University of Alberta

Sequence stratigraphy and underlying tectonism of the Northern Richardson Mountains and adjacent Mackenzie Delta related to the formation of the Arctic Ocean

by

Ryan A. Millar

A thesis submitted in partial fulfillment of the requirements for the degree of

Master of Science

Department of Earth and Atmospheric Sciences

University of Alberta

ABSTRACT

Jurassic-Cretaceous rifting within Arctic North America that eventually resulted in the formation of the Arctic Ocean greatly affected deposition within nearshore terrestrial basins in surrounding areas, such as the Brooks-Mackenzie Basin and the Sverdrup Basin. In this thesis, measured stratigraphic sections and detrital U-Pb zircon data from outcrops within the Northern Richardson Mountains are integrated with well-log and core data from the adjacent Mackenzie Delta to establish a model-independent sequence stratigraphic framework for the Brooks-Mackenzie Basin. This framework is then used to elucidate the underlying tectonic forces responsible for the observed stratigraphy, relating patterns of deposition to various phases of rift development. The proposed interpretation classifies the sub-Jurassic unconformity as a first-order sequence boundary, demarcating a change in tectonic setting from pre-rift to rift, meaning it is also classified as the rift onset unconformity for the Arctic Ocean. The overlying Bug Creek Group is largely progradational, representing a first-order lowstand systems tract corresponding to early syn-rift strata. Detrital zircon data from the Bug Creek Group lacks syn-depositional zircons and resemble the underlying Permian, suggesting a recycled source. A change in the detrital zircon signature is observed within the uppermost Aklavik Formation, representing a new source. This also coincides with a rapid transition to the lower offshore deposits of the Husky Formation caused by normal faulting in the Husky Lakes Fault Zone, which is associated with a dramatic basin expansion. Maximum transgression occurs above the arenaceous member of the Husky Formation, likely near the Jurassic-Cretaceous boundary, representing a first-order maximum flooding surface and rift-climax. Above the rift climax, the overall progradational signature represents a first-order HST and post-rift deposits. The sub-Hauterivian basal Kamik

unconformity is observed at the base of the subsequent FSST. This first-order sequence boundary is approximately time equivalent to the breakup unconformity for the Arctic Ocean, with the overlying Kamik Formation resembling the Isachsen Formation in the Sverdrup Basin.

“We keep moving forward, opening new doors, and doing new things, because we’re curious and curiosity keeps leading us down new paths.” – Walt Disney

“Now this is not the end. It is not even the beginning of the end. But it is, perhaps, the end of the beginning.” – Winston Churchill

Acknowledgements

I have many people to thank, foremost my parents. I have the best parents in the world. I cannot thank them enough for their continued support, love, and encouragement. I think all the hikes and travelling as a child stimulated my curiosity in the natural world; perhaps it was all the time we spent together in the mountains that led me to start considering how things like the mountains formed in the first place.

I thank my girlfriend, Kylie Wilson, for her help, love, and support throughout this process. She is also pursuing a Masters, and in a field unrelated to her undergraduate degree. Seeing her drive and perseverance when tackling new challenges has been a constant source of inspiration.

This work would not have been possible without the guidance and support of Dr. Thomas Hadlari. I cannot thank him enough. Specifically, I thank him for his patience during the writing process and for allowing me to build the project my own way. He has been a great mentor and has taught me many lessons, both personal and professional. We didn't always agree on the interpretation (I think I was almost always wrong…), but I truly valued the conversations we would have when we interpreted things differently. I wish we were able to have more talks about geology at Last Defence Lounge near the end of my thesis, but hopefully we can resume that again shortly. It was a pleasure to work with such a talented scientist and curious mind.

I thank Dr. Octavian Catuneanu for taking me on as a student and introducing me to the project. His research was heavily relied upon throughout, and I thank him for his comments on sequence stratigraphy and excellent classroom lectures.

My great friends Cole and Scott are thanked for their support. Their friendship made graduate school about far more than writing papers. They were both members of the Ichnology

Research Group (IRG), and I would also like to thank the IRG more generally, both the students and Dr.'s Gingras, Zonneveld, and Pemberton. As someone who came from a very small lab group, inviting me to eat lunch in the lab and including me on your field trips truly meant a lot.

Thank you to Dr. Benjamin Daniels and Emily Ellefson (AKA "Team Strat") for being wonderful field partners. I will never forget our time in the Northern Richardson Mountains. To the entire field team, you helped make the trip to Aklavik one of the highlights of my life. We had a great team. Thank you in particular to Caleb Charlie for his help in the field and the owners and staff at Bessie's Bunkhouse. We would spend long days in the field, and their help and support back at camp was a huge part of our team's success.

Thank you to the many other academics or researchers who were involved along the way, particularly Terry Poulton, Larry Lane, and Jim Dixon. Thank you to Bill Dwyer and Richard Fontaine for all of their hard work and assistance in the core lab.

Thank you to the Research Affiliate Program, Geo-mapping for Energy and Minerals Program, and the University of Alberta for financing this work. I feel incredibly fortunate to have been given this opportunity.

Thank you to all my friends who supported me along the way, particularly my old friends, most of whom I've known since Kindergarten or before. You have been one of the most important constants of my life. I may technically be an "only child", but you are my brothers.

Last, but most certainly not least, thank you to the people of Aklavik. Going to Aklavik was a life-changing experience. I have never felt a more loving and inviting people. Thank you for teaching me about your traditions and way of life. It was a true honour to be included in the whale hunt. I can't wait to go back one day.

Table of Contents

List of Figures

Chapter 1: Introduction

TIME AND SPACE

The current work is presented as a part of broader, ongoing research at the Geological Survey of Canada (GSC) focused on characterizing the tectonic evolution of Arctic Canada during the Mesozoic, the Era spanning 250 to 65 million years ago (Ma), specifically concerning both the older (approximately 200 to 126 Ma) rifting associated with the incipient Arctic Ocean and the younger (less than approximately 113 Ma) development of the North American Cordillera (Fig. 1-1). In this thesis, the primary focus is on the older opening of the Arctic Ocean. Consequently, the Jurassic to mid-Early Cretaceous period is examined (200 to approximately 120 Ma). Understanding the Jurassic to mid-Early Cretaceous period is critical to evaluating the formation of the Arctic Ocean because, though there is disagreement on the precise formation dynamics (e.g., Embry, 1990, 2000; Lane, 1997), little disagreement exists on timing, with the overwhelming majority of publications supporting key tectonic reorganization related to the opening of the Arctic Ocean during this period. Therefore, regardless of formation dynamics, this is the crucial period for understanding how the region evolved from a tectonic and stratigraphic perspective.

Regarding the study area, the geographical extent encompasses the Northern Richardson Mountains and the Mackenzie Delta, both of which contain strata deposited within the Canadian portion of the ancestral Brooks-Mackenzie Basin (defined by Balkwill et al., 1983; Fig. 1-2). These two adjacent areas are the main focus for four reasons. First, this area is located just south of the Arctic Ocean and would have been dramatically affected by its development, meaning

observations from the study area can provide important insights into the nature and timing of tectonic events related to the formation of the Arctic Ocean on a broader scale.

The second reason is data availability and accessibility. Because of inherent problems involved in studying the Arctic Ocean directly (e.g., ice cover, remoteness, financial cost, water depth, and other geological factors including sediment cover and overprinting due to igneous activity), there is little geological data within the ocean basin itself, though geophysical data does exist (e.g., Vogt et al., 1979). Therefore, to assess the formation dynamics, previous geological studies have commonly examined nearshore or terrestrial basins demarcating the Arctic Ocean (e.g., the Sverdrup Basin; Hadlari et al., 2016), rather than examining the Arctic Ocean itself. Aside from the reasons listed above, this approach is also beneficial because (1) surrounding basins may contain exposed outcrops (e.g., outcrops on Ellef Ringnes Island in the Sverdrup Basin; Tullius et al., 2014) and (2) these basins commonly contain publicly available data derived from petroleum exploration (e.g., well-logs, core, or seismic data). The same logic is applied here by focusing the geological investigation on the predominantly terrestrial Brooks-Mackenzie Basin, which contains a significant amount of subsurface data within the Mackenzie Delta (Fig. 1-3) and abundant outcrop data from the Northern Richardson Mountains (Fig. 1-4).

Thirdly, the Mackenzie Delta has significant petroleum potential (NRCan, 2019). Petroleum investigation within the area has a long history. Following the discovery of oil and gas in Prudhoe Bay Alaska in 1968, companies operating in Canada began to intensify their investigations into the Mackenzie Delta, which resulted in the discovery of petroleum in this region by Imperial Oil in 1970. Since 1970, drilling in the area has expanded, resulting in numerous discoveries amounting to considerable reserves estimated at 1 to 1.2 billion barrels of

recoverable oil resource and 9 to 10.4 trillion cubic feet of marketable gas resource (Beaufort Regional Environmental Assessment, 2013). Therefore, any potential insights stemming from this work could have additional economic considerations.

Finally, though this area has been studied extensively in the past (e.g., Operation Porcupine, a large-scale mapping project led by D.K. Norris beginning in the 1960s and culminating in a synthesis edited by Norris (1997)), it represents a locality with a relative dearth of new data or studies. Therefore, in light of both advances in sedimentary geology (e.g., modern facies analysis and sequence stratigraphy) and new laboratory techniques (e.g., detrital zircon U-Pb geochronology), re-examining this area is expected to advance a better understanding of the local geology within the broader context, namely how it is related to the formation of the Arctic Ocean and surrounding areas.

PROJECT BACKGROUND AND MOTIVATIONS

The underlying mechanics of how the Arctic Ocean opened has stimulated much debate, as it is a relevant topic for advancing the understanding of fundamental plate tectonic processes (e.g., rift dynamics) from an academic standpoint, and the distribution of oil and natural gas accumulations (within both the Arctic Ocean basin itself and other demarcating basins affected by its development) from an economic standpoint. Academic investigations stem from S.W. Carey's seminal work on *oroclines*[1] (Carey, 1955), where he first described a potential link

[1] Defined as "an orogenic system which has been flexed in plan to a horse-shoe or elbow shape" (Carey, 1955, pg. 257)

between the opening of the Arctic Ocean and the North American Cordillera, or the Rocky Mountains, through this newly developed concept.

Oroclines are essentially a bent segment of a mountain range, with a prominent orocline present in Alaska (Fig. 1-1). Carey (1955) asserted that forces responsible for bending the mountain belt would be associated with rotation, transcurrent displacement, and tensional opening inland (Figs. 1-1, 1-2). In the case of the Rocky Mountain orocline in Alaska, Carey (1955) proposed that tensional opening inland was expressed through rifting that resulted in the opening of the Arctic Ocean. Though the nature of the relationship between the North American Cordillera and the Arctic Ocean is now being re-assessed (e.g., Hadlari et al., 2017), this represents the first conceptual framework describing the mechanism in which the Arctic Ocean opened (via rifting of continental crust in response to tectonic forces that were also responsible for "bending" the North American Cordillera).

Ensuing work has focused on refining this general concept. Examples of additional early developments include constraining the timing of the opening to post-Triassic (e.g., <201 Ma; Tailleur, 1969), locating the hypothesized rotation pole within the Mackenzie Delta (e.g., Rickwood, 1970; Fig. 1-2), and attempts to elucidate internal complexities beyond the general opening dynamics (e.g., Vogt and Ostenso, 1970). Grantz et al. (1979) provided the first regional synopsis of the tectonic development of the Alaskan margin, which borders the western edge of the Arctic Ocean, based primarily on seismic data, but also bathymetry, gravity, paleomagnetic, and geomagnetic data. This paper is normally credited with the development of what is now commonly known as the "anticlockwise rotation hypothesis" or "windshield wiper hypothesis", though it was refined and improved by Grantz et al. (2011). The reason this paper is credited,

rather than older works like Carey (1955), mainly has to do with the specificity of the geodynamic model presented and the fact that the interpretation is based on multiple data sets, rather than broader conceptualizations (e.g., the idea of oroclines).

According to the hypothesis of Grantz et al. (1979, 2011), generally speaking, the Canadian Arctic Islands and Arctic Alaska would have once formed a conjugate margin, with Arctic Alaska rifting away from the Canadian Arctic Islands around a rotation pole located within the Mackenzie Delta toward the position observed today, resulting in the formation of the southern Arctic Ocean basin (i.e., below the Lomonosov Ridge; Fig. 1-2A), known as the Amerasia Basin. The northern basin in the Arctic Ocean, the Eurasia Basin, was not formed until much later and is beyond the scope of this project.

Many academics studying the geology of Arctic North America accept some variation of the hypothesis proposed by Grantz et al. (1979, 2011), though other hypotheses have been circulated (reviewed in Lawver and Scotese, 1990). In recent years, however, the debate surrounding the opening of the Arctic Ocean has reemerged. This has been primarily driven by technological advances in terms of available geophysical techniques (e.g., Døssing et al., 2013; Chian et al., 2016), which can provide additional constraints on tectonic origin and development, and laboratory techniques (e.g., U-Pb detrital zircon geochronology), which can be used to establish sedimentary provenance or to date specific events (e.g., Anfinson et al., 2012, 2016; Gottlieb et al., 2014; Midwinter et al., 2016). Both of these advancements can provide quantitative support for various geodynamic models, resulting in improved precision and understanding. Additionally, though many recent studies still support or invoke some form of anticlockwise rotation (e.g., Shepard et al., 2013; Hadlari et al., 2016; Midwinter et al., 2016; Till,

2016), this model is not universally accepted (e.g., Lane, 1997, 2007; Colpron and Nelson, 2009; Miller et al., 2010), which continues to drive academic debate and investigation.

From an economic perspective, the formation of the Arctic Ocean plays a profound role in sediment routing, distribution of depositional environments, and structural complexity. Furthermore, the opening of the Arctic Ocean affects not only the ocean basin itself, but also nearby terrestrial basins, such as the Brooks-Mackenzie Basin within the study area (Fig. 1-2). An adequate understanding of fundamental formation dynamics is therefore vital to predicting petroleum accumulations, as the location, quality, and continuity of petroleum play elements (source, reservoir, and seal) are highly dependent on the historical arrangement of depositional systems (i.e., paleogeography) and structural complexity (i.e., faulting patterns).

Though some areas within the study area have been exploited, for example, the Tuktoyaktuk Peninsula (Fig. 1-3), development in Arctic Canada has largely stagnated. Therefore, to stimulate development, Natural Resources Canada (NRCan) began funding geological research initiatives focused on enhancing the regional understanding through the Geo-mapping for Energy and Minerals (GEM) Program, anticipating that an improved regional understanding would result in increased private investment. GEM began in 2008 with a $100 million investment over 5 years and was renewed in 2013. As of 2019, research funded by the GEM Program has “generat[ed] $40 million in direct employment opportunities and indirect investment of over $300 million” (NRCan, 2019).

INTENTIONS

This thesis intends to do four things: (1) re-evaluate existing sedimentology and depositional environments, (2) establish a sequence stratigraphic framework and hierarchy, (3) present new U-Pb detrital zircon data, and (4) relate the study area to the nearby Sverdrup Basin. The aim in completing these four objectives is a better understanding of the underlying tectonic forces, as well as their spatial and temporal extent, which are responsible for the observed stratigraphy. This contributes to ongoing discussions regarding the opening of the Arctic Ocean, in an attempt to define events with greater precision, increase predictive power, and in general conceive of a better understanding of the tectonic evolution of Arctic North America during the Mesozoic.

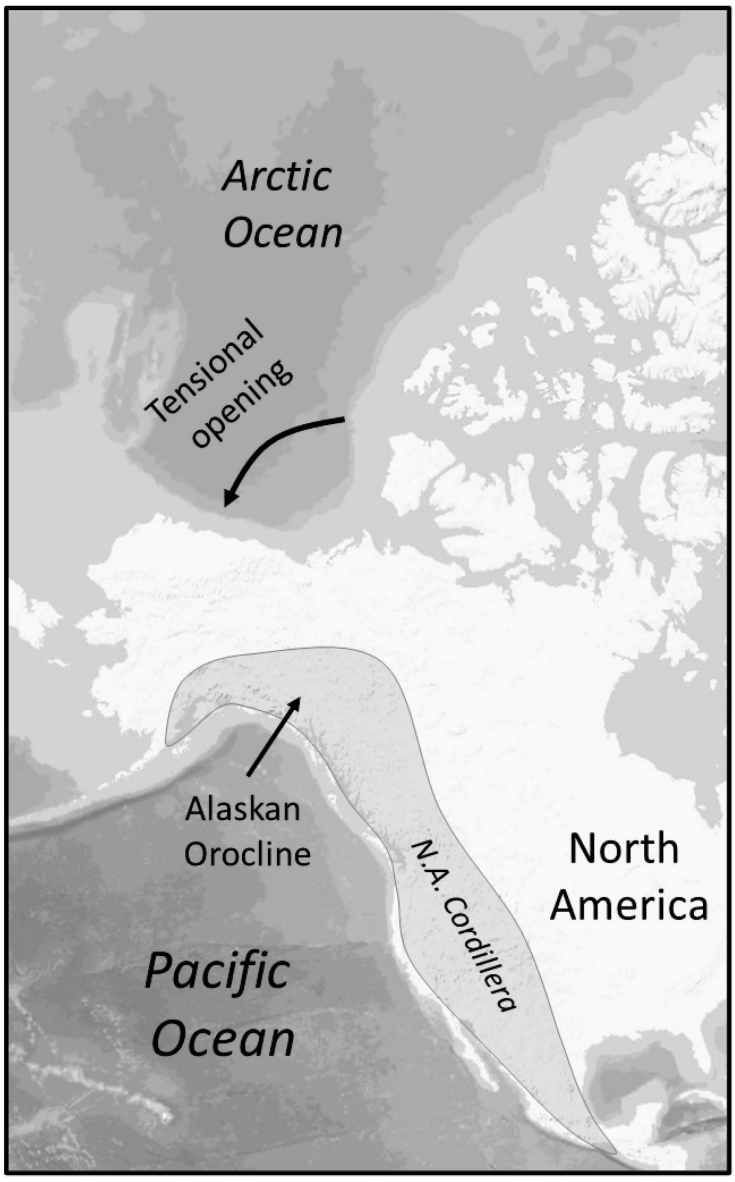

Figure 1-1: Map of Arctic North America highlighting the Alaskan orocline and the Arctic Ocean. Approximate outline of the North American (N.A.) Cordillera is shown in grey. Source of basemap: Ersi, USGS, NOAA.

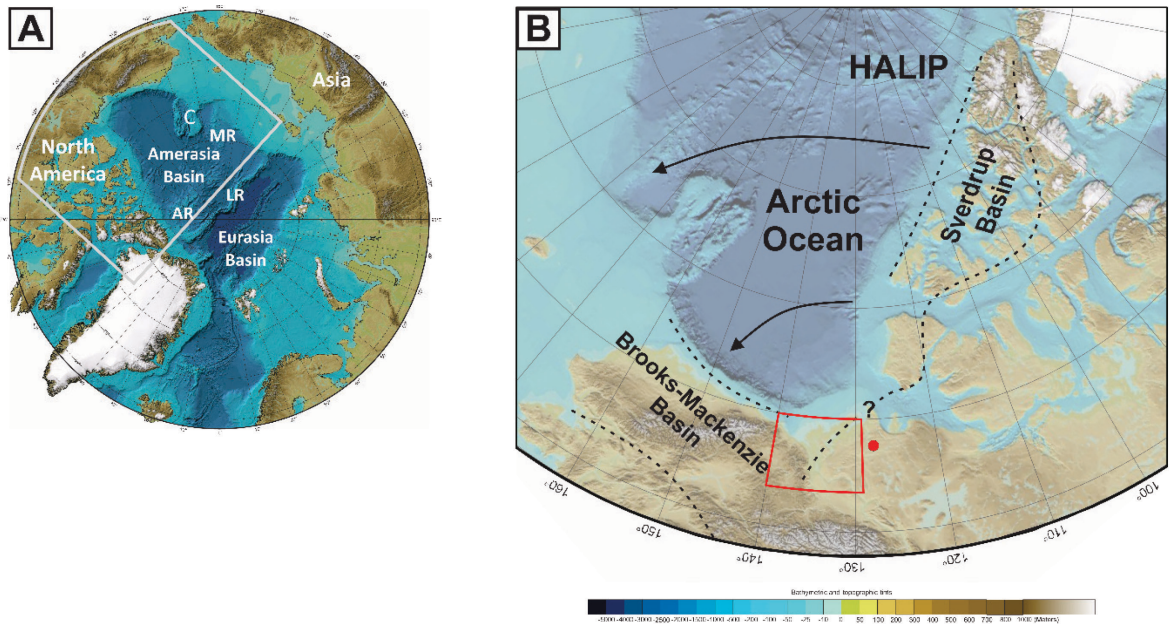

Figure 1-2: (A) Circum-Arctic bathymetric map from Jakobsson et al. (2012). AR: Alpha Ridge, C: Chukchi Borderland, LR: Lomonosov Ridge, MR: Mendeleev Ridge. The location of (B) is outlined in grey. **(B)** Bathymetric map showing the outline of the Sverdrup and Brooks-Mackenzie basins modified after Balkwill et al. (1983). The red dot is the hypothesized pivot point after Rickwood (1970); Grantz et al. (2011). The red box outlines the location of the study area shown in Fig. 1-3A.

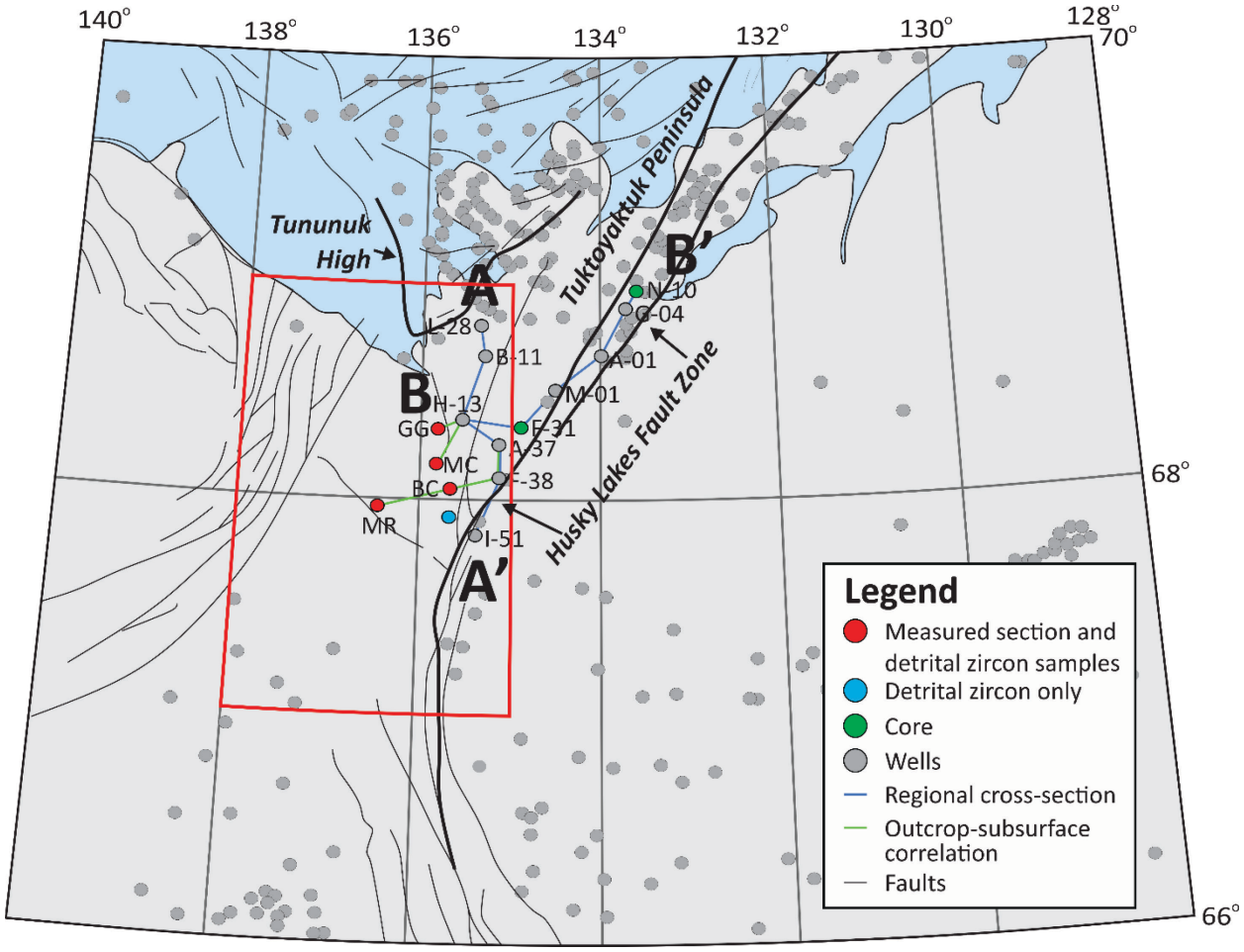

Figure 1-3: Map of study area showing wells, cross-sections, the location of measured sections, and detrital zircon sample locations. Faults from Norris (1985). BC: Bug Creek, GG: Grizzly Gorge, MC: Martin Creek, MR: Murray Ridge. The red box shows the outline of Fig. 1-4.

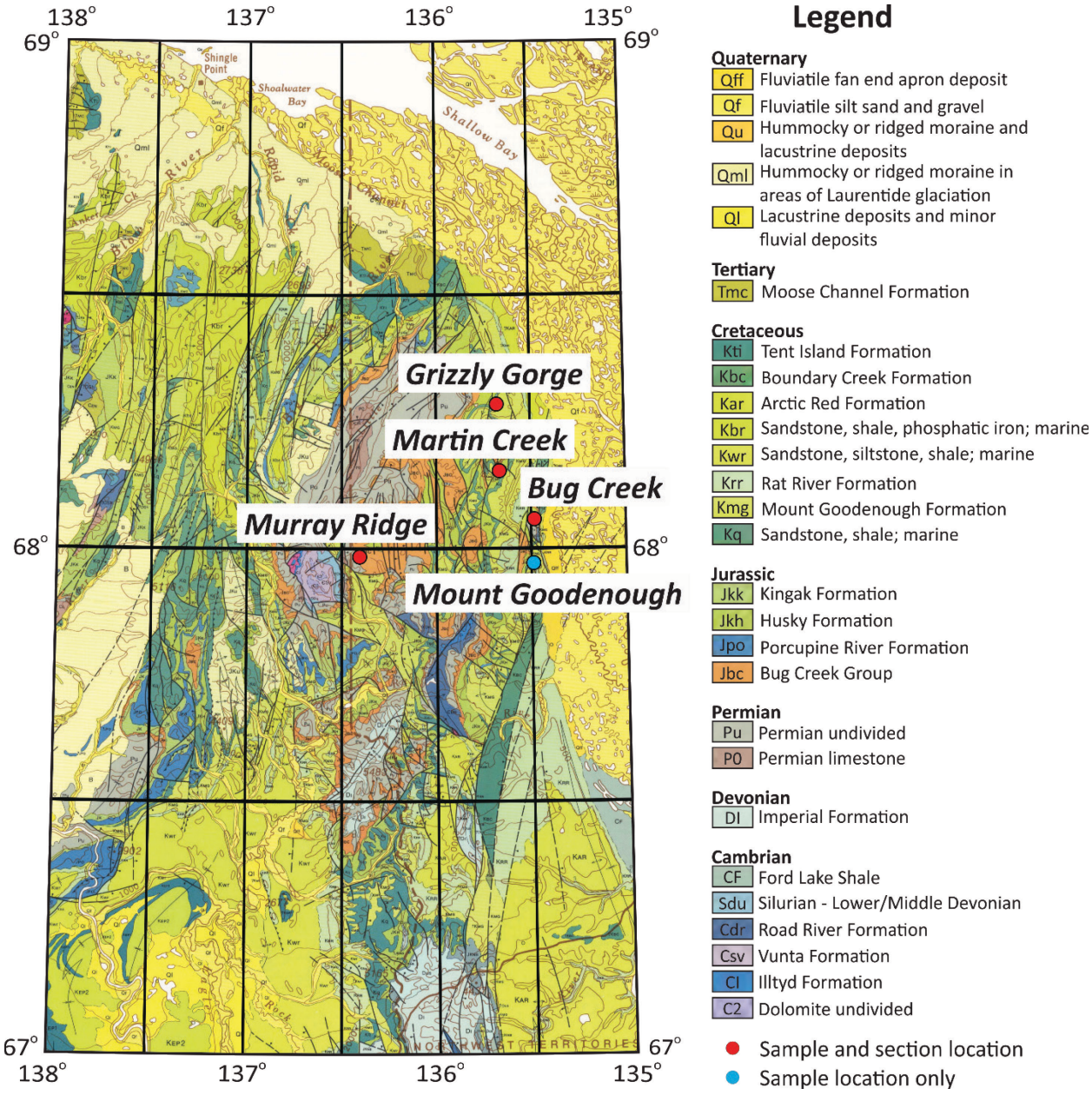

Figure 1-4: Geological map of outcrops within the Northern Richardson Mountains modified after Norris (1985).

BIBLIOGRAPHY

Anfinson, O.A., Leier, A.L., Embry, A.F., and Dewing, K., 2012. Detrital zircon geochronology and provenance of the Neoproterozoic to Late Devonian Franklinian Basin, Canadian Arctic Islands. Geological Society of America Bulletin, 124(3-4), p. 415 – 430.

Anfinson, O.A., Embry, A.F., and Stockli, D.F., 2016. Geochronologic constraints on the Permian-Triassic northern source region of the Sverdrup Basin, Canadian Arctic Islands. Tectonophysics, 691, p. 206 – 219.

Balkwill, H.R., Cook, D.G., Detterman, R.L., Embry, A.F., Hakansson, E., Miall, A.D., Poulton, T.P., and Young, F.G., 1983. Arctic North America and northern Greenland. In: Moullade, M., and Nairn, A.E.M. (eds.), The Phanerozoic Geology of the World II, Elsevier, New York, p. 1 – 31.

Beaufort Regional Environmental Assessment (BREA), 2013. Oil and Gas Exploration and Development Activity Forecast. Accessed August 28, 2020. <https://www.beaufortrea.ca/wp-content/uploads/2012/03/NCR-5358624-v4-BREA_-_FINAL_UPDATE_-_EXPLORATION_AND_ACTIVITY_FORECAST-__MAY_2013.pdf>

Carey, S.W., 1955. The orocline concept in geotectonics. Paper and Proceedings of the Royal Society of Tasmania, 89, p. 255 – 288.

Chian, D., Jackson, H.R., Hutchinson, D.R., Shimeld, J.W., Oakey, G.N., Lebedeva-Ivanova, N., Li, Q., Saltus, R.W., and Mosher, D.C., 2016. Distribution of crustal types in Canada Basin, Arctic Ocean. Tectonophysics, 691, p. 8 – 30.

Colpron, M., and Nelson, J.L., 2009. A Palaeozoic Northwest Passage: incursion of Caledonian, Baltican and Siberian terranes into eastern Panthalassa, and the early evolution of the North

American Cordillera. In: Cawood, P.A., and Kröner, A. (eds.), Earth Accretionary Systems in Space and Time, The Geological Society, London, Special Publication, 318, p. 273 – 307.

Døssing, A., Jackson, H.R., Matzka, J., Einarsson, I., Rasmussen, T.M., Olesen, A.V., and Brozena, J.M., 2013. On the origin of the Amerasia Basin and the High Arctic Large Igneous Province—Results of new aeromagnetic data. Earth and Planetary Science Letters, 363, p. 219 – 230.

Embry, A.F., 1990. Geological and geophysical evidence in support of anticlockwise rotation of northern Alaska. Marine Geology, 93, p. 317 – 329.

Embry, A.F., 2000. Counterclockwise rotation of the Arctic Alaska Plate: Best available model or untenable hypothesis for the opening of the Amerasia Basin. Polarforschung, 68, p. 247 – 255.

Gottlieb, E.S., Meisling, K.E., Miller, E.L., and Mull, C.G., 2014. Closing the Canada Basin: Detrital zircon geochronology relationship between the North Slope of Arctic Alaska and the Franklinian mobile belt of Arctic Canada. Geosphere, 10(6), p. 1366 – 1384.

Grantz, A., Eittreim, S., and Dinter, D.A., 1979. Geology and tectonic development of the continental margin north of Alaska. Tectonophysics, 15, p. 263 – 291.

Grantz, A., Hart, P.E., and Childers, V.A., 2011. Geology and tectonic development of the Amerasia and Canada Basins, Arctic Ocean. In: Spencer, A.M., Embry, A.F., Gautier, D.L., and Sørenson, K. (eds.), Arctic Petroleum Geology, Memoir 35, Geological Society, London, p. 771 – 799.

Hadlari, T., Midwinter, D., Galloway, J.M., Dewing, K., and Durbano, A.M., 2016. Mesozoic rift to post-rift tectonostratigraphy of the Sverdrup Basin, Canadian Arctic. Marine and Petroleum Geology, 76, p. 148 – 158.

Hadlari, T., Midwinter, D., Poulton, T.P., and Matthews, W.A., 2017. A Pangean rim of fire: Reviewing the Triassic of western Laurentia. Lithosphere, 9(4), p. 579 – 582.

Jakobsson, M., Mayer, L.A., Coakley, B., Dowdeswell, J.A., Forbes, S., Fridman, B., Hodnesdal, H., Noormets, R., Pedersen, R., Rebesco, M., Schenke, H.W. Zarayskaya, Y., Accettella, A.D., Armstrong, A., Anderson, R.M., Bienhoff, P., Camerlenghi, A., Church, I., Edwards, M., Gardner, J.V., Hall, J.K., Hell, B., Hestvik, O.B., Kristoffersen, Y., Marcussen, C., Mohammad, R., Mosher, D., Nghiem, S.V., Pedrosa, M.T., Travaglini, P.G., and Weatherall, P., 2012**.** The International Bathymetric Chart of the Arctic Ocean (IBCAO) Version 3.0. Geophysical Research Letters, doi:10:1029/2012GL052219.

Lane, L.S., 1997. Canada Basin, Arctic Ocean: evidence against a rotational origin. Tectonophysics, 16(3), p. 309 – 322.

Lane, L.S., 2007. Devonian-Carboniferous paleogeography and orogenesis, northern Yukon and adjacent Arctic Alaska. Canadian Journal of Earth Science, 44(5), p. 679 – 694.

Lawver, L.A., and Scotese, C.R., 1990. A review of tectonic models for the evolution of the Canada Basin. In: Grantz, A., Johnson, G.L., and Sweeney, J.F. (eds.), The Arctic Ocean Region, The Geology of North America, 1, p. 593 – 618.

Midwinter, D., Hadlari, T., Davis, W.J., and Dewing, K., 2016. Dual provenance signatures of the Triassic northern Laurentian margin from detrital-zircon U-Pb and Hf-isotopic analysis of Triassic-Jurassic strata in the Sverdrup Basin. Lithosphere, 8(6), p. 668 – 683.

Miller, E.L., Gehrels, G.E., Pease, V., and Sokolov, S., 2010. Stratigraphy and U-Pb detrital zircon geochronology of Wrangel Islands, Russia: implications for Arctic paleogeography. AAPG Bulletin, 94(5), p. 665 – 692.

Norris, D.K., 1985. Geology of the Northern Yukon and Northwest District of Mackenzie. Geological Survey of Canada, "A" Series Map 1581A. <https://doi.org/10.4095/120537>.

Norris, D.K. (eds.), 1997. Geology and Mineral and hydrocarbon potential of northern Yukon Territory and Northwestern District of Mackenzie, Geological Survey of Canada Bulletin, 422.

NRCan, 2019. About Geo-mapping for Energy and Minerals (GEM) program. Accessed June 2, 2020. <https://www.nrcan.gc.ca/science-data/earth-sciences/earth-sciences-resources/earth-sciences-federal-programs/gem-geo-mapping-energy-minerals/about-geo-mapping-energy-minerals-gem-program/21817>.

Rickwood, F.K., 1970. The Prudhoe Bay Field. In: Adkinson, W.L., and Brosgè, W.P. (eds.), Proceedings of the geological seminar on the North Slope of Alaska, AAPG, Pacific Section, L1 – L11.

Shepard, G.E., Müller, R.D., and Seton, M., 2013. The tectonic evolution of the Arctic Pangea breakup: Integrating constraints from surface geology and geophysics with mantle structure. Earth-Science Reviews, 124, p. 148 – 183.

Tailleur, L.L., 1969. Rifting speculation of the geology of Alaska's North Slope. Oil and Gas Journal, 19, p. 128 – 130.

Till, A.B., 2016. A synthesis of Jurassic and Early Cretaceous crustal evolution along the southern margin of the Arctic Alaska-Chukotka microplate and implications for defining tectonic boundaries active during opening of Arctic Ocean basins. Lithosphere, 8(3), p. 219 – 237.

Tullius, D.N., Leier, A.L., Galloway, J.M., Embry, A.F., and Pedersen, P.K., 2014. Sedimentology and stratigraphy of the Lower Cretaceous Isachsen Formation: Ellef Ringnes Island, Sverdrup Basin, Canadian Arctic Archipelago. Marine and Petroleum Geology, 57, p. 135 – 151.

Vogt, P.R., and Ostenso, N.A., 1970. Magnetic and gravity profiles across the Alpha Cordillera and their relation to Arctic sea-floor spreading. Journal of Geophysical Research, 75(26), p. 4925 – 4937.

Vogt, P.R., Taylor, P.T., Kovacs, L.C., and Johnson, G.L., 1979. Detailed aeromagnetic investigation of the Arctic Basin. Journal of Geophysical Research, 84(B3), p. 1071 – 1089.

Chapter 2: Sequence stratigraphy and underlying tectonism of the Northern Richardson Mountains and adjacent Mackenzie Delta related to the formation of the Arctic Ocean

INTRODUCTION

This chapter attempts to enhance the understanding of fundamental plate tectonic processes by developing a model-independent sequence stratigraphic framework (*sensu* Catuneanu, 2019a) for Jurassic to mid-Early Cretaceous strata deposited within the Brooks-Mackenzie Basin (Figs. 1-2 to 1-4). Like the approach of Hadlari et al. (2016) applied to the Sverdrup Basin, focusing on the adjacent Brooks-Mackenzie Basin is expected to reveal tectonic insights related to the formation of the Arctic Ocean, as the stratigraphic expressions preserved within the Brooks-Mackenzie Basin are largely controlled by the opening of the Arctic Ocean during this period. This framework is developed in multiple steps. First, facies associations (*sensu* Collinson, 1969) are defined based on outcrop and core observations, as well as previous studies (e.g., Dixon, 1982, 1991, 2004; Poulton et al., 1982; Poulton, 1997; Barnett, 2003). Second, the vertical arrangement of depositional environments and the overall geometry of the basin are examined using a pair of regional cross-sections (Fig. 1-3). Third, systems tracts are defined based on stratal stacking patterns and bounding surfaces from a combination of core, outcrop, and well log data (Figs. 1-3 and 1-4). Results are also supported by new U-Pb detrital zircon data obtained from samples in the Northern Richardson Mountains (Fig. 1-4). Finally, this framework is used to elucidate underlying tectonic signatures. The underlying tectonic signatures are then compared to the nearby Sverdrup Basin (e.g., Hadlari et al., 2016). The Brooks Mackenzie and Sverdrup

basins together demarcate the North American portion of the Arctic Ocean, with any correlation being the likely result of large-scale rifting.

The opening of the Arctic Ocean

The Arctic Ocean contains two major basins, the Amerasia and Eurasia basins, which are separated by the Lomonosov Ridge (Fig. 1-2). The opening of the Eurasia Basin via seafloor spreading began approximately 60 Ma and is still active (Vogt and Avery, 1974). This is well established due to the presence of clear magnetic anomalies (Vogt and Avery, 1974; Brozena et al., 2003). The model of formation for the sub-triangular Amerasia Basin is contested, with multiple tectonic models proposed. However, most authors (e.g., Embry, 1990; Embry and Dixon, 1990; Shepard et al., 2013; Gottlieb et al., 2014; Hadlari et al., 2016; Midwinter et al., 2016; Till, 2016) favor a form of anticlockwise rotational opening proposed by Grantz et al. (1979, 2011) in which Arctic Alaska and the Canadian Arctic Islands once formed a conjugate margin, with Arctic Alaska rifting away from Arctic Canada to the position observed today (Fig. 1-2). In this model, the study area is located near the approximate pivot point (Fig. 1-2B), and the resulting, time-equivalent deposits would have formed within the context of rifting. This also agrees with previous assertions by other authors regarding the tectonic setting of the study area from the Jurassic to the mid-Early Cretaceous (e.g., Dixon, 1997) and published seismic interpretations showing normal faulting, which is indicative of rifting (e.g., Dietrich, 1996).

Idealized rift succession

Rift basins form due to continental extension, resulting in the generation of grabens and half-grabens at the newly developing continental margin and oceanic crust between the severed continental fragments. The development of rift basins occurs in a relatively distinct and

predictable fashion summarized in Figure 2-1. Though unique rift basins can differ due to variations in climate (e.g., humid vs. arid environments) or sea-level, unique underlying stratigraphic patterns emerge that are differentiable from those observed in passive margin settings (Prosser, 1993; Martins-Neto and Catuneanu, 2010; Holz et al., 2017). The differing stratigraphic signature between passive margins and rift basins is due to the differing nature of tectonic forces acting in each setting. In passive margin settings, where active faulting is absent and the area is tectonically stable, tectonic subsidence is largely driven by prolonged thermal subsidence (Vail et al., 1977; Martins-Neto and Catuneanu, 2010) that is also approximately linear (Prosser et al., 1993). This results in eustasy, or sea-level fluctuations, being the dominant force responsible for shifting shoreline trajectories. In rift basins, by contrast, fault-generated subsidence plays the key role in the generation of accommodation space, with eustatic forces subordinated. Given that this subsidence generating mechanism (fault generated subsidence) is comparatively instantaneous and intermittently active (vs. eustatic forces that are more predictable and constant), successions tend to exhibit prolonged periods of progradation followed by sharp flooding surfaces and marine transgressions (Martins-Neto and Catuneanu, 2010).

General models for the conceptual understanding or predictive framework of rift basins have also been developed, in terms of both the way faulting proceeds (e.g., Gupta et al., 1998) and the predictable association of facies that occurs as a result of the faulting (e.g., Prosser, 1993; Fig. 2-1), which are both best described in terms of the various stages of rift development. In general, rift basins develop above a basal rift-onset unconformity (ROU), which demarcates a change in the tectonic setting from pre-rift to rift. In the early stages, isolated fault blocks

dominate, but as rifting proceeds, isolated fault blocks are linked into a more continuous fault array (Fig. 2-1B; Gupta et al., 1998). Because faulting is the main control on accommodation in rift basins, the pattern of generally isolated depocenters in early phases of rifting followed by a regionally continuous depocenter mirrors the faulting pattern as extension proceeds (Fig. 2-1B; Gupta et al., 1998). Furthermore, the transition from isolated faults to a regionally continuous fault array is associated with a dramatic increase in tectonic subsidence, which expands the catchment area and greatly increases accommodation, regardless of whether or not extension rates increase (Gupta et al., 1998). This transition from isolated to continuous depocenters, and the resulting increase in the catchment area and accommodation space, approximately coincides with the transition from "rift initiation" to "rift climax" of Prosser (1993) when discussing the resulting stratigraphy (Fig. 2-1A).

During the earlier rift initiation phase, when sediment is concentrated in numerous, isolated fault-bound depocenters, sediment supply is generally able to keep pace with the rate of created accommodation space, which in the early stages of rift basin development is relatively low. This results in mainly shallow marine or fluvial deposits that onlap the underlying basement, also being arranged in a progradational pattern (Holz et al., 2017). When isolated fault-bound basins become contiguous with increased rifting, sediment supply is unable to keep pace with the dramatic increase in accommodation space and sedimentary facies begin to backstep, resulting in a basin expansion. The rift climax of Prosser (1993) occurs at the time of maximum retrogradation, or backstepping, of facies. During this phase, mud-dominant strata are deposited over most of the basin, with the deposition of coarser material limited to the basin margin.

Prosser (1993) defines two additional phases after the rift climax: immediate post-rift and late post-rift. During the immediate post-rift phase (e.g., immediately after a major faulting event), the rate of normal faulting, and thus the rate of fault-generated accommodation space, greatly decreases. Furthermore, newly exposed terrains (e.g., headwall areas that become exposed during syn-rift faulting), can act as a new source of sediment, increasing supply. This increases the rate of sediment influx. The combination of a general decrease in fault-generated subsidence and a general increase in available sediment commonly results in progradation during the immediate post-rift phase. The late post-rift phase is typically associated with transgression, possibly due to the degradation of source material (e.g., the tilted, exposed footwall), but this may not always be the case (Prosser, 1993). In instances where rifts proceed to the breakup phase (i.e., a successful rift vs. a failed rift), as is the case with the Arctic Ocean (Chian et al., 2016), the severing of continental crust and the generation of oceanic crust results in a predictable association of facies known as the "breakup sequence" (*sensu* Soares et al., 2012).

The concept of a "breakup sequence" was developed at the divergent continental margins of Newfoundland and Iberia (Soares et al., 2012), which represents a magma poor rifted margin (Wilson, 1975), similar to the Arctic Ocean (Hadlari et al., 2016). The breakup sequence is interpreted to represent the transitional period between lithospheric breakup and the onset of thermal relaxation (Soares et al., 2012). This is similar to the "rift termination systems tract" of Holz et al. (2017), the "transitional sequence" of Moore (1992), or the "early post-rift phase" of Nøttvedt et al. (1995).

Conceptually, the breakup sequence evolved from the "breakup unconformity" (BU) of Falvey (1974), which was hypothesized to form as a result of erosion during a phase of uplift just

before breakup. The conceptual evolution of the BU to a larger breakup sequence was necessary primarily to recognize that breakup is a protracted event, meaning a predictable association of facies can be recognized, rather than a single unconformity, though the unconformity (the BU or BU equivalent) is also present. The expression of the breakup sequence can vary depending on the proximity to the continental margin (Soares et al., 2012), but in all areas, it is bound by an unconformity or correlative conformity at the base and can be partitioned into distinct phases. Within the inner proximate margin (e.g., the interpreted location of the study area in relation to the opening of the Arctic Ocean) at the type section for the breakup sequence (offshore Iberia and Newfoundland; Soares et al., 2012), this includes, from base to top, an unconformity, a forced regressive unit, and an overall transgressive package, representing a phase of coarse clastic infill of remnant topography followed by deposition of finer-grained material (Nøttvedt et al., 1995).

GEOLOGICAL BACKGROUND

Jurassic to mid-Early Cretaceous strata underlying the Mackenzie Delta (Fig. 1-3) and outcropping within the Northern Richardson Mountains (Fig. 1-4) were deposited within the Brooks-Mackenzie Basin, which was defined by Balkwill et al. (1983) to reflect the relative continuity between strata deposited within the northern regions of the Northwest Territories, Yukon, and Arctic Alaska before the breakup that eventually resulted in the formation of the Arctic Ocean (Fig. 1-2B). This basin was one of two active depocenters within Arctic North America from the Jurassic to mid-Early Cretaceous, the other being the Sverdrup Basin. However, because of the size of the Brooks-Mackenzie Basin, combined with the fact that it crosses political

borders (Canada and the United States), the American and Canadian portions are commonly examined separately. Few publications on the tectonic setting of the Canadian portion of the Brooks-Mackenzie Basin from the Jurassic to mid-Early Cretaceous are available. However, some publications (e.g., Dixon, 1997; Dixon et al., 2019) suggest a three-phase tectonic history: a rift phase from at least the Early Jurassic to Aptian, followed by a hybrid rifting and compressional phase during the Albian, and lastly a compressional phase from the Cenomanian to present.

Local features within the study area affecting deposition from the Jurassic to mid-Early Cretaceous are also assumed to be rift-related according to the interpretation of Dixon (1997). For example, the Husky Lakes Fault Zone (HLFZ, formerly Eskimo Lakes Fault Zone, Hadlari et al., 2020; Fig. 1-3) is interpreted as a pair of normal faults (Cook et al., 1987) that borders the Kugmallit Trough to the southeast, which represents a major depocenter for much of the Jurassic to mid-Early Cretaceous succession. Paleohighs displaying horst-graben geometry are also intermittently active throughout the Jurassic to mid-Early Cretaceous period and affect deposition, particularly the Tununuk High (Fig. 1-3; Dixon et al., 2019).

The prominent sub-Mount Goodenough unconformity, which truncates strata older than the Late Hauterivian, also greatly affects the thickness of preserved sediment within the study area. This unconformity is associated with major normal faulting, also along the HLFZ, based on interpreted seismic data (see Dietrich, 1996, Fig. 24).

Sedimentology, age, and depositional environment

Jurassic to mid-Early Cretaceous successions within the study area are dominantly clastic, oscillating between mud-rich and sand-rich lithologies (Fig. 2-2). Strata are divided into mappable formations on lithostratigraphic grounds using the stratigraphic nomenclature defined by

Jeletzky (1967), Dixon (1982, 1991), Poulton et al. (1982), and Dixon and Jeletzky (1991), with depositional ages derived from macro- and micro-fossil evidence (Jeletzky, 1960, 1967, 1980; Poulton et al., 1982; and Dixon and Jeletzky, 1991). Depositional environments are also derived from the studies cited previously, as well as Dixon (2002), which examined cores in the area. Depositional environments are also expanded upon when discussing facies associations in the next section. Regional paleogeographic evolution at formation scale based on the work of Poulton (1997) and Dixon (1991, 2004) can be seen in Figure 2-3.

Bug Creek Group (Sinemurian to Oxfordian)

The lower portion of the Jurassic succession (Sinemurian to Oxfordian), was initially defined by Jeletzky (1967) as the Bug Creek Formation, but later raised to group status by Poulton et al. (1982) containing three mud-dominant and two sand-dominant formations. At the basal contact, the Bug Creek Group onlaps Permian strata, indicating period(s) of non-deposition or erosion before Jurassic deposition (Poulton et al., 1982; Poulton, 1997). This contact is referred to as the sub-Jurassic unconformity. The lowermost unit, the Murray Ridge Formation, contains a thin basal sandstone in certain eastern localities called the Scho Creek member, which is interpreted as a transgressive shoreface of marine origin or possibly a fluvial to fan-type sandstone (Poulton et al., 1982). The Murray Ridge Formation transitions upwards into an open marine setting (Poulton et al., 1982) characterized by mudstone deposition. The Almstrom Creek Formation above is sand-dominant, but also contains intervals of sandstone-siltstone interbeds, with at least two cleaning-upward successions where fully developed (Dixon, 1982; Poulton et al., 1982). The third formation of the Bug Creek Group, the Manuel Creek Formation, is dominantly mudstone where present, with deposition being limited to central portions of the

basin (Poulton et al., 1982), likely representing the maximum transgression of facies during Bug Creek Group time (Dixon, 1982). The upper two formations of the Bug Creek Group together form a regional coarsening upward sequence, gradationally transitioning from interbedded sandstone-mudstones of the Richardson Mountains Formation to the sandstone-dominant Aklavik Formation. Dixon (1982) recognized an unconformity within the Aklavik Formation, which separates the formation into a lower and upper portion demarcated by "a tongue of Richardson Mountain-type strata" (Dixon, 1982). Later work by Barnett (2003) interpreted this formation as a wave-dominated delta likely sourced by few confined braided channel systems, resulting in a paleoshoreline oriented approximately northeast-southwest (Fig. 2-3A; Poulton, 1997). To the northwest, the Bug Creek Group transitions into the shale-dominant Kingak Formation.

Husky Formation (Oxfordian to Berriasian)

The deposition of the Husky Formation coincides with a significant basin expansion associated with activation along the HLFZ (Dixon, 1982). The Husky Formation was initially named and described by Jeletzky (1967) using outcrops within the Northern Richardson Mountains. He defined four members from base to top: lower, arenaceous, red-weathering, and upper. In the subsurface, the Husky Formation is divided into only two members: lower and upper (Dixon, 1982), with the former comprising the Lower and the arenaceous members of Jeletzky (1967), while the latter corresponds to the red-weathering and the upper members. The vertical profile contains two locally apparent coarsening- and cleaning-upward trends, with the first transitioning from the shale deposits of the lower member to the thin, sandy deposits of the arenaceous member, while the second gradationally coarsens upwards into the well-developed, sand-dominant Martin Creek Formation.

Jeletzky (1967) dated the lowermost Husky Formation as Lower Kimmeridgian based on fossil evidence from outcrop, which was later confirmed by fossils collected from the subsurface (Brideaux et al., 1975). The Jurassic-Cretaceous boundary occurs at or near the lithological boundary between the arenaceous and red-weathering members (Jeletzky, 1967). The upper contact between the Husky Formation and the overlying Martin Creek Formation is commonly conformable, with the boundary chosen where sandstone becomes prominent (Dixon, 1982) during approximately Berriasian time (Dixon and Jeletzky, 1991).

Parsons Group (Berriasian to Hauterivian)

The Martin Creek Formation, named by Dixon and Jeletzky (1991), is the lowermost formation of the Parsons Group, which also includes the McGuire and Kamik formations above. The Martin Creek Formation is dated as upper Berriasian to lower Valanginian (Dixon and Jeletzky, 1991). The formation is sand-dominant, commonly containing ripple laminae, shell debris, parallel laminations, and hummocky cross-stratification, which is interpreted to represent a high-energy environment with strong wave action (Dixon and Jeletzky, 1991). This formation is up to 200 m thick in the Mackenzie Delta and thins towards the west (Dixon, 1991). Regional mapping suggests the paleoshoreline at Martin Creek time was also oriented northeast-southwest (Fig. 2-3B; Dixon, 1991, 2004).

The upper contact with the lower to middle Valanginian McGuire Formation is commonly erosional, as interstratified mudstone-siltstone are abruptly deposited atop the Martin Creek Formation (Dixon and Jeletzky, 1991). The McGuire Formation is interpreted as an open marine shale, generally deposited below the storm wave-base (Dixon and Jeletzky, 1991). Like the Bug

Creek Group and Husky Formation below, the Martin Creek and McGuire formations are both laterally equivalent to the Kingak Formation in Yukon and Arctic Alaska (Dixon, 1991).

The uppermost formation of the Parsons Group, the Kamik Formation named by Dixon (1982), has been informally divided into two members by Dixon (1991): a lower, sandstone-dominant member that is mainly fluvial to overbank in origin, and an upper interbedded member of marine origin. The lower contact with the underlying McGuire Formation varies depending on the locality. In western areas of the Northern Richardson Mountains, the contact is gradational over a maximum of approximately 10 meters (Dixon, 1991), whereas on the eastern flanks of the Northern Richardson Mountains and within the subsurface of the Mackenzie Delta, the contact is abrupt or gradational over a short distance. Where the contact is abrupt in eastern areas, Dixon (1982) suggests erosion is associated with deposition. Where gradational in western areas, the contact is associated with deposits transitioning from more distal to more proximal marine environments. The lower member terminates with a transgression, marking a return to marine deposition within the upper member, which contains multiple coarsening upward successions (Dixon, 1991).

Relatively few micro- and macro-fossils have been recovered from the Kamik Formation. However, those that are present record a Valanginian to Hauterivian age (Myhr and Gunther, 1974), which is also supported by Jeletzky (1960), who used fossiliferous strata from above and below the Kamik Formation to suggest a middle or late Valanginian to middle Hauterivian age. This is consistent with more recent dating from foraminifera and palynological data suggestive of a Hauterivian age (McNeil, pers. comm.).

Mount Goodenough Formation (Barremian to Aptian)

Dixon and Jeletzky (1991) formally named the Mount Goodenough Formation after the type section at Mount Goodenough, also dating it as Barremian to Aptian. The shale-dominant formation contains fossil data indicative of a marine shelf setting (Dixon and Jeletzky, 1991). The basal contact is a regional unconformity, the magnitude of which can vary widely throughout the Northern Richardson Mountains and Mackenzie Delta, greatly affecting the preserved thickness or presence of underlying formations. The magnitude of the unconformity is believed to be related to paleohighs, such as the Cache Creek Uplift and the Husky Lakes Arch (Fig. 1-3), as well as the cessation of extensional faulting (Dixon, 2004).

Rat River Formation (Aptian)

The Aptian age Rat River Formation is not a main focus of this study, but is briefly described for completeness, as it forms a regionally extensive shallowing upward sequence with the Mount Goodenough Formation and was sampled for U-Pb detrital zircon data. The formation is characterized by sandstone-shale interbeds arranged within three coarsening-upwards cycles where fully preserved (Dixon and Jeletzky, 1991). The nature of the basal contact with the Mount Goodenough Formation may be gradational or abrupt (Dixon and Jeletzky, 1991). The formation is interpreted as entirely marine in origin, with interbedded sections being deposited below fair-weather wave base and the more homogenous sand-dominant sections being deposited above fair-weather wave base (Dixon and Jeletzky, 1991).

DATA AND METHODS

This work encompasses separate field, laboratory, and interpretive methodologies across four distinct data sets: outcrop, core, geophysical well-log, and U-Pb detrital zircon data.

Data collection

Fieldwork completed in the Northern Richardson Mountains during the summer of 2018 focused on the stratigraphic analysis of four measured sections, the collection of sandstone samples for U-Pb detrital zircon analysis, and the collection of mudstone samples for palynology (in prep). Section selection was informed by the work of previous authors, particularly Dixon (1982), Poulton et al. (1982), Dixon (1991), and Dixon and Jeletzky (1991), all of whom previously described sections within the study area at formation scale.

The collection and documentation of lab-derived data was facilitated by the Geological Survey of Canada (GSC). Well-log data was compiled from LAS files stored at the GSC and viewed using geoSCOUT©, which was also used to establish core locations and core-depth intervals. The core data appearing here was viewed at the GSC Sample Repository, which is also the storage location.

Methodology

Facies analysis

Modern facies analysis (e.g., James and Dalrymple, 2010) was used to establish and or/verify previously interpreted depositional environments (e.g., Dixon, 1982, 1991; Poulton et al. 1982; Dixon and Jeletzky, 1991) using measured stratigraphic sections, core, and well-log data. When measuring stratigraphic sections or analyzing core data, the primary focus was grain size, sorting, maturity, grading, sedimentary structures, and biogenic structures (ichnology). Strata

were then subdivided into facies and facies associations (FA) using the integrated core-outcrop dataset. Individual facies were interpreted to represent a distinct environment deposited under specific conditions (e.g., water level, water energy, salinity) and later grouped into FA, which are broadly defined as "groups of facies genetically related to one another and which have some environmental significance" (Collinson, 1969). The classification and nomenclature used to define depositional environments broadly follow Catuneanu (2006) (see Catuneanu, 2006, Figure 2.4), as well as MacEachern and Pemberton (1992) within the marine realm and Miall (1977) within the continental realm.

After FA and depositional environments were elucidated at isolated points (e.g., within specific cores and measured outcrop sections), results and observations were correlated to the gamma-ray signature of geophysical well-logs, assuming an inversely proportional relationship between sand content and gamma-ray reading, a common practice when evaluating stratigraphy (Catuneanu, 2006). Next, results were correlated throughout the subsurface using selected well logs in two stratigraphic cross-sections (Fig. 1-3). The integrated data set was also used to evaluate stratal stacking patterns, which are key to the sequence stratigraphic methodology.

Sequence stratigraphy

The sequence stratigraphic methodology is ubiquitous in sedimentary geology. The power and popularity of this methodology is largely due to applicability and ease of integration across multiple data sets at varying scales of observation (high-resolution core data, mid-resolution well-log data, and low-resolution seismic data), as well as its predictive nature. Broadly defined, sequence stratigraphy is a type of stratigraphy that deals with the description, interpretation,

classification, and nomenclature of sedimentary strata based on their stacking patterns, which form in response to changes in accommodation (*sensu* Jervey, 1988) and sediment supply.

Accommodation is defined as "space, created by sea-level rise, subsidence or both of two, in which sediment can be accreted" (Van Wagoner, 1995), which can be measured independent of sediment supply (Catuneanu, 2019a). Sediment supply may be defined "… in terms of influx of sediment to a depositional area (i.e., sediment supply), or in terms of rates of sedimentation" (Catuneanu, 2019a), both of which are fundamentally associated with the amount of material (i.e., sediment) being transported from the area in which it was generated (i.e., the source) to the area where it is eventually deposited (i.e., the sink). In essence, all stratigraphic expressions, or stratal stacking patterns, recorded in the rock record are the result of the interplay of processes responsible for creating or eliminating space for sediment to fill (i.e., accommodation) and the filling of that space (i.e., sedimentation).

Stratal stacking patterns afford the definition of systems tracts. Four systems tracts have been defined in downstream-controlled settings (falling-stage systems tract (FSST); lowstand systems tract (LST); transgressive systems tract (TST); and highstand systems tract (HST)). A general summary explaining how each stratal stacking pattern and systems tract relates to accommodation and sedimentation can be seen in Figure 2-4A.

Additionally, because sequences can occur at multiple scales (Fig. 2-4B), a stratigraphic hierarchy was also defined. This hierarchy was defined between first-order unconformities, which demarcate changes in tectonic setting (Catuneanu, 2019b). For example, rift-related strata are separated from underlying pre-rift strata by the ROU at the base, which by definition marks the onset of rifting, and the BU at the top, which marks the completion of a successful rift (Falvey,

1974). Within first-order sequences, multiple lower ranked sequences (e.g., second- and third-order sequences) may be classified, which are related to changes in accommodation and sedimentation on a smaller scale (Fig. 2-4B).

For a more in-depth discussion of sequence stratigraphy, see Catuneanu (2019a). For more detail on stratigraphic hierarchy, see Catuneanu (2019b).

U-Pb detrital zircon geochronology

U-Pb detrital zircon data provides a powerful quantitative tool that is commonly applied to sedimentary geology to evaluate sedimentary provenance within a basin, as the spectrum of age ranges associated with the detrital zircon grains within a particular sample reflects the age of the magmatic or metamorphic rocks within the source terranes (e.g., Røhr et al., 2010). Therefore, if the age of surrounding magmatic and metamorphic terrains is known, the source region may be implied or constrained based on the age spectrum of a given sample. However, in many instances, recycled sedimentary rocks also act as a primary source (e.g., Hadlari et al., 2012), meaning they are at least one depositional cycle removed from the original igneous or metamorphic source. Changes in the detrital zircon age spectrum can have further implications regarding basinal evolution, as changes in provenance and sediment routing, expressed through a change in age spectrum at different chronological intervals, can be the result of tectonic events shaping basinal development and the surrounding landscape.

Detrital U-Pb zircon data from fourteen sandstone samples ranging in age from the earliest Jurassic to Aptian is presented here. Samples were collected from the Northern Richardson Mountains during the summer of 2017 and are currently archived at the GSC. Samples were processed at the University of Calgary following Matthews and Guest (2016).

RESULTS

Facies analysis

Two facies associations (FA) are defined: shoreface and alluvial, reflecting a range of depositional environments from deep marine to fluvial and overbank. The results and interpretations are based on a combination of outcrop and core data, with reference to previous author's interpretations, particularly Dixon (1982), Poulton et al. (1982), Dixon and Jeletzky (1991), and Barnet (2003). Figures 2-5 and 2-7 to 2-9 show outcrop and core expressions of various facies, while Figure 2-6 shows the gamma-ray signature and core schematic of selected cored intervals.

Table 2-1: Facies association descriptions and interpretations.

Facies Association	Description	Interpretation
Shoreface		
S1: Laminated mudstone	Black, highly fissile, almost entirely mud sized grains, few small thin (mm to cm-scale) silt to very-fine grained sandstone interbeds, highly recessive in outcrop (Fig. 2-5A), no observed trace fossils	Lower offshore, deposition below normal storm wave base from suspension fallout, rare hurricane-level storms responsible for silt to very-fine grained sandstone interbeds, potentially anoxic due to lack of trace fossils (Gingras et al., 2011)
S2: Bioturbated mudstone	Heavily bioturbated with a diverse assemblage of trace fossils including *Schaubcylindrichnus*, *Palaeophycus*, *Planolites,* and *Phycosiphon* (Fig. 2-8A, B), sedimentary structures largely obscured by bioturbation, some minor parallel wavy laminations, increased relative proportion of silt and sand-sized grains in comparison to S1	Upper offshore, distal *Cruziana* ichnofacies (*sensu* Seilacher, 1967), increased number of storms influencing deposition at shallower water depths, diverse trace fossil assemblage suggests an oxygenated water column
S3: Interbedded sandstone and bioturbated siltstone	Interstratified, interbeds ranging from cm to dm scale, rare m scale; sandstone commonly arranged in fining upward packages with an erosional base and gradational upper contact, sedimentary structures include parallel laminations that are both concave up (i.e., swaley cross-stratification; SCS) and concave down (i.e., hummocky cross-stratification; HCS) in nature (Fig. 2-5B, C, D), some symmetric ripples; siltstone commonly heavily bioturbated, including *Phycosiphon, Planolites, Chondrites,* and *Schaubcylindrichnus*, which largely obscures primary sedimentary structures	Offshore-shoreface transition zone, *Cruziana* ichnofacies, deposition above the storm wave base and below fair-weather wave base, storm-influenced conditions result in alternating periods of low (i.e., not during a storm) and high (i.e., during a storm) energy levels

Table 2-1 cont.: Facies association descriptions and interpretations.

Facies Association	Description	Interpretation
S4: Argillaceous sandstone	Cream to grey colour, fine-grained sandstone, and siltstone, some parallelly bedded units with abrupt basal contacts are observed, overall sedimentary structures are obscured by the high levels of bioturbation (e.g., *Chondrites*, *Schaubcylindrichnus*, *Asterosoma*, *Teichichnus*, *Palaeophycus*, *Zoophycos*, and *Ophiomorpha*; e.g., Figs. 2-7C, D, F), bivalve shells, leaf fragments, and carbonaceous debris are also locally common (Fig. 2-7D)	Lower shoreface, proximal *Cruziana* ichnofacies, consistently above fair-weather wave base, oxygen-rich, carbonaceous debris, and leaf fragments could suggest deposition occurred near a delta
S5: Fine to medium-grained sandstone	Well-sorted, mature, concave up parallel laminations (SCS), rare concave down laminations (HCS), erosive surfaces, and cross-bedding (e.g., Fig. 2-5G, H, 2-8C), a minimal but diverse assemblage of trace fossils including *Cylindrichnus, Diplocraterion, Planolites,* and *Skolithos* is also present; however, appears massive and structureless in most expressions (e.g., Fig. 2-5E, F, 2-7G, 2-8C)	Middle shoreface to foreshore, *Skolithos* ichnofacies (*sensu* Seilacher, 1967), SCS and HCS are storm derived, cross-beds likely represent migrating sub-aqueous dunes forming during fair weather conditions, overall lack of sedimentary and biogenic structures may be attributed to uniformity of grain size and mineralogy or cryptic bioturbation (e.g., Pemberton et al., 2008)

Table 2-1 cont.: Facies association descriptions and interpretations.

Facies Association	Description	Interpretation
Alluvial		
A1: Cross-bedded sandstone and conglomerate	Coarse-grained sandstone typically arranged in fining upward packages, individual packages are demarcated by erosive contacts often accompanied by a pebble horizon (e.g., Fig. 2-9F); pebbles are commonly on the mm to cm-scale, sub-rounded, sub-angular, and composed of chert, with some associated carbonaceous debris also present (e.g., Fig. 2-9G); planar cross-bedded sandstone dominates most individual packages (e.g., Fig. 2-9E), minor ripple laminations (e.g., Fig. 2-9F), no bioturbation	Amalgamated fluvial channel system, braided river, high depositional energy, multiple erosive surfaces, and conglomerate horizons represent periods of increased flow or bar migration indicative of variable discharge rates, planar cross-beds are interpreted to represent 3-D dune migration, paucity of fine-grained material or heterolithic bedding suggests unstable channel banks
A2: Interbedded siltstone and sandstone	Discrete, commonly lenticular interbeds of silt to very-fine-grained sandstone on the cm to dm scale, may be arranged in coarsening upward packages, usually bound by sharp and weakly erosive contacts (e.g., Fig. 2-9A, B); siltstone interbeds are commonly grey to dark grey and weakly bioturbated; sandstone interbeds are light beige to grey; both siltstone and sandstone interbeds are relatively structureless, root traces locally abundant (e.g., Fig. 2-9B); horizons of bituminous coal may also be present, commonly at the top of conformable successions (e.g., Fig. 2-9C)	Broadly classified as overbank to include crevasse splay, floodplain, swamp, and marsh sub-environments; abundant root traces suggests a continental environment, massive and mildly bioturbated siltstone to mudstone beds are interpreted to represent floodplain deposits; periodically active crevasse splays (e.g., Fig 2-9B) are deposited when channel levees are breached, resulting in a coarsening upward trend representing the same physical process as deltaic progradation into the floodplain (Miall, 1996); coal deposits representative of marshes or swamps

FA1: Shoreface

FA1 is associated with the deposition of a shallowing upward shoreface succession deposited under fully-marine conditions. Five facies (S1 to S5) commonly demarcated by gradational contacts were observed within FA1, which are described below in stratigraphic order from base to top (i.e., deep to shallow water).

S1: Laminated mudstone

The laminated mudstone facies is present within the Husky and Mount Goodenough formations. It is typically black and highly fissile (i.e., shale), being almost entirely composed of mud-sized grains with few thin (mm to cm-scale) siltstone to very-fine grained sandstone interbeds. In core and outcrop (e.g., Bug Creek section, Fig. 2-5A and Martin Creek section, Fig. 2-5K), the highly recessive nature of this facies makes detailed sedimentological analysis challenging, though a gradational upper contact with S2 (described next) is present in all occurrences of this facies. No biogenic structures were observed.

S1: Lower offshore

The laminated mudstone facies is interpreted as lower offshore (*sensu* MacEachern and Pemberton, 1992), characteristic of deposition below the normal storm wave base. The predominant lack of sand-sized particles suggests wave energy was consistently low to nil, with sedimentation likely occurring from suspension fallout. Some deviations from this form of sedimentation are suggested based on the rare silt to fine-grained sandstone interbeds, which are interpreted as tempestites derived from major storms (e.g., hurricane-level events) that are stronger than more common, seasonal storms. The lack of trace fossils within this facies could

suggest an anoxic environment, which can occur under deep marine conditions (Gingras et al., 2011).

S2: Bioturbated mudstone

The bioturbated mudstone facies varies slightly by formation. For example, within the Husky and McGuire formations, this facies is heavily bioturbated with a diverse assemblage of trace fossils including *Schaubcylindrichnus*, *Palaeophycus*, *Planolites,* and *Phycosiphon* (Fig. 2-8A, D). An increased relative proportion of silt and sand-sized grains is also observed, some of which contain wavy laminations, while others appear fully bioturbated. The same facies in the Murray Ridge Formation, by contrast, appears to contain a monospecific *Zoophycos* assemblage and no silt-sized grains (Fig. 2-7A-C). However, this is only based on one data point (e.g., Shell Napoiak F-31 core; Fig. 2-6, 7 A-C) due to a lack of core within the Murray Ridge Formation and the recessive nature of this formation in outcrop.

S2: Upper offshore

The observed trace fossil assemblage is associated with a low-energy environment typical of the distal *Cruziana* ichnofacies (Seilacher, 1967), which is interpreted to represent an upper offshore environment (MacEachern and Pemberton, 1992). In comparison to the laminated mudstone facies (S1), the elevated concentration of silt and sand-sized particles likely represents an increased number of storms influencing deposition at the shallower depths of the upper offshore. This is also supported by the presence of observable trace fossils, indicative of an oxygenated water column (Gingras et al., 2011), which would also be expected in shallower water.

S3: Interbedded sandstone and bioturbated siltstone

Two alternating fabrics, bioturbated siltstone and parallel laminated sandstone, dominate this facies, with interbeds ranging from cm to dm scale, rarely m scale. The sandstone-dominant interbeds are commonly arranged in fining upward successions with an erosional base and gradational upper contact. Sedimentary structures include parallel laminations that are both concave up and concave down in nature (e.g., Fig. 2-5C, D), as well as symmetric ripples. Furthermore, a general change in the degree of bioturbation from the base to the top of sandstone-dominant beds can also be observed, with the lower portion of beds commonly being unbioturbated, while the upper portion may contain bioturbation (e.g., Fig. 2-5B). The fine-grained interbeds (e.g., siltstone-dominant) are commonly heavily bioturbated, including *Phycosiphon, Planolites, Chondrites,* and *Schaubcylindrichnus* (Fig. 2-8B), which obscures primary sedimentary structures.

S3: Transition zone

This facies is interpreted as the offshore-shoreface transition zone, representing deposition above the storm wave base and below the fair-weather wave base. Storm-influenced conditions in the transition zone result in alternating periods of low (i.e., not during a storm) and high (i.e., during a storm) energy levels. During storms, increasingly turbulent water lowers the wave-base, causing minor erosion of the fair-weather seafloor, and moves coarser material (e.g., sand-sized particles) basinward. The coarsest sand is normally deposited above the erosive surface when energy is highest, decreasing in grain size as the storm wanes, resulting in the observed normally graded beds. Additionally, the parallel concave down (i.e., hummocks) and concave up (i.e., swales) laminations present within sandstone interbeds are interpreted as

hummocky cross-stratification (HCS) and swaley cross-stratification (SCS), respectively. These sedimentary structures are interpreted as tempestites deposited during storms, consistent with the interpretation of numerous other authors (e.g., Dott and Bourgeois, 1982; Duke, 1985). As energy from the storm decreases, opportunistic organisms recolonize the substrate, something they are unable to do during the height of the storm surge, explaining the relative increase in bioturbation in the upper parts of the storm-derived beds (MacEachern and Pemberton, 1992). When the storm ceases completely, the calm conditions result in the deposition of fine-grained material that is dominantly siltstone, with these conditions facilitating extensive bioturbation from sea-dwelling organisms.

S4: Argillaceous sandstone

This facies was observed within the Almstrom Creek and Martin Creek formations, where it is commonly cream to grey in colour (e.g., Fig. 2-7F), comprised of fine-grained sandstone and silt-sized particles. Some parallelly bedded units with abrupt basal contacts are observed, though overall sedimentary structures are obscured by the high levels of bioturbation, with the observed assemblage containing *Chondrites*, *Schaubcylindrichnus*, *Asterosoma*, *Teichichnus*, *Palaeophycus*, *Zoophycos*, and *Ophiomorpha* (e.g., Figs. 2-7F), Additionally, bivalve shells, leaf fragments, and carbonaceous fragments are also locally common (Fig. 2-7D).

S4: Lower shoreface

A lower shoreface environment is interpreted within the argillaceous sandstone facies. The high proportion of sand-sized grains within this facies suggests that energy was continuously high, consistent with deposition at the lower extent of the fair-weather wave-base. Additionally, trace fossils indicate a fully-marine, oxygen-rich setting typical of the proximal *Cruziana*

ichnofacies, which is also interpreted to represent the lower shoreface (MacEachern and Pemberton, 1992).

S5: Fine to medium-grained sandstone

The fine to medium-grained sandstone facies was observed within the Almstrom Creek, Aklavik, Martin Creek, and Kamik formations. It is commonly well-sorted and mature, displaying a range of sedimentary structures including concave up parallel laminations, rare concave down laminations, erosive surfaces, and cross-bedding (e.g., Fig. 2-5G, H, 2-8C). However, in most instances, this facies appears massive and structureless (e.g., Fig. 2-5E, F, 2-7G). Bioturbation is largely absent within this facies, with only rare examples of *Cylindrichnus, Diplocraterion, Planolites,* and *Skolithos* traces.

S5: Middle shoreface to foreshore

The fine to medium-grained sandstone facies is interpreted to represent the middle shoreface to foreshore, representing deposition consistently above the fair-weather wave base. This interpretation is supported by the relative uniformity and maturity of sand-sized grains, as well as a trace fossil assemblage representative of the *Skolithos* ichnofacies. Additionally, similar to S3, the presence of parallel laminations are interpreted to represent storm-derived SCS and HCS. The observed cross-beds likely represent migrating sub-aqueous dunes more commonly associated with fair weather conditions. The overall structureless and unbioturbated nature of much of this facies could be attributed to uniformity of grain size and mineralogy, but the massive nature could also be associated with cryptic bioturbation and deposition within the foreshore (Pemberton et al., 2008).

FA2: Alluvial

FA2 is interpreted to represent alluvial sediment largely deposited in a continental setting. This FA has been divided into two facies (A1 and A2), representing braided river and overbank depositional environments.

A1: Cross-bedded sandstone and conglomerate

The cross-bedded sandstone and conglomerate facies are prevalent within the lower member of the Kamik Formation (e.g., Parsons N-10 core; Fig. 2-9C-G), where it appears as fine- to coarse-grained sandstone typically arranged in fining upward packages. Individual packages are demarcated by erosive contacts, which may also be accompanied by a pebble horizon (e.g., Fig. 2-9F). Pebbles are commonly on the mm to cm-scale, sub-rounded, sub-angular, and composed of chert, with some associated carbonaceous debris also present (e.g., Fig. 2-9G). Planar cross-bedded sandstone dominates most individual packages (e.g., Fig. 2-9E), though ripple laminations can also be observed in the upper portions (e.g., Fig. 2-9F). Bioturbation is virtually absent from this facies, with the only exception being *Planolites* burrows near contacts with facies A2.

A1: Braided river

This facies is interpreted to represent an amalgamated fluvial channel system within a braided river. High depositional energy is inferred from the increased grain size. Multiple erosive surfaces and conglomerate horizons are interpreted to represent periods of increased flow or bar migration, which can be indicative of variable discharge rates expected within braided rivers. Planar cross-beds are interpreted to represent 3-D dune migration, while the paucity of fine-

grained material or heterolithic bedding suggests unstable channel banks, both of which are common in braided systems (Miall, 1977).

A2: Interbedded siltstone-sandstone

The interbedded siltstone-sandstone facies was observed within the lowermost cored interval of the Kamik Formation in the Parsons N-10 core (e.g., Fig. 2-9A, B). It is composed of discrete, lenticular interbeds of silt to very fine-grained sandstone. Individual beds are on the cm to dm scale, normally arranged in coarsening upward packages bound by sharp and weakly erosive contacts (e.g., Fig. 2-9A, B). Siltstone interbeds are commonly grey to dark grey and weakly bioturbated, while sandstone interbeds are light beige to grey. Both siltstone and sandstone interbeds are relatively structureless, though root traces are locally abundant (e.g., Fig. 2-9B). Horizons of bituminous coal are also present (e.g., Fig. 2-9C)

A2: Overbank

This facies is interpreted to represent a range of depositional sub-environments broadly classified as overbank, which would include crevasse splays, floodplains, swamps, and marches. The abundance of root traces suggests a continental environment. Massive and mildly bioturbated siltstone to mudstone beds are interpreted to represent floodplain deposits, with periodically active crevasse splays (e.g., Fig 2-9A, B) deposited when channel levees are breached during episodic flooding events, resulting in a coarsening upward trend representing the same physical process as deltaic progradation into the floodplain (Miall, 1996). Coal deposits, which often occur on top of conformable sequences (e.g., Fig. 2-9C), are interpreted to represent marshes or swamps.

Depositional history and basin geometry

Two regional cross-sections overlain with interpreted depositional environments are presented to show the overall stratigraphic evolution and geometry of the study area. Cross-section A-A' (Fig. 2-10A) is oriented N-S from the Tununuk High to the basin margin (Fig. 1-3), meaning it is roughly perpendicular to the Jurassic shoreline (Fig. 6A). The datum for this cross-section is a MFS within the Husky Formation above unless the surface has been removed by subsequent erosion associated with the sub-Mount Goodenough unconformity (e.g., Treeless Creek I-51 well at the southern-most extent of the cross-section in Fig. 2-10A). Cross-section B-B' (Fig. 2-10B) is oriented approximately NE-SW (Fig. 1-3) with the base of the alluvial deposits within the lowermost Kamik Formation selected as the datum. This section is positioned roughly parallel to the Cretaceous shoreline according to the Dixon (1991, 2004) interpretation (Fig. 2-3 B, C, D). Positioning a cross-section perpendicular to the Cretaceous shoreline is not possible due to a lack of well-log data.

An overall regression, transgression, second regression, and second transgression of facies and depositional environments are observed throughout the Jurassic to the mid-Early Cretaceous period, with maximum transgression occurring in the Late Jurassic (Husky time) and maximum regression occurring around the Hauterivian (Kamik time). On a more detailed scale, deposition above the sub-Jurassic unconformity begins with the earliest Jurassic Murray Ridge Formation, which is interpreted as upper offshore marine (Table 2-1, S2). The overlying contact with the Almstrom Creek Formation appears sharp throughout the section, consistent with observations within the Napoiak F-31 core (Figs. 2-6A, 2-7A, B, C). Above, two phases of shallow marine facies are present within the Almstrom Creek Formation that appear broadly

symmetrical, with the thickest accumulation of sandstone present in the Beaverhouse Creek H-13 well, the approximate midpoint of the cross-section between the craton and the Tununuk High (Fig. 1-3, 2-10A). Above the Almstrom Creek Formation, an asymmetrical geometry is observed, with the Manuel Creek-Aklavik interval being approximately 20 meters in the south (e.g., Union Aklavik F-38) and about 100 meters in the north (e.g., Unak B-11).

A relatively gradational facies transition is observed in distal portions of the basin (e.g., Unak B-11), whereas the Manuel Creek Formation is absent in more proximal settings (e.g., Union Aklavik F-38). The absence of the Manuel Creek Formation in proximal areas may be associated with tilting and erosion, as proposed by Poulton et al. (1982) and Dixon (1982), or due to the transition to sandier facies in more proximal areas. The two upper formations of the Bug Creek Group, the Richardson Mountains and Aklavik formations, form a gradational contact, though the transition to the sandstone-dominant Aklavik Formation is punctuated by multiple phases of sandstone development, with each phase extending further northward than the previous phase (Fig. 2-10A).

Complex stratigraphic geometry is apparent within the Aklavik Formation (first noted by Dixon, 1982), where it transitions from a single or amalgamated shoreface (e.g., Union Aklavik F-38) to a shoreface with two distinct components. The clearest example of this partitioning is seen in the Aklavik A-37 well, where a lower Aklavik sandstone is demarcated by a gradational base and sharp flooding surface above, which is distinct from a second upper Aklavik sandstone containing a sharp basal and upper contact. Moving basinward (e.g., Unak B-11), the sharp nature of the basal contact within the upper Aklavik sandstone appears to become gradational.

Cross-section B-B' depicts primarily the Late Jurassic to the mid-Early Cretaceous portion of the study interval, but also shows the same general geometry within the Bug Creek Group as cross-section A-A'. Above the Bug Creek Group, a significant basin expansion is observed, resulting in the depositional limits of the overlying Husky Formation expanding north-eastward into the Kugmallit Trough (Fig. 2-10B) and above the Tununuk High (Fig. 2-10A). The deposition of Husky Formation shales also represents the maximum backstepping of facies, with relatively thick accumulations of lower offshore facies persisting until the gradual transition to the regionally extensive, sandstone-dominant Martin Creek Formation. The comparatively thin McGuire Formation marks a return to offshore deposits, with a sharp and erosive contact present between it and the underlying Martin Creek Formation (Fig. 2-8D). The nature of the overlying McGuire—Kamik contact appears sharp throughout the section, with alluvial deposition dominating the lower Kamik. A gradual return to marine deposition is recorded throughout the upper portion of the Kamik Formation where overlying strata are not eroded by the sub-Mount Goodenough unconformity. For example, in the Parsons L-43 well (Fig. 2-10B), a transition from braided fluvial (A1) and overbank (A2) deposits to marine (S4/5) deposits in the uppermost Kamik Formation are observed over approximately 100 meters. By contrast, in Beaverhouse H-13, only approximately 10 meters of the lower Kamik Formation is present. Trends show the magnitude of erosion below the sub-Mount Goodenough unconformity increasing south-westward towards the Cache Creek High and north-eastward towards the Husky Lakes Arch (e.g., Fig. 1-3, 2-10B).

Sequence stratigraphy

The sequence stratigraphy of four measured sections from the Northern Richardson Mountains (Figs. 1-4, 2-11) is described, augmented by core data where appropriate (Figs. 1-3, 2-

6 to 2-9). Measured sections are then correlated to the subsurface, which is used to establish stratal stacking patterns and systems tracts, the foundation of the sequence stratigraphic methodology. Schematic illustrations, correlations, and interpretations can be seen in Figures 2-11 to 2-16.

Murray Ridge and Bug Creek sections

Description. The Murray Ridge and Bug Creek sections are discussed together, as the Bug Creek Group is the subject of focus in both sections (Fig. 2-12). In both cases, the Early Jurassic Murray Ridge Formation overlies Permian deposits, representing the sub-Jurassic unconformity. At the Murray Ridge section, a sharp contact between S2 (lower offshore) of the Murray Ridge Formation and S3 (transition zone) of the Almstrom Creek Formation is observed. Additionally, this contact is also sharp and erosive when viewed in core (e.g., Shell Napoiak F-31; Fig. 2-7A, B, C, 2-13A), being associated with a sharp facies transition, distinct pebble lag, and vertical burrows (*Skolithos*) filled by the overlying sediment (Fig. 2-13A). Above this contact, at least three fining- then coarsening-upward pairs oscillating between S2/3 and S4/5 are observed, with the main coarse clastic intervals corresponding to the Almstrom Creek Formation, the Little Bell member of the Richardson Mountains Formation, and the Aklavik Formation. The bottom two pairs (Almstrom Creek Formation and Little Bell member) appear bound by gradational contacts on both the base and the top, while the nature of demarcating contacts surrounding the Aklavik Formation cannot be assessed at Murray Ridge, as the lower contact with the Richardson Mountains Formation is obscured due to rock-fall and the upper contact with the Husky Formation is not present (Fig. 2-12).

In comparison to the Murray Ridge section, the Bug Creek section displays the gradational contact between the Richardson Mountains and Aklavik formations, as well as the abrupt nature of the overlying contact with the Husky Formation (Figs. 2-5A, D). First, the lower contact with the Richardson Mountains Formation displays an interbedded nature. The frequency and thickness of sandstone interbeds increases upwards until strata are exclusively sandstone (Fig. 2-12). The upper contact between the Aklavik and Husky formations is abrupt, with highly fissile mudstones of the Husky Formation sharply overlying the Aklavik Formation (Fig. 2-5A). However, as described earlier and as shown within Figures 2-10A and 2-12A, the subsurface (e.g., Shell Aklavik A-37 well) highlights the complex stratigraphic geometry displayed within the Aklavik Formation, where a lower Aklavik shoreface (S5) is separated from an upper Aklavik shoreface (S5) by a fine-grained facies (S2/3) (called a "tongue of Richardson Mountains-type strata" by Dixon, 1982). The fine-grained facies appear bound by sharp contacts on both sides, with the lower contact representing a sharp flooding surface and the upper contact being associated with the unconformity labelled the "intra-Aklavik unconformity" in Figure 2-12.

Correlation with the subsurface, stratal stacking patterns, and systems tracts. The basal contact, the sub-Jurassic unconformity, is interpreted as a SU overprinted by a younger WRS, with the lowermost Murray Ridge Formation representing a TST. This interpretation is supported by the fact that no Triassic sediment is present below this surface (Poulton et al., 1982), indicating a period(s) of non-deposition or an erosive event, consistent with the development of a SU. The erosive contact between the Murray Ridge Formation and the overlying Almstrom Creek Formation is interpreted to represent a *Glossifungites* surface (*sensu* Seilacher, 1964; Fig. 2-13A), which represents an erosive discontinuity associated with a firmground (Pemberton and Frey,

1984). Though the lack of data makes interpreting the sequence stratigraphic significance of this contact speculative, the most likely interpretation is a BSFR reworked by a younger RSME. The erosive nature of the RSME can explain why the contact is demarcated by a *Glossifungites* surface, which by definition requires the erosion of an underlying firmground (Pemberton and Frey, 1984). The overlying deposits transition from S3 at the base to S4 above, meaning they accumulated during a period of regression and progradation, which also fulfils the criteria of a RSME (see Catuneanu, 2006, Fig. 4.9). Consequently, strata above represent a FSST. The top of the FSST is marked by a SU containing a thick shell horizon and a distinct increase in grain size (Figs. 2-6A, 2-7E). The overlying LST is comparatively thin (Fig. 2-14). Above, the multiple TST-HST pairs indicate a period of continued relative sea-level rise, likely lasting until the deposition of the upper Aklavik sandstone.

The complex nature of the upper portion of the Aklavik Formation (e.g., the partitioned shoreface in Shell Aklavik A-37) is interpreted to be the result of erosion during a relative sea-level fall. This interpretation is supported by the observed sharp-based shoreface (*sensu* Plint and Nummedal, 2000) within the upper Aklavik at the Shell Aklavik A-37 well, which represents a FSST at the top of the Bug Creek Group. The magnitude of erosion is interpreted to increase moving southward, wherein the muddier facies separating the distinct shorefaces in Shell Aklavik A-37 are entirely eroded within the Union Aklavik F-38 well and the Bug Creek section. Furthermore, this would imply that the seemingly uniform shoreface at the Bug Creek section and Union Aklavik F-38 well (Fig. 2-12) may contain two amalgamated components: a lower HST that is distinct from an upper FSST. Additional support for this interpretation is seen in more distal correlations (e.g., Unak B-11 well; Fig. 2-10A), wherein the sharp contact at the base of the upper Aklavik appears

to become more gradational away from the basin margin, which would also be expected as the regression continues when relative sea-level begins to rise during the subsequent LST.

Martin Creek section

Description. The Martin Creek section (Fig. 2-15) spans the lower member of the Husky Formation to the Martin Creek Formation. The entire section displays an overall coarsening-upwards stacking pattern, transitioning gradually from S1 within the Husky Formation at the base of the section to S5 within the Martin Creek Formation at the top of the section, but is internally composed of multiple fining-/coarsening-upward sequences of lesser magnitude (Fig. 2-15). The first observable coarsening upward section culminates in the arenaceous member, representing S3. Above the arenaceous member, much of the Husky formation remains shale dominant (S1 to S2), with at least one additional coarsening upwards succession being present within the Husky Formation (Fig. 2-15). The major coarsening upward interval observed in this section ends with the Martin Creek Formation, a regionally extensive and thick sand-body.

Correlation with the subsurface, stratal stacking patterns, and systems tracts. The correlation of the Martin Creek section to the Beaverhouse H-13 well 24km away is relatively straightforward, with multiple easily correlatable MRS (Fig. 2-15A), representing a relatively simple succession containing exclusively HST-TST pairs. The lack of any observable LST or FSST indicates that observed strata developed under a period of constant positive accommodation or base-level rise. Each HST is bound by a MRS at the top, except for the final HST within the Martin Creek Formation, seen as an erosional contact and sharp facies transition (e.g., within the Parsons N-10 Core; Figs. 2-6B, 2-8D, 2-13C), which is interpreted as a MRS overprinted by a younger WRS responsible for the observed erosion.

Grizzly Gorge section

Description. The entire Parsons Group and the Mount Goodenough Formation were observed at the Grizzly Gorge section (Fig. 2-16). At the base of the section, Martin Creek sandstones display a coarsening upward trend, which terminates at the contact with the McGuire Formation. Similar to observations discussed previously in association with the contact in the Parsons N-10 core (Figs. 2-8D, 2-13C), the contact between the Martin Creek and McGuire formations is sharp, with some minor backstepping observed. A thin phase of sandstone development is observed within the McGuire Formation, occurring approximately 10 meters above the Martin Creek-McGuire contact. The basal contact of the Kamik Formation appears sharp, with no gradational change from more interbedded deposits below. Sandstone beds in the lowermost Kamik are fine-grained, containing parallel laminations, minor wave ripples, and minimal bioturbation. Grain size remains constant until approximately fifteen meters above the basal contact, where another major contact is observed, which is labelled the "intra-Kamik contact" in Figure 2-16A. This contact is marked by an abrupt increase in grain size to medium, or coarse locally, and a distinctive pebble horizon traceable across the outcrop (Fig. 2-13D). Sandstone above the contact appears relatively homogeneous with no bioturbation, though major iron staining and chemical weathering hamper sedimentological observations. A third major contact, presumed to be the sub-Mount Goodenough unconformity, occurs almost ten meters above the intra-Kamik contact. Notably, no large-scale interbedded deposits characteristic of the upper member of the Kamik Formation are present here, indicating the sub-Mount Goodenough unconformity is associated with extensive erosion at this locality. Above the

sub-Mount Goodenough unconformity, a backstepping marine facies within the Mount Goodenough Formation is observed.

Correlation with the subsurface, stratal stacking patterns, and systems tracts. Many observable similarities exist between the Grizzly Gorge section and the nearby Beaverhouse Creek H-13 well (Fig. 2-16A). Like at the Martin Creek section, the Martin Creek Formation here represents an HST, which terminates above the Martin Creek-McGuire contact, with overlying backstepping facies representing a thin TST. The minor phase of sandstone development observed at the Grizzly Gorge section correlates with a low-gamma signature in the Beaverhouse H-13 well at approximately 420 meters (Fig. 2-16). Above, the McGuire-Kamik contact appears sharp in both outcrop and well-log, where it is marked by an abrupt shift to sandstone deposition and lower gamma readings. Because the overlying Kamik deposits are interpreted as marine, this contact is interpreted to be associated with the development of a sharp-based shoreface during a time of relative sea-level fall (Plint and Nummedal, 2000), meaning the basal Kamik contact is a RSME at these locations. Applying this interpretation, the lowermost Kamik interval would represent an FSST (Fig. 2-16).

The intra-Kamik contact also correlates between outcrop and the Beaverhouse H-13 well log, as the distinct increase in grain size observable in outcrop (Figs. 2-5J, 2-13D) corresponds with another abrupt shift to the left on the gamma-ray log at approximately 380m (Fig. 2-16A). The thickness of the lowermost Kamik (e.g., between the base Kamik and intra-Kamik contacts) is relatively consistent between outcrop and well-log. However, the strata between the intra-Kamik contact and the sub-Mount Goodenough unconformity are approximately twice as thick at Beaverhouse Creek H-13 in comparison to the Grizzly Gorge section, suggesting the magnitude

of the sub-Mount Goodenough unconformity increases moving westwards towards the Cache Creek High, consistent with other authors' observations (e.g., Dixon, 2004). The intra-Kamik unconformity is interpreted as a SU based on the erosive nature of the contact, and the fact that underlying deposits are associated with a FSST, meaning the overlying alluvial deposits (also observed in the Parson N-10 core; Fig. 2-9) represent a LST. The sub-Mount Goodenough unconformity at this location is interpreted as a SU overprinted by a younger WRS. Though not viewed directly in this section, much of the upper Kamik Formation records a gradual transgression and a return to marine deposition (Fig. 2-10B; Dixon, 1982). The fact that this strata is missing is most likely associated with erosion accompanied by the development of a SU, with the overlying offshore marine (e.g., S1/2) deposits of the Mount Goodenough representing a major transgression.

U-Pb detrital zircon geochronology

Results from the fourteen detrital zircon samples retrieved from 5 locations within the Northern Richardson Mountains (Fig. 1-4) provide quantitative support for later tectonic interpretations. Photographs of each sample are shown in Figures 2-17 and 2-18. Detrital zircon age spectra are shown in Figure 2-19. The full dataset is shown in Appendix A.

Permian

The underlying Permian strata were sampled at two locations: the Murray Ridge and Bug Creek sections (Figs. 1-4, 2-17 C, D, and 2-18A, G), amounting to a total of 352 analyzed grains. In both cases, samples were taken at the top of the regional coarsening upward package below the sub-Jurassic unconformity separating Permian deposits from overlying Jurassic strata. Zircons from both samples fall predominantly within three age groups: a small Neoarchean (2900—2500

Ma) component, a broad Paleoproterozoic to Neoproterozoic (2000—900 Ma) assemblage, and a trimodal Neoproterozoic to Devonian (700—320 Ma) range with peaks at approximately 420, 550, and 650 Ma. A hiatus is present from 680—880 Ma in the Bug Creek sample. The same hiatus is observed within the Murray Ridge sample, though it begins at approximately 1000 Ma.

Bug Creek Group and Husky Formation

Five samples were taken from the Bug Creek Group (Figs. 2-18B-F), representing 1242 analyzed zircon grains. Four samples were obtained at the Murray Ridge section (Fig. 2-17C), with the fifth sample from the Aklavik Formation at the Bug Creek section (Fig. 2-17D). Pre-Aklavik strata display similar probability density curves, with a limited but continuous Mesoarchean to Paleoproterozoic (2900—2100 Ma) component containing a minor peak at approximately 2750 Ma and increasing in density from the Paleoproterozoic to the Neoproterozoic (2100—900 Ma) with three local peaks at approximately 1480, 1160, and 1040 Ma. The highest relative proportion of grains in pre-Aklavik strata are concentrated around a narrow peak at approximately 450 Ma, with the youngest grain recording a 363 Ma age.

A departure from the pre-Aklavik trend is observed within both samples of the Aklavik Formation and the sample of the overlying arenaceous member of the Husky Formation taken from the Martin Creek section, which contains a dominant peak at approximately 1900 Ma not observed in older samples. However, the size of this peak is comparatively less prominent in the Aklavik Formation at Murray Ridge and the arenaceous member at Martin Creek. Furthermore, this peak is not present within the sample of the arenaceous member at the Mount Goodenough section, nor is it present in any younger strata. The youngest grains from this interval are from

the Aklavik Formation at the Murray Ridge section, dated as 184 Ma, representing the first record of Mesozoic aged zircons, though they are older than the age of deposition.

Parsons Group

Two samples of the Parsons Group from the Martin Creek and Kamik formations were retrieved from the Grizzly Gorge section (Fig. 2-17F, 2-18 K, I), with a total of 583 grains analyzed. Similar to underlying strata, a broad spectrum from approximately 2100 to 900 Ma is present with a well-defined local maximum at 1100 Ma. The Martin Creek sample contains a local maximum just before the Paleozoic at approximately 560 Ma, though a similar local high is present in the Kamik Formation at approximately 540 Ma. Like all underlying strata, both samples have another local maximum centered around approximately 460 Ma. The Martin Creek sample has a small number of grains forming no well-defined peaks younger than 460 Ma, with the youngest recorded grain being 147 Ma. A total of 5 Mesozoic grains are present, representing just under 2% of the relative proportion. The Kamik Formation also contains a total of 5 Mesozoic grains, again representing about 2%. However, two well-defined peaks at approximately 160 and 235 Ma are observed, with the youngest recorded age being 159 Ma, which is older than the age of deposition.

Mount Goodenough and Rat River Formations

The sample of the Mount Goodenough Formation taken from Grizzly Gorge is very similar to the underlying Kamik Formation. However, the sample was retrieved from strata within the lower Mount Goodenough Formation presumed to be a transgressive shoreface, meaning the sediment was likely locally derived from the erosion of underlying strata (e.g., the Kamik Formation) at this location, which explains the similarity. The final two samples of the upper

Mount Goodenough and Rat River formations were retrieved from the Mount Goodenough section (Figs. 2-17A, 2-18M, N). In both samples, prominent peaks are present at approximately 450 and 1100 Ma. The youngest recorded data points are 166 and 154 Ma for the Mount Goodenough and Rat River Formations, respectively, which again is older than the age of deposition.

DISCUSSION

Summary of detrital zircon provenance

The Permian resembles the Devonian Imperial Formation, which is interpreted to reflect source material from predominantly north western Laurentia (Fig. 2-19; Lemieux et al., 2011). Most of the Jurassic Bug Creek Group also displays a similar age spectrum to that of the Devonian and Permian, suggesting multiple phases of recycling. The uppermost formation of the Bug Creek Group, the Aklavik Formation, is distinguished based on a prominent peak at approximately 1.8 – 2 Ga, like the peak observed within the Mississippian and Cambrian (Fig. 2-19; Hadlari et al., 2012). This change in character within the Bug Creek Group may reflect the difference between type 1 and type 2 detrital zircon sources present within the Northwest Territories (Hadlari et al., 2012). The first Mesozoic aged zircons do not appear until the deposition of the Aklavik Formation. The sources of these grains may reflect input from the Yukon-Tanana terrane to the south (e.g., Nelson et al., 2006; Colpron et al., 2015), suggesting an expanded catchment.

Hierarchy of stratigraphic surfaces and systems tracts

Having established the main sequence stratigraphic surfaces and systems tracts in the results section above, the hierarchical rank may be established, which arises because

stratigraphic surfaces and systems tracts can be observed at different scales (Fig. 2-4B; Catuneanu, 2019b). The largest observed sequence stratigraphic surfaces and systems tracts (i.e., first-order) are defined first, then internal systems tracts and stratigraphic surfaces of lower rank. Results are shown in Figure 2-20 and correlated throughout the subsurface in Figure 2-21 using the two cross-sections also depicted in Figure 2-10.

First-order LST (Sinemurian to Kimmeridgian)

The interval spanning the sub-Jurassic unconformity to the intra-Aklavik unconformity is interpreted as a first-order LST, which represents the majority of the Bug Creek Group. The nature of the demarcating contacts and the overall progradational signature (i.e., normal regressive stacking pattern) supports this interpretation. The basal contact is the sub-Jurassic unconformity, interpreted as a first-order SU reworked by a younger WRS. The sub-Jurassic unconformity is geographically broad and represents a hiatus of over 50 Ma, as all Triassic sediment is absent below this contact, suggesting a period of base-level fall before deposition of this first-order LST. The MRS bounding the top of this systems tract is interpreted with reference to the lithostratigraphy (Fig. 2-10) and the maximum progradation of sandstone-dominant facies into the basin during the first major phase of deposition, which occurred at or very near the top of the Bug Creek Group. In total, this first-order LST persisted for approximately 40 My based on available biostratigraphic data (e.g., Poulton et al., 1982; Fig. 2-2).

Internally, this sequence is composed of a second-order TST-HST pair, which in turn may be sub-divided into multiple third-order systems tracts. Early transgression (i.e., the second-order TST) spans the Murray Ridge to Almstrom Creek interval, with the second-order MFS within the lowermost Manuel Creek Formation. Above, a well-developed second-order HST is observed,

terminating at the intra-Aklavik unconformity. Within this second-order sequence, at least six third-order TST-HST pairs are present (Fig. 2-20).

First-order TST (Kimmeridgian to Berriasian)

The interval spanning the intra-Aklavik unconformity to the MFS above the arenaceous member of the Husky Formation is interpreted as a first-order TST. The MFS above the arenaceous member is chosen as a first-order bounding surface for two main reasons. First, it demarcates a change in stratal stacking pattern from retrogradational below to progradational above (i.e., marks the maximum backstepping of facies). Second, it is located within the thickest accumulation of offshore marine deposits (e.g., S1 in Table 2-1 within the Husky Formation) observed within the Jurassic to the mid-Early Cretaceous interval (Fig. 2-10). Three second-order systems tracts (TST-HST-TST; Fig. 2-20) are observed internally, with the second-order MRS present at the top of the arenaceous member.

First-order HST (Berriasian to Hauterivian)

Relative sea-level continues to rise above the first-order TST described previously, but the stratal stacking pattern becomes progradational. As a result, overlying strata represent a first-order HST. The upper contact is the RSME below the Kamik Formation. Internally, a thick second-order HST from the Husky Formation to the top of the Martin Creek Formation is observed. A thin TST-HST pair is present within the lowermost McGuire Formation, beginning at the sharp WRS above the Martin Creek Formation (Fig. 2-13C).

First-order FSST (Hauterivian)

A thin first-order FSST represents a relative-sea level fall above the previous HST. The RSME was observed at Grizzly Gorge and can also be identified using the gamma-ray signature

(Figs. 2-16, 2-19, 2-20). Where present, this surface is located at the base of the Kamik Formation (e.g., Fig. 2-16). It may also be eroded by the overlying SU (e.g., Pex Napartok M-01, Fig. 2-21). The upper contact is the subaerial unconformity within the lower Kamik Formation labeled the intra-Kamik contact in Figure 2-16. The intra-Kamik unconformity is interpreted as a first-order SU primarily because it is erosive and demarcates a transition from marine deposits below to fluvial deposits above (Figs. 2-5J, 2-9, 2-10, 2-16).

First-order LST (Hauterivian)

Above the intra-Kamik unconformity, regionally extensive fluvial deposits representing a first-order LST are observed (Figs. 2-5J, 2-9, 2-10). The MRS bounding the upper limit of this systems tract is chosen with reference to the gamma-ray signature. Little internal sub-division is possible.

First-order TST (Hauterivian to Barremian)

Relative sea-level continues to rise above the first-order LST, but the rate of created accommodation surpasses sediment supply, resulting in a first-order TST. This TST represents the majority of the Kamik Formation and lowermost Mount Goodenough Formation when not eroded below the sub-Mount Goodenough unconformity (Figs. 2-10, 2-16, 2-20). During this TST, the depositional environment transitions from continental fluvial near the base of the Kamik Formation to lower offshore in the basal Mount Goodenough Formation.

Underlying tectonism

Important tectonic events related to the opening of the Arctic Ocean are now examined based on the sequence stratigraphic framework (Fig. 2-20) and U-Pb detrital zircon geochronology (Fig. 2-19). Results suggest that rifting began in the Sinemurian (approximately

200 Ma), with the sub-Jurassic unconformity representing the ROU. Recalling the criteria for identifying the ROU (e.g., broad, angular unconformity, approximately time-equivalent to the earliest deformation or active stretching; Falvey, 1974; Fig. 2-1), the sub-Jurassic unconformity represents the best fit. It is angular and broad, with all Triassic strata absent below this surface within the study area. Additionally, this unconformity is time equivalent to other basal Jurassic unconformities in northern Alaska (e.g., Grantz and May 1982; Hubbard et al., 1987; and Grantz et al., 2011) and the Sverdrup Basin (e.g., Hadlari et al., 2016) that have also been interpreted as the ROU, providing a sense of regional consistency.

Above the ROU, the overlying first-order LST corresponds to syn-rift strata (*sensu* Prosser, 1993), deposited over an approximately 40 My period from the Sinemurian to the Oxfordian. The source of syn-rift strata is most likely derived from a recycled suite, as most of the Early Jurassic Bug Creek Group strata greatly resembles the underlying Permian, suggesting the weathering of local deposits was a prominent source of sediment during the Jurassic, with no active primary source (e.g., igneous or metamorphic rocks) contributing syn-depositional zircon grains. This pattern of resembling the Permian changes dramatically within the upper Aklavik, which contains a large 1900 Ma spike, suggesting a new source.

The intra-Aklavik unconformity, which separates the majority of the Bug Creek Group from the uppermost Aklavik Formation and overlying Husky Formation, is interpreted as the syn-rift unconformity (*sensu* Nøttvedt et al., 1995). This contact coincides with a dramatic basin expansion (e.g., Figs. 2-3A, B, 2-10) and a rapid transition to a lower offshore environment of deposition (e.g., S1; Fig. 2-13B), which is consistent with the transition from syn-rift to rift climax of Prosser (1993).

On a broader scale, this basin expansion may be associated with a transition from multiple regionally isolated sub-basins to a more regionally continuous basin (Fig. 2-1B; Gupta et al., 1998). Here, the underlying tectonic mechanism responsible for this transition is interpreted to be associated with normal fault activation along the HLFZ (Fig. 1-3). This is also supported by seismic data (e.g., Dietrich, 1996), paleogeographic trends (Dixon, 1991, 2004; Fig. 2-3), and correlates to what Hubbard et al. (1987) consider to be the earlier failed rift stage in Arctic Alaska. Furthermore, Mesozoic detrital zircon grains are present above this contact. The source of these grains is likely the developing North American Cordillera to the south (e.g., Colpron et al., 2015; Fig. 1-1), which is also evidence of an expanded catchment. The overlying first-order HST spanning the Husky-McGuire interval is considered early post-rift (*sensu* Prosser, 1993).

The basal-Kamik unconformity is proposed as a likely candidate for the BU, which defines the base of the breakup sequence above (*sensu* Soares et al., 2012). The breakup sequence is interpreted to begin with a FSST (Soares et al., 2012), with a FSST being present within the lowermost Kamik. Additionally, many studies of continental breakup suggest an influx of coarse clastic material in the earliest phase of breakup (e.g., Nøttvedt et al., 1995; Soares et al., 2012), resulting in early progradation immediately above the BU (i.e., at the base of the breakup sequence). Within the study area, this would correspond to the braided river deposits (e.g., A1 in Table 2-1) within the lower Kamik immediately above the intra-Kamik unconformity (Fig. 2-10). This is also reconcilable with interpretations within the Sverdrup Basin.

Comparison to the Sverdrup Basin

The 200 – 190 Ma unconformity at the base of the Heiberg Group has been interpreted to represent the ROU for the Arctic Ocean within the Sverdrup Basin (Hadlari et al., 2016). This

correlates to the sub-Jurassic unconformity within the study area. The timing of basinal expansion (Kimmeridgian to Berriasian; rift climax) within the study area also appears to correlate with the rift climax within the Sverdrup Basin's Deer Bay Formation (Fig. 2-22; Hadlari et al., 2016). Further similarities between the Isachsen Formation of the Sverdrup Basin and the Kamik Formation of the Brooks-Mackenzie Basin are observed. Within the Isachsen Formation, a prominent sub-Hauterivian unconformity between underlying shoreline/deltaic deposits and overlying fluvial deposits is interpreted as the breakup unconformity. A similar contact is observed within the Kamik Formation (i.e., the intra Kamik unconformity; Grizzly Gorge section; Fig. 2-13D, 2-16), which is also interpreted to represent the breakup unconformity. Above this contact, a similar association of transgressive facies occurs, with fluvial sandstones transitioning upwards into floodplain deposits and eventually fully marine deposits by the Aptian (e.g., Paterson Island, Rondon, and Walker Island members in the Sverdrup Basin; Tullius et al., 2014).

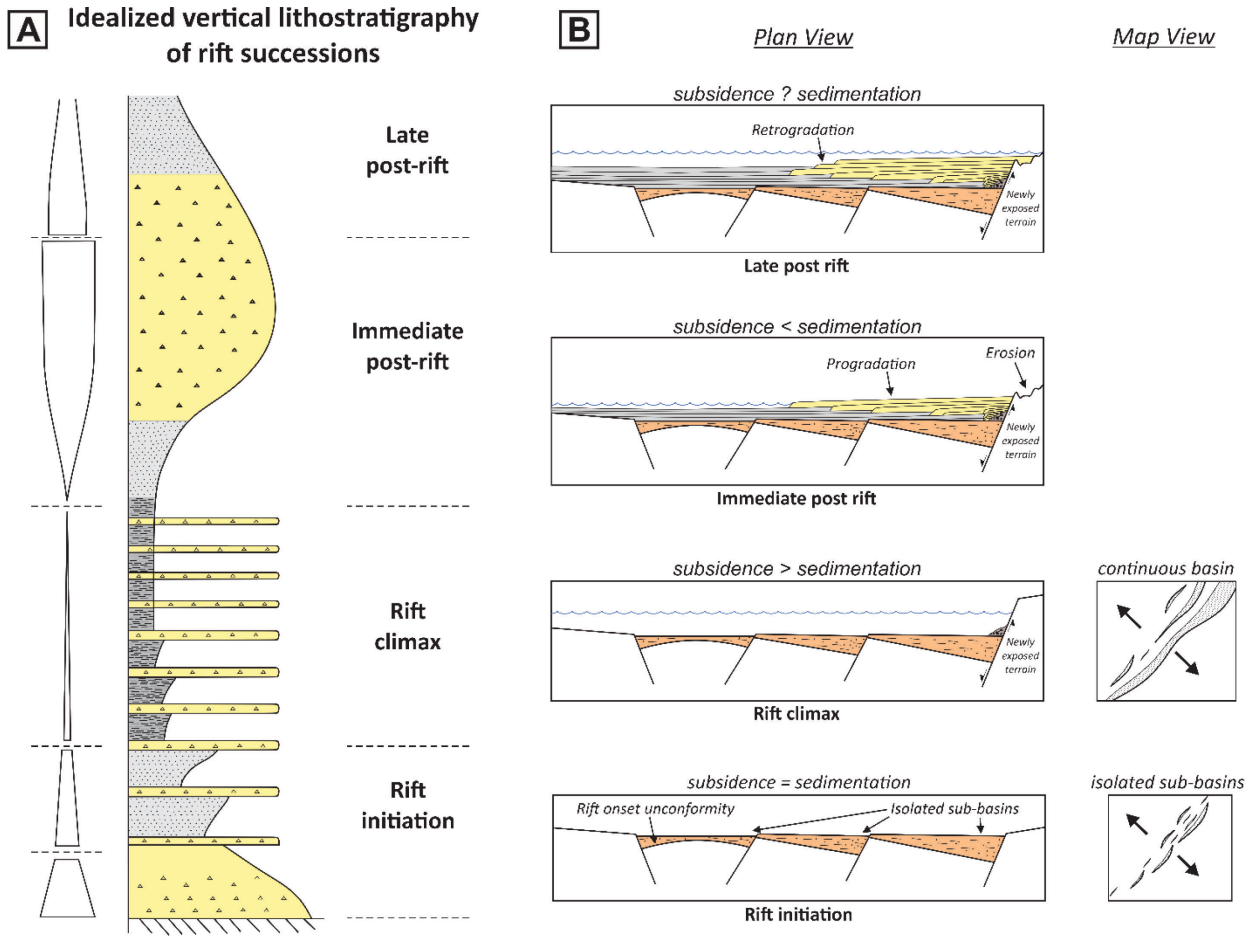

Figure 2-1: (A) Idealized rift succession modified after Prosser (1993) with a schematic illustration at each stage of development. **(B)** Various phases of rift development. The rift initiation phase is associated with early fault block rotation, resulting in isolated depocenters commonly exhibiting a progradational pattern. Rift climax as isolated fault blocks amalgamate, which also greatly increases accommodation space. The immediate post-rift phase is associated with erosion on newly tilted and exposed fault blocks, which also act as a source for sediment, generally resulting in progradation. The late-post rift phase is potentially associated with transgression as the source degrades. Based on Prosser (1993).

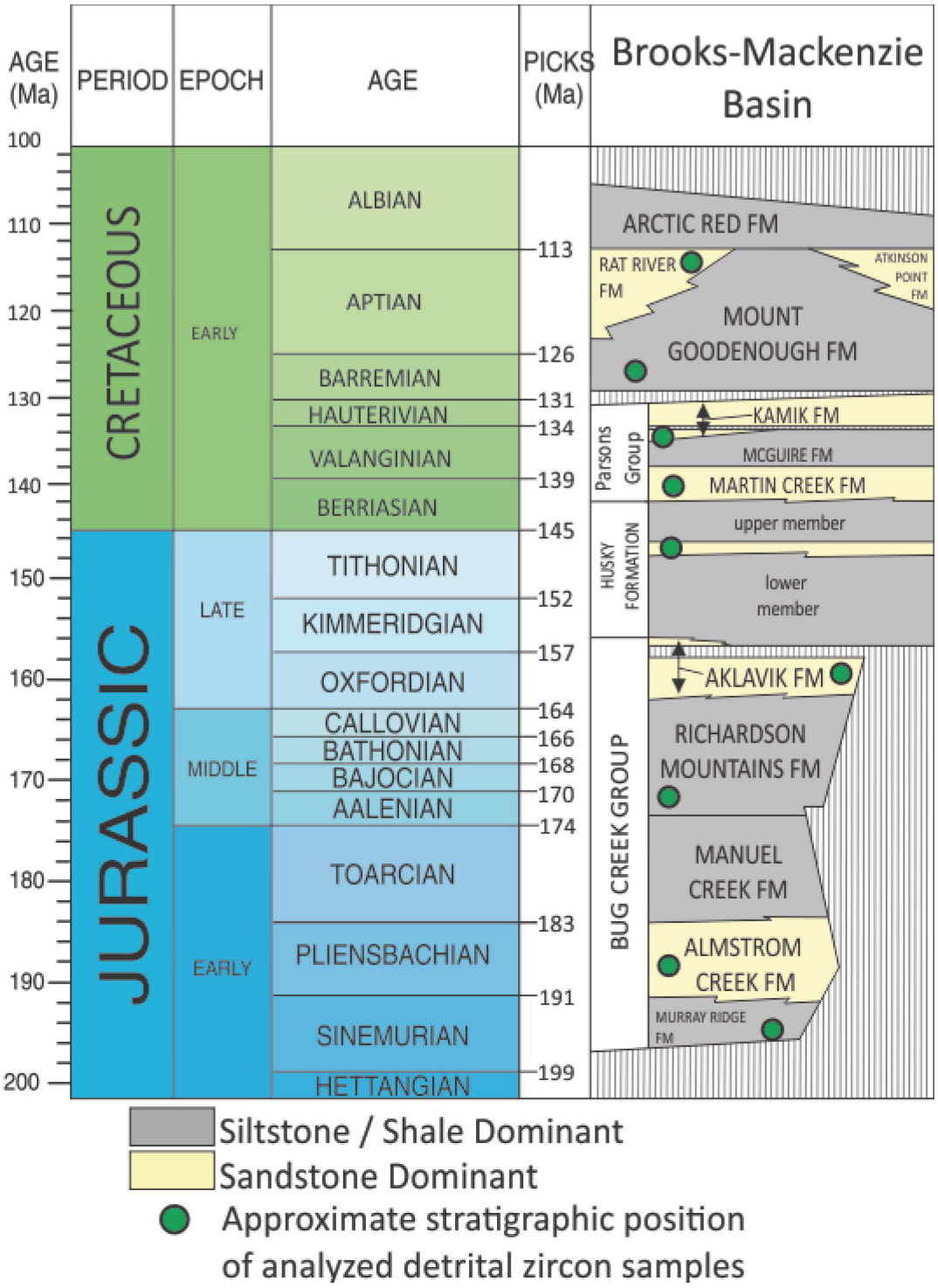

Figure 2-2: Table of Formations modified after Poulton et al. (1982) and Dixon and Jeletzky (1991).

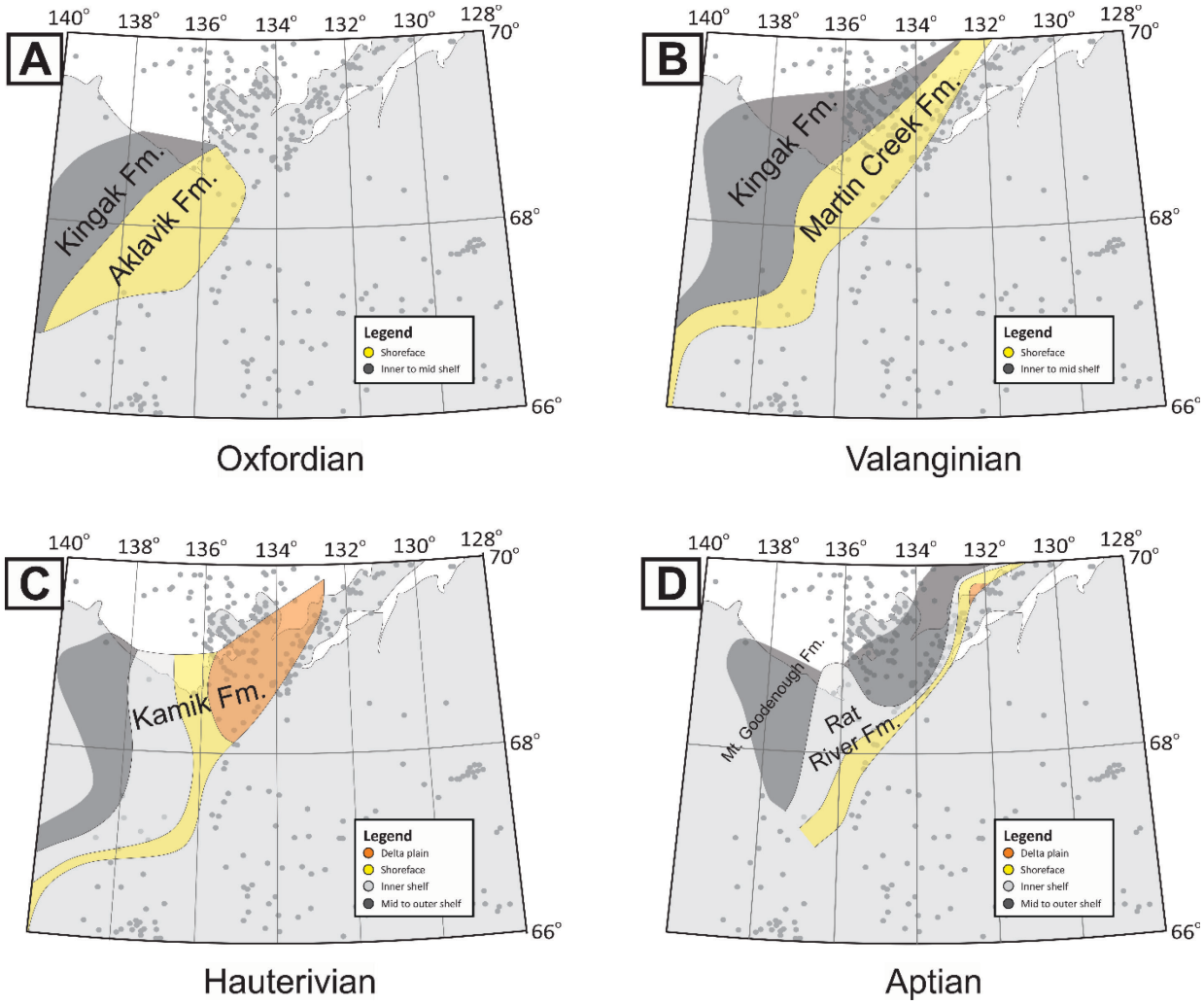

Figure 2-3: Paleogeographic maps. **(A)** modified after Poulton (1997), **(B, C, and D)** modified after Dixon (1991, 2004).

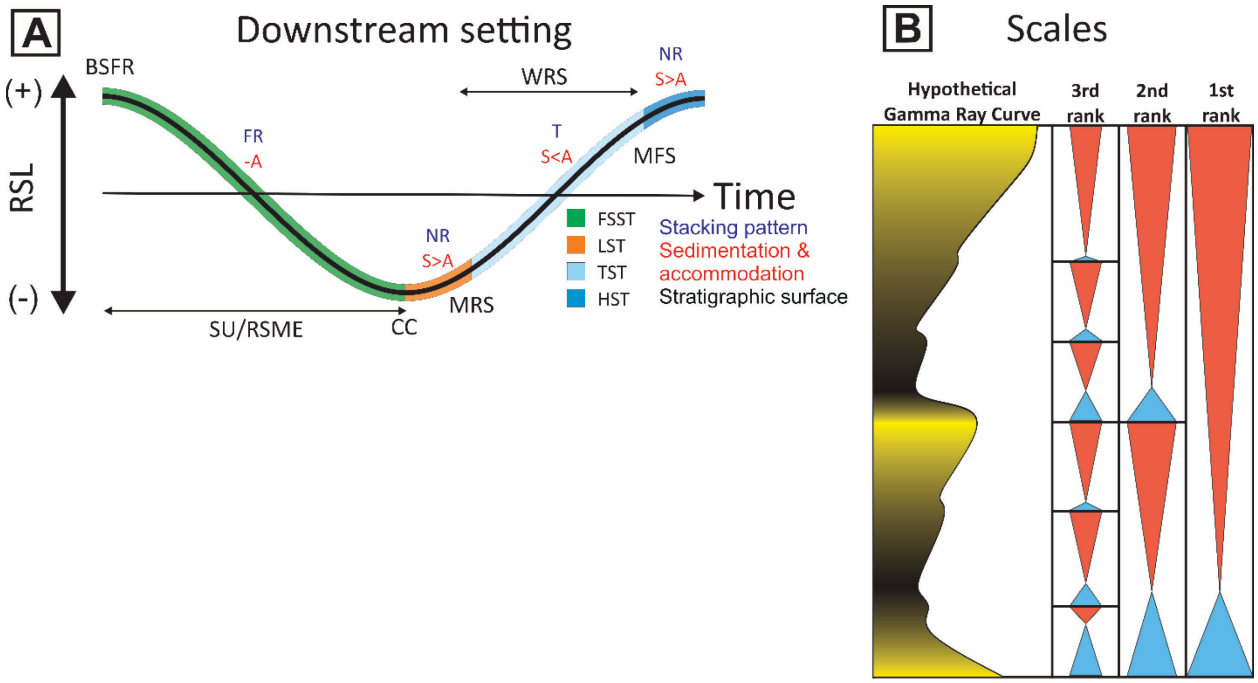

Figure 2-4: Summary figure of some key principles in sequence stratigraphy. **(A)** Diagram showing nomenclature of systems tracts in the downstream (i.e., marine) setting, and how they relate to time, base level, accommodation, and sedimentation. A: accommodation, BFSR: basal surface of forced regression, FR: forced regression, FSST: falling stage systems tract, HST: highstand systems tract, LST: lowstand systems tract, MRS: maximum regressive surface, MFS: maximum flooding surface, NR: normal regression, RSME: regressive surface of marine erosion, S: sedimentation, SU: subaerial unconformity, TST: transgressive systems tract, WRS: wave ravinement surface. **(B)** Schematic diagram displaying the concept of hierarchy, with "higher-order" sequences being composed of multiple "lower-order" sequences.

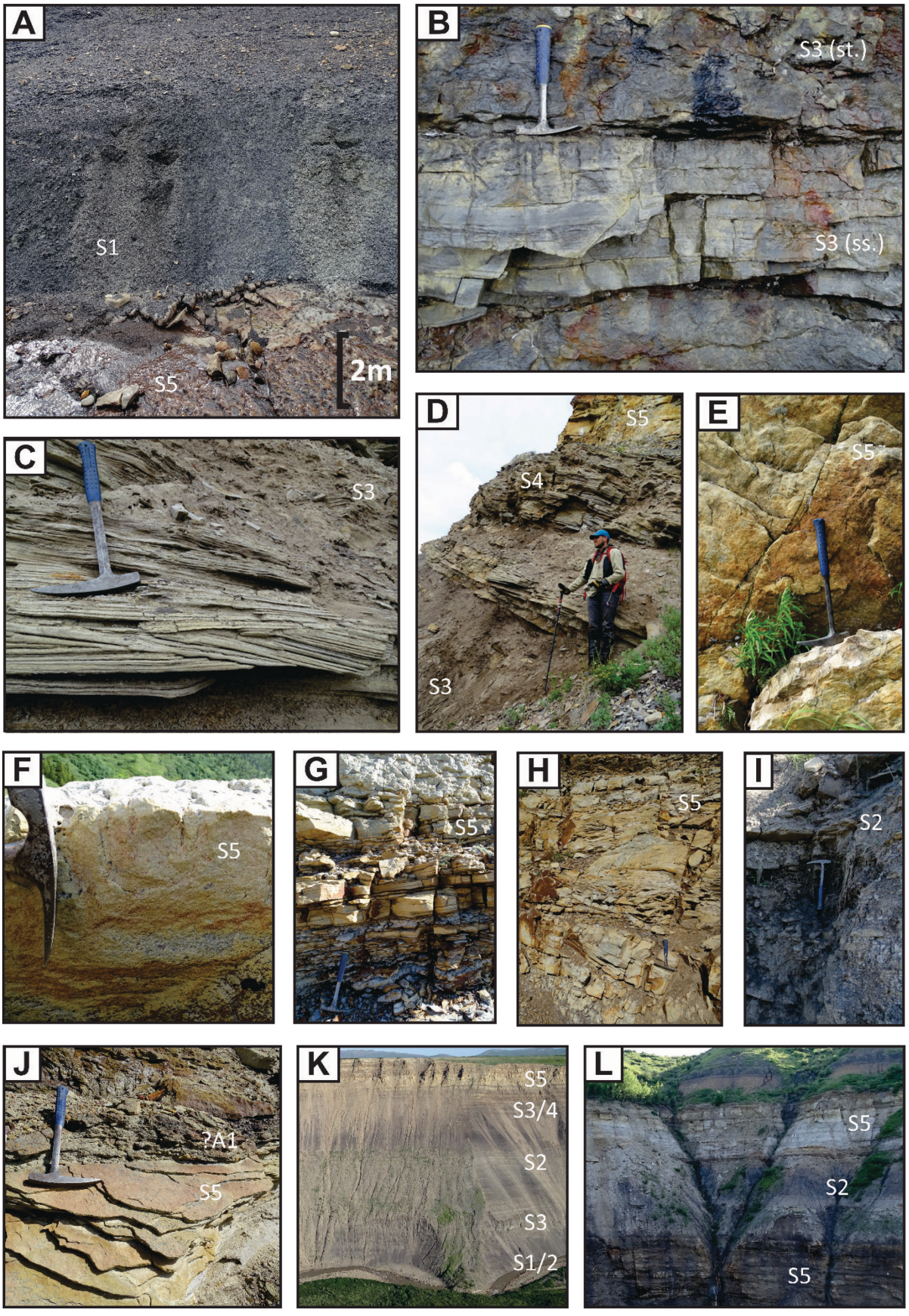
A
S1
S5
2m
B
S3 (st.)
S3 (ss.)
C
S3
D
S5
S4
S3
E
S5
F
S5
G
S5
H
S5
I
S2
J
?A1
S5
K
S5
S3/4
S2
S3
S1/2
L
S5
S2
S5

Figure 2-5 (previous page): Photo plate showing various facies in outcrop. The exact locations of photographs within the measured section are shown in Figs. 2-11, 2-14, and 2-15. **(A)** From the Bug Creek section: S1 in Husky Formation and S5 in Aklavik Formation. **(B)** From the Murray Ridge sections: S3 in the Almstrom Creek Formation (ss.: sandstone, st.: siltstone). **(C)** From the Bug Creek section: S3 in the Richardson Mountains Formation. **(D)** From the Bug Creek section: S3/4 in the Richardson Mountains Formation and S5 in the Aklavik Formation. **(E)** From the Bug Creek section: S5 in the Aklavik Formation. **(F)** From the Bug Creek section: S5 in the Aklavik Formation. **(G and H)** From the Martin Creek section: S5 within the Martin Creek Formation. **(I)** From the Martin Creek section: S2 in the Husky Formation. **(J)** From the Grizzly Gorge section: S5 and ?A1 in the Kamik Formation. **(K)** Aerial photo of the Martin Creek section showing multiple facies of FA1. **(L)** Aerial photo of the Grizzly Gorge section showing various facies of FA1.

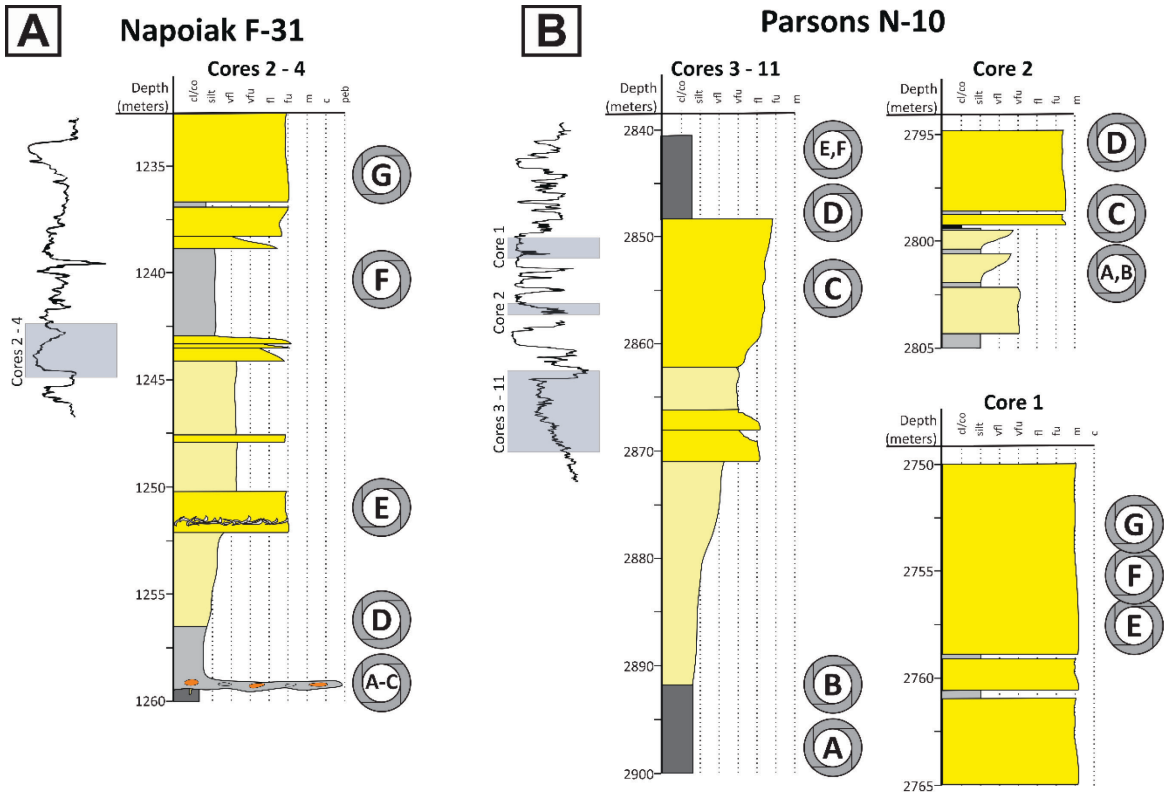

Figure 2-6: Schematic illustration of the four cored intervals described here. The locations of the wells are shown in Figures 1-3. **(A)** Photographs are shown in Fig. 2-7. **(B)** Photographs are shown in Fig. 2-8 (cores 3 –10) and 2-9 (cores 1 and 2).

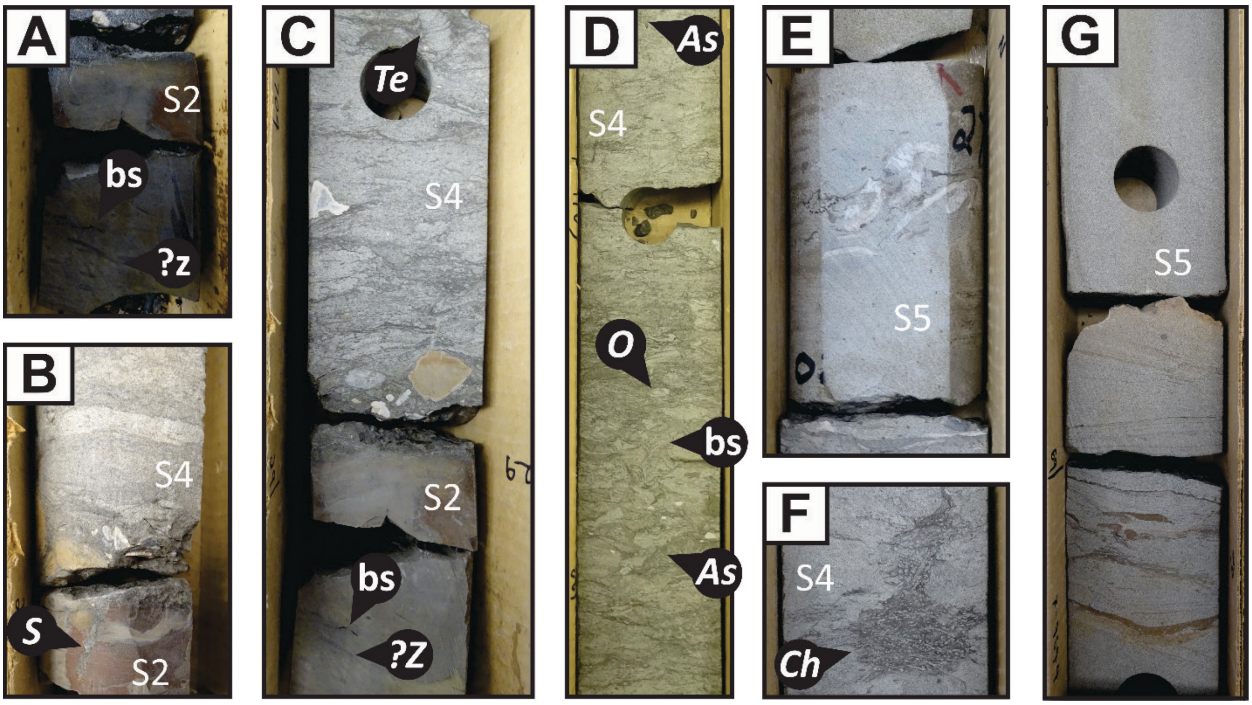

Figure 2-7: Photo plate showing various facies within the Murray Ridge and Almstrom Creek formations in the Shell Napoiak F-31 core. Exact locations of photographs within the well-log are shown in Figure 2-6A. **(A)** The Murray Ridge Formation, bs: bivalve shell, *z: Zoophycos*. **(B/C)** The erosive contact between the Murray Ridge Formation and Almstrom Creek Formation, bs: bivalve shell, *S: Skolithos, Te: Teichichnus, Z: Zoophycos*. **(D, F)** S4 within the Almstrom Creek Formation, *As: Asterosoma, Ch: Chondrites, O: Ophiomorpha, Z: Zoophycos*. **(E, G)** S5 within the Almstrom Creek Formation.

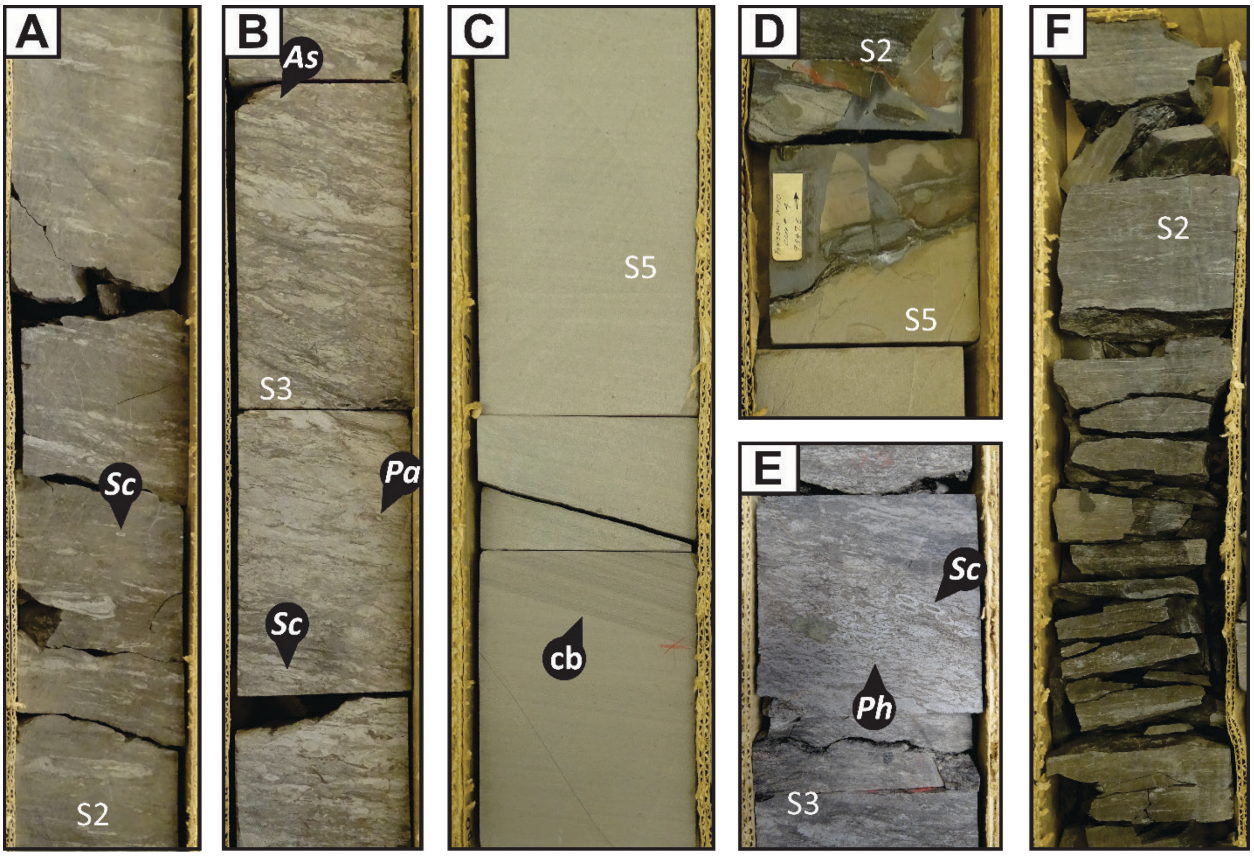

Figure 2-8: Photo plate showing various facies within the Husky, Martin Creek, and McGuire formations in the Parsons N-10 core. The exact locations of photographs within the well-log are shown in Figure 2-6B. **(A/B)** S2 within the Husky Formation, *As: Asterosoma, Pa: Palaeophycus, Sc: Schaubcylindrichnus*. **(C)** S5 within the Martin Creek Formation (cb: crossbed. **(D)** Erosive contact between the underlying Martin Creek Formation and the overlying McGuire Formation. **(E/F)** S2 within the McGuire Formation, *Ph: Phycosiphon, Sc: Schaubcylindrichnus.*

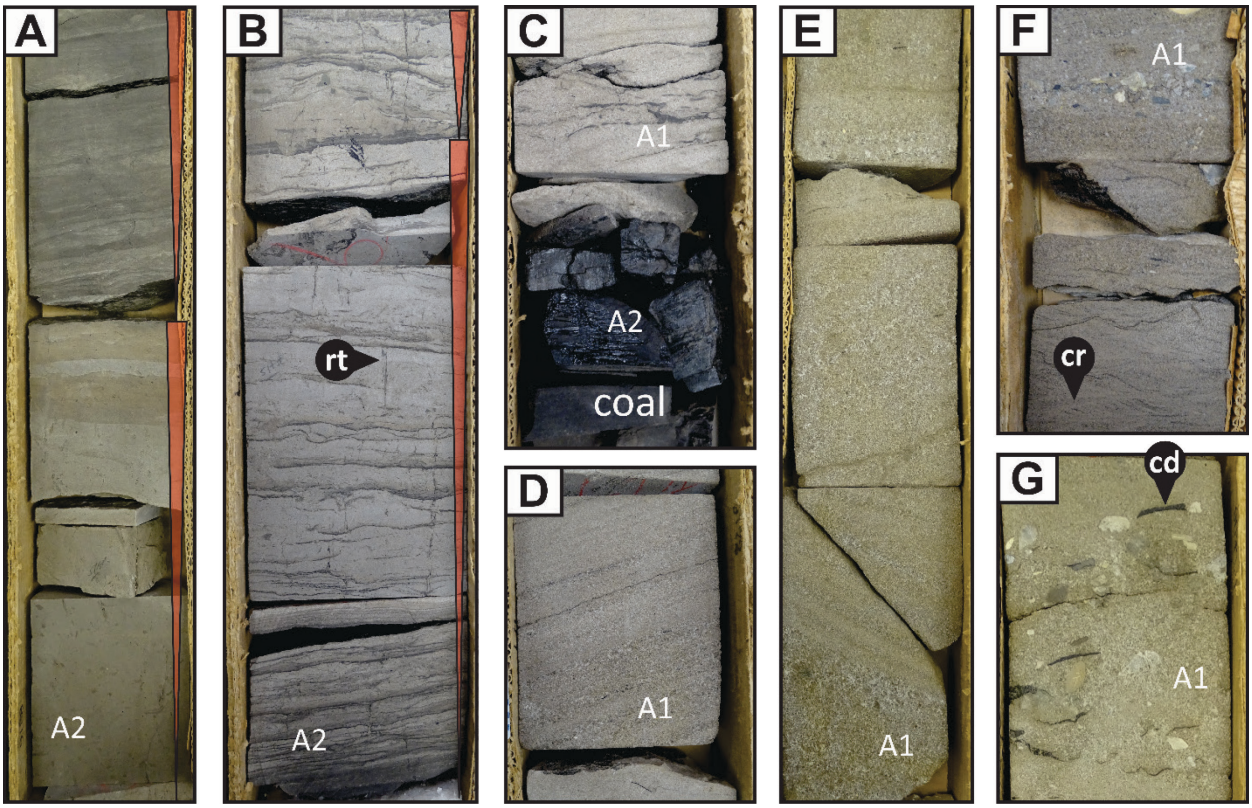

Figure 2-9: Photo plate showing various facies within the Lower Member of the Kamik Formation in the Parsons N-10 core. The exact locations of photographs within the well-log are shown in Figure 2-6B. **(A/B)** A2 coarsening upwards packages are interpreted to represent crevasse splay deposits, rt: root trace. **(C)** Coal deposits (A2) eroded by overlying sandstone facies (A1). **(D – G)** Facies A1 showing coarse to fine-grained sandstone, cd: carboniferous debris, cr: climbing ripples.

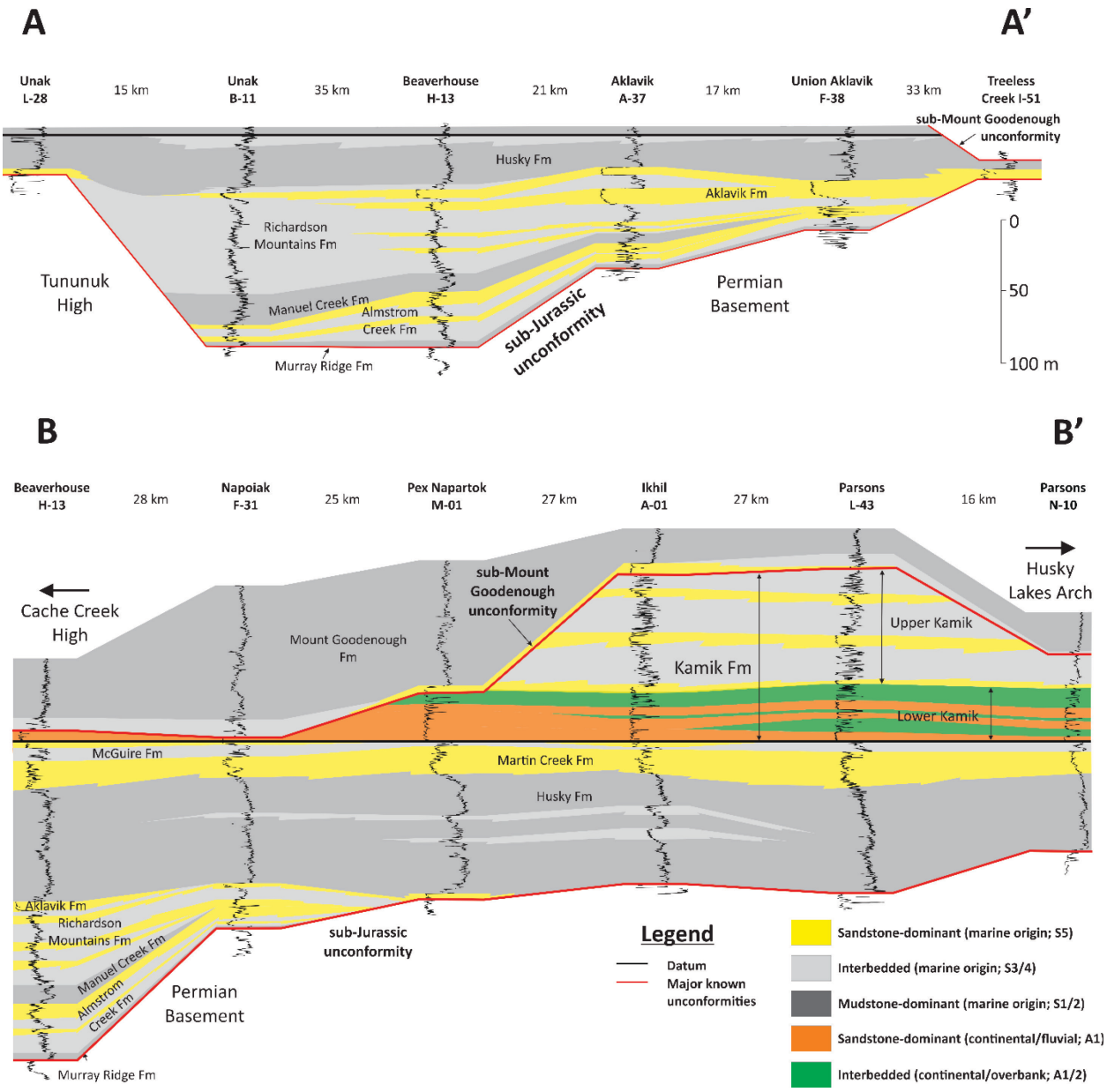

Figure 2-10: Lithostratigraphic cross-section and environment of deposition correlation. Location of the cross-section shown in Fig. 1-3. Vertical scale in meters.

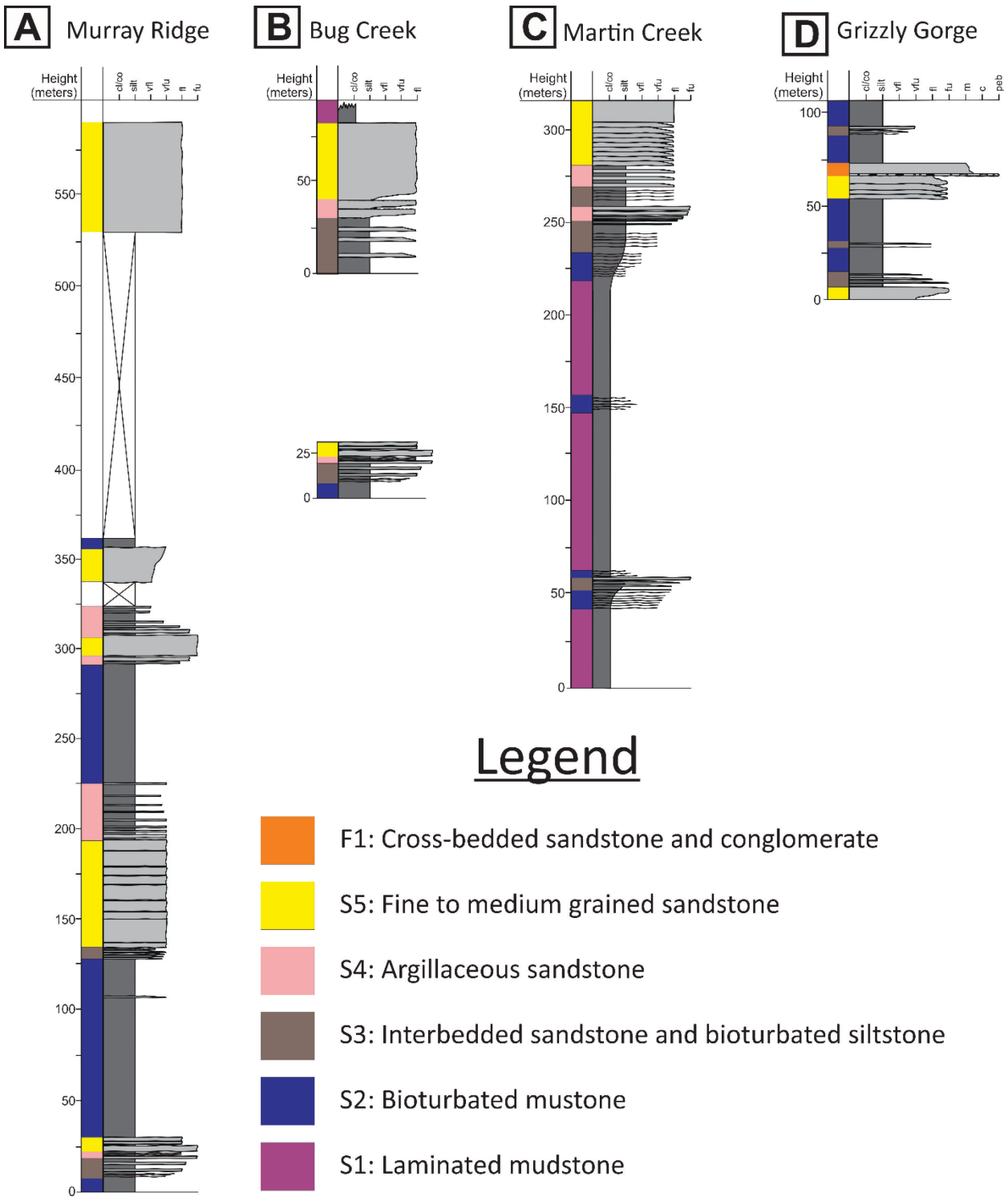

Figure 2-11: Measured outcrop sections and facies from the Northern Richardson Mountains. Location in Figure 1-4.

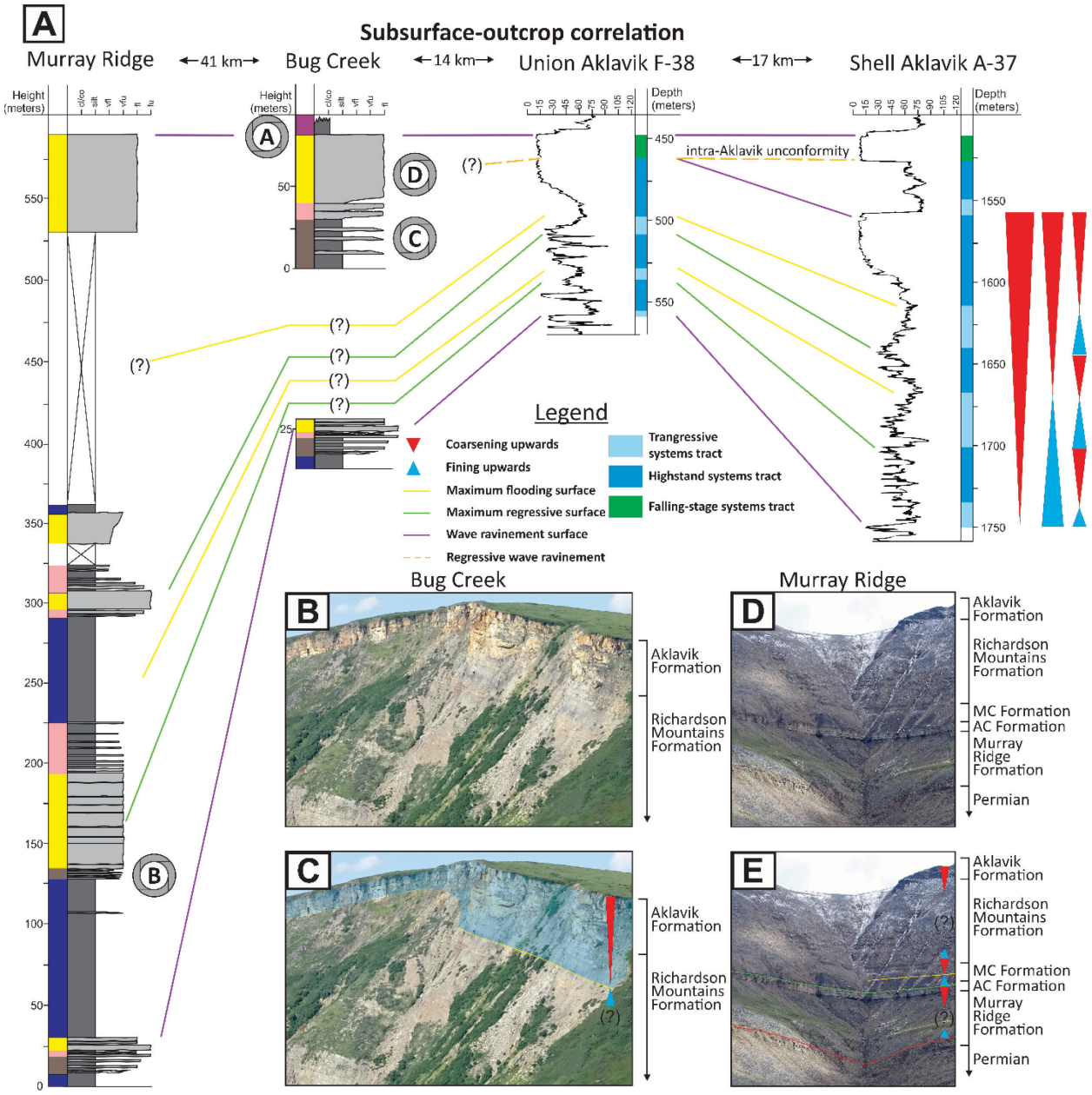
A
Subsurface-outcrop correlation
Murray Ridge
41 km
Bug Creek
14 km
Union Aklavik F-38
17 km
Shell Aklavik A-37
Height (meters)
Depth (meters)
intra-Aklavik unconformity
(?)
Legend
Coarsening upwards
Fining upwards
Maximum flooding surface
Maximum regressive surface
Wave ravinement surface
Regressive wave ravinement
Trangressive systems tract
Highstand systems tract
Falling-stage systems tract
Bug Creek
Murray Ridge
B
C
D
E
Aklavik Formation
Richardson Mountains Formation
MC Formation
AC Formation
Murray Ridge Formation
Permian

Figure 2-12 (previous page): Correlation of the Bug Creek Group in measured outcrop sections with the subsurface. **(A)** Correlation of sequence stratigraphic surfaces. Murray Ridge section detrital zircon sample numbers from base to top: P-MR-103, SC-MR-203, AC-MR-298, RM-MR-437, AK-MR-645. Bug Creek section detrital zircon samples numbers from base to top: P-BC-33, AK-BC-195. **(B)** Aerial photo of the Bug Creek section. **(C)** Grain size trends and systems tracts in the Bug Creek section. **(D)** Aerial photo of the Murray Ridge section. **(E)** Grain size trends and systems tracts in the Murray Ridge section.

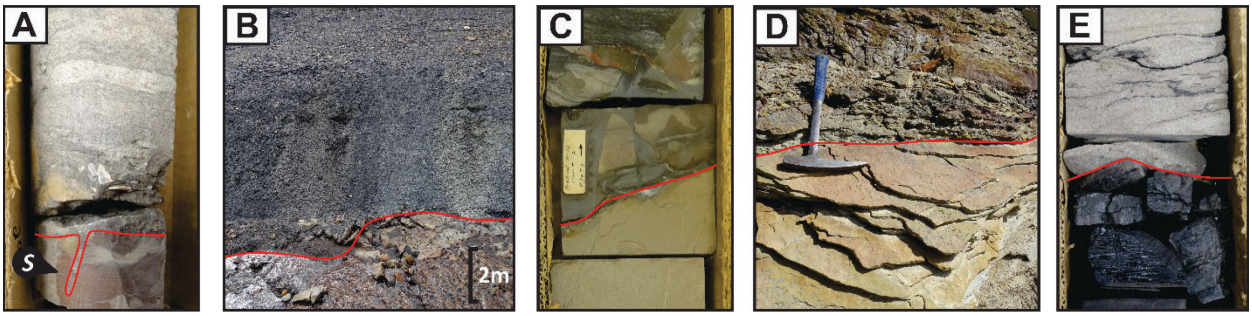

Figure 2-13: Some important sequence stratigraphic contacts. **(A)** *Glossifungites* surface at the contact between the Murray Ridge and Almstrom Creek formations (untraced image in Fig. 2-7B). **(B)** WRS at the contact between the Aklavik and Husky formations (untraced image in Fig. 2-5A). **(C)** WRS at the contact between the Martin Creek and McGuire formations (untraced image in Fig. 2-6D). **(D)** SU within the Kamik Formation (untraced image in Fig. 2-5J). **(E)** SU within the Kamik Formation (untraced image in Fig. 2-9C).

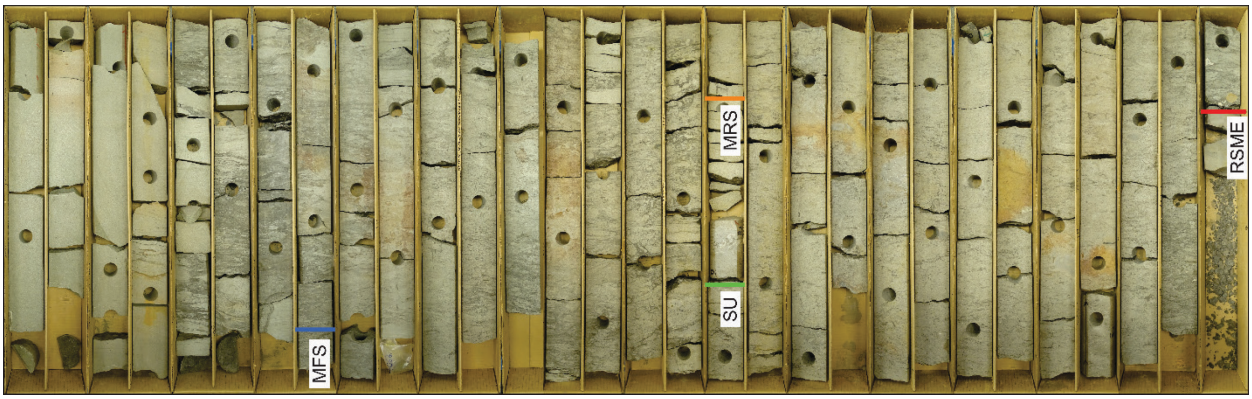

Figure 2-14: Sequence stratigraphic interpretation of the Shell Napoiak F-31 core (base bottom right), Murray Ridge Formation to McGuire Formation interval. RSME: regressive surface of marine erosion, SU: subaerial unconformity, MRS: maximum regressive surface, and MFS: maximum flooding surface. Location of the core shown in Fig. 1-3. Gamma-ray signature is shown in Fig. 9A.

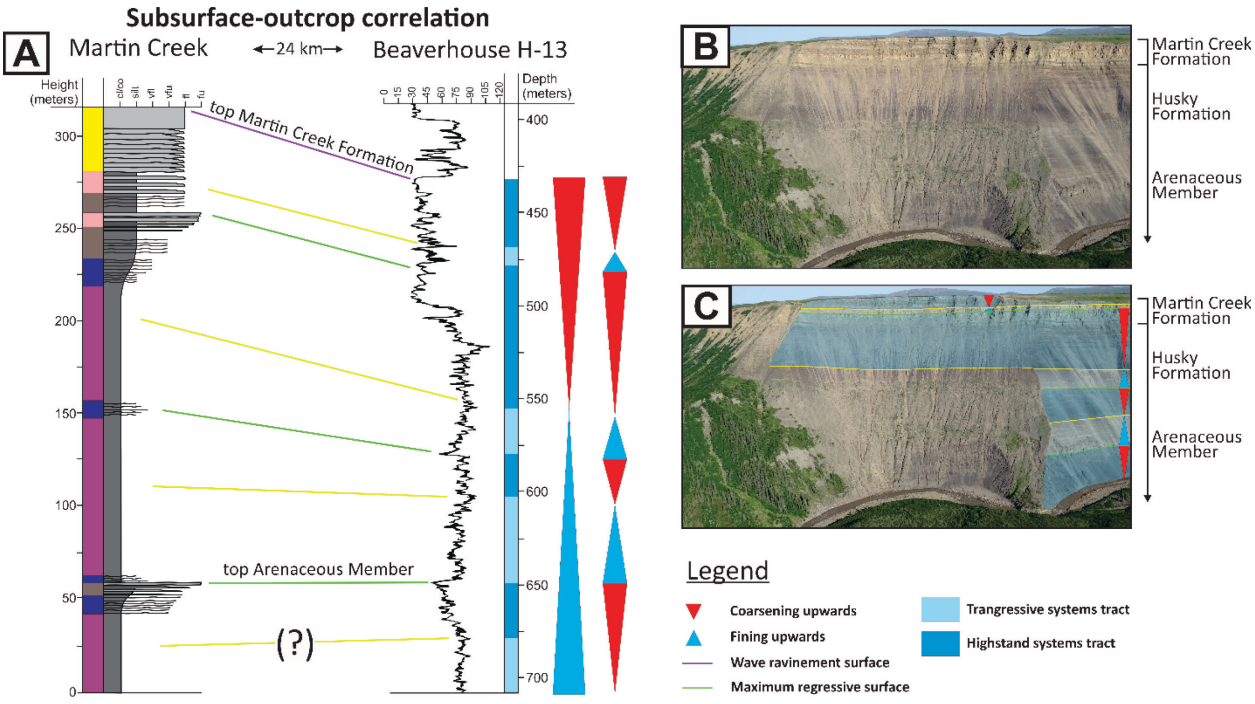

Figure 2-15: Correlation of the Martin Creek measured outcrop section with the subsurface. **(A)** Correlation of sequence stratigraphic surfaces. Martin Creek section detrital zircon sample number: HK-MC-60. **(B)** Aerial photo of the Martin Creek section. **(C)** Grain size trends and systems tracts.

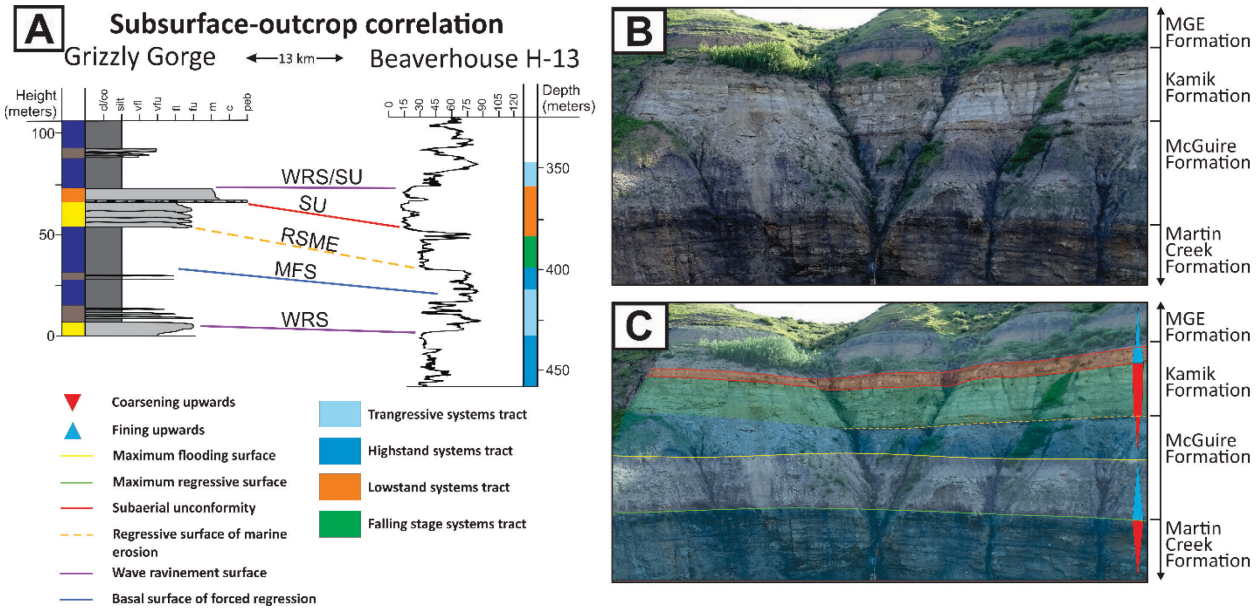

Figure 2-16: Correlation of the Grizzly Gorge measured outcrop sections with the subsurface. **(A)** correlation of sequence stratigraphic surfaces. Grizzly Gorge section detrital zircon sample numbers from base to top: MC-GG-13, K-GG-75, MGE-GG-94. **(B)** Aerial photo of the Grizzly Gorge section. **(C)** Grain size trends and systems tracts.

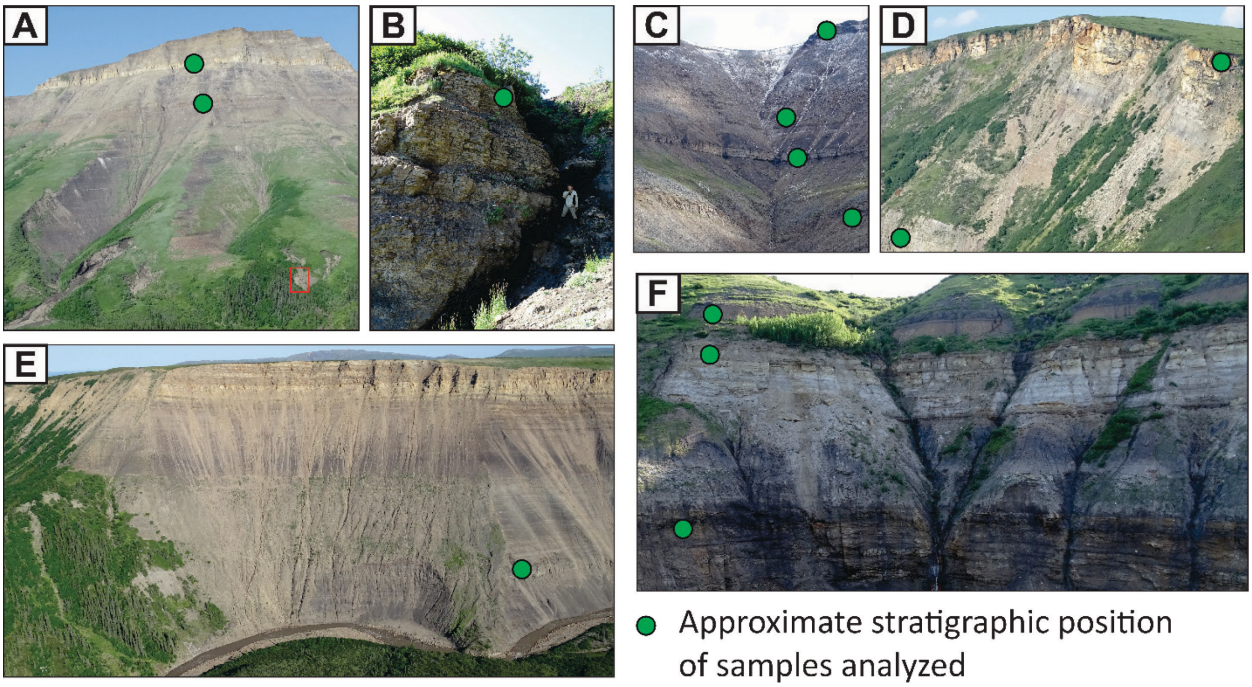

Figure 2-17: Outcrop photos and approximate stratigraphic position of detrital zircon samples. **(A)** Mount Goodenough section. Detrital zircon sample numbers from base to top: MGE-MGE-425, MGE-RR. The red box shows the location of (B). **(B)** Arenaceous Member. Detrital zircon sample number: HK-MGE-18. **(C)** Murray Ridge section. Detrital zircon sample numbers from base to top: P-MR-103, SC-MR-203, AC-MR-298, RM-MR-437, AK-MR-645. **(D)** Bug Creek section. Detrital zircon sample numbers from base to top: P-BC-33, AK-BC-195. **(E)** Martin Creek section. Detrital zircon sample number: HK-MC-60. **(F)** Grizzly Gorge section. Detrital zircon sample numbers from base to top: MC-GG-13, K-GG-75, MGE-GG-94.

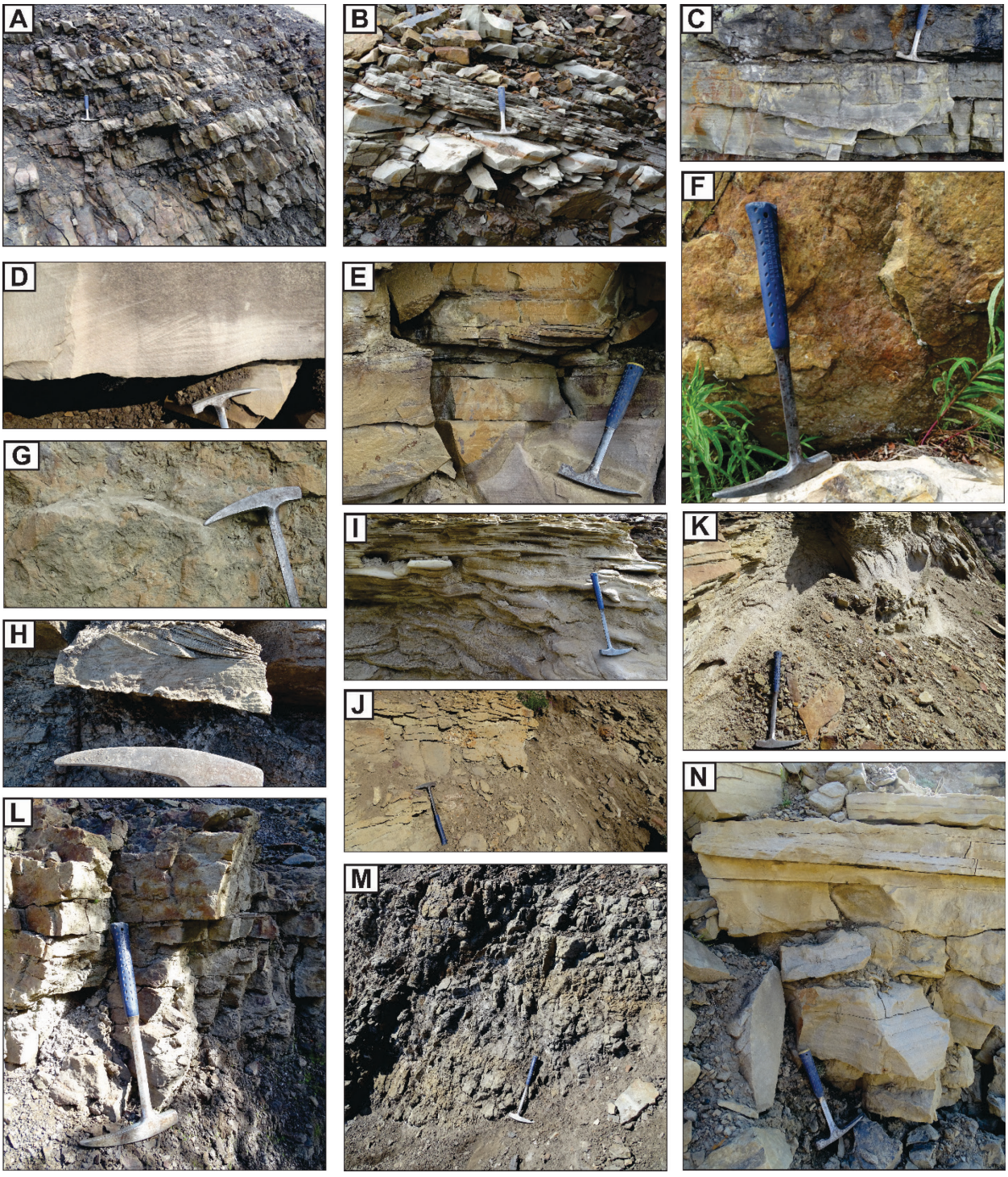
A
B
C
D
E
F
G
I
K
H
J
L
M
N

Figure 2-18 (previous page): (A) Permian sample P-MR-103 at the Murray Ridge Section. **(B)** Scho Creek Member of the Murray Ridge Formation sample SC-MR-203 at the Murray Ridge section. **(C)** Almstrom Creek Formation sample AC-MR-298 at the Murray Ridge section. **(D)** Richardson Mountains Formation sample RM-MR-437 at the Murray Ridge section. **(E)** Aklavik Formation sample AK-MR-645 at the Murray Ridge section. **(F)** Aklavik Formation sample AK-BC-195 at the Bug Creek section. **(G)** Permian sample P-BC-33 at the Bug Creek section. **(H)** Arenaceous Member of the Husky Formation sample HK-MC-60 at the Martin Creek section. **(I)** Martin Creek Formation sample MC-GG-13 at the Grizzly Gorge section. **(J)** Mount Goodenough Formation sample MGE-GG-94 at the Grizzly Gorge section. **(K)** Kamik Formation sample K-GG-75 at the Grizzly Gorge section. **(L)** Arenaceous Member of the Husky Formation sample HK-MGE-18 at the Mount Goodenough section. **(M)** Mount Goodenough Formation sample MGE-MGE-425 at the Mount Goodenough section. **(N)** Rat River Formation sample MGE-RR at the Mount Goodenough section.

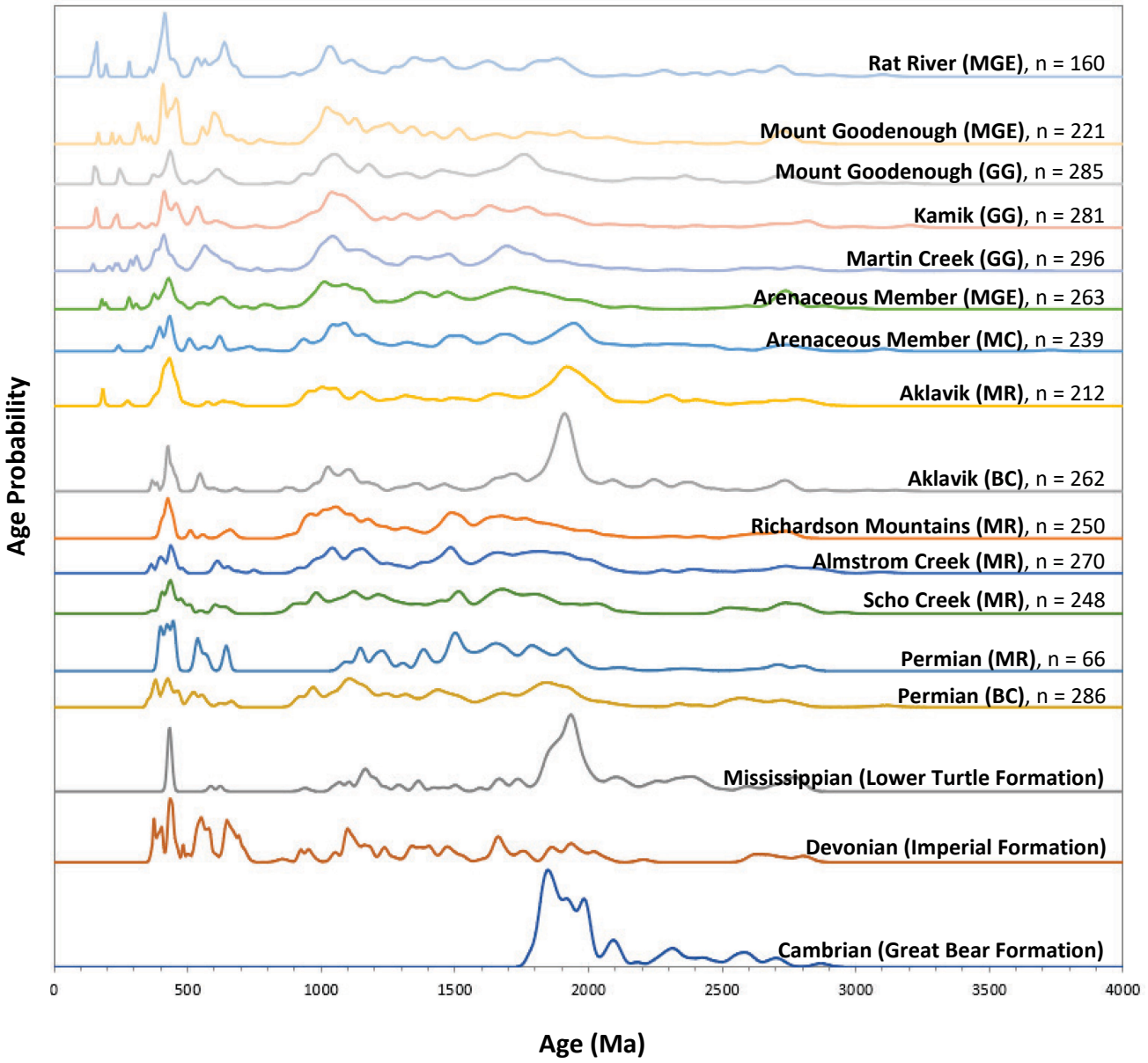

Figure 2-19: Detrital zircon data from the Northern Richardson Mountains. Mississippian and Devonian reference curves from Lemieux et al., 2011. Cambrian reference curve from Hadlari et al., 2012)

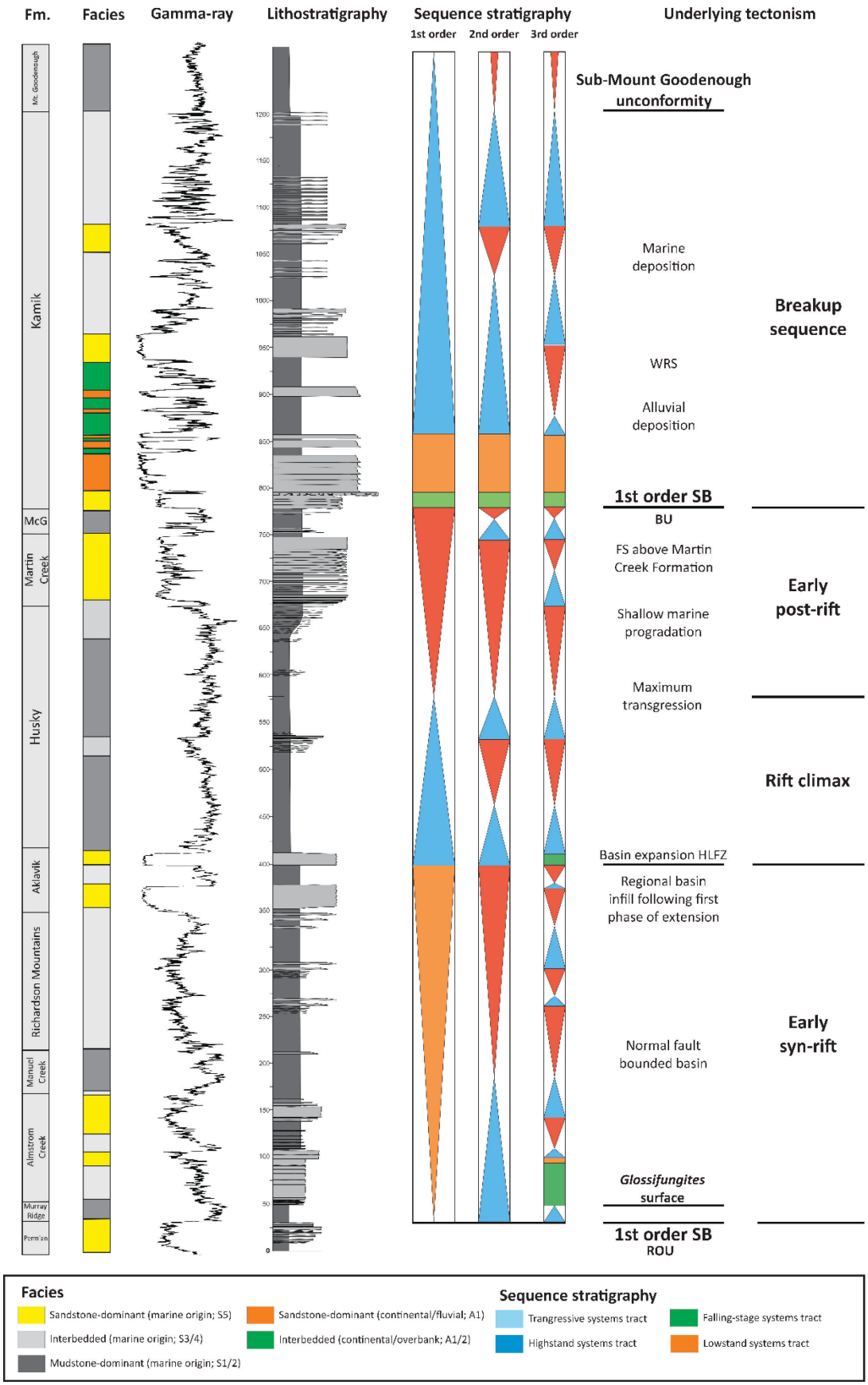
Fm.
Facies
Gamma-ray
Lithostratigraphy
Sequence stratigraphy
1st order
2nd order
3rd order
Underlying tectonism
Mt. Goodenough
Kamik
McG
Martin Creek
Husky
Akiavik
Richardson Mountains
Manuel Creek
Almstrom Creek
Murray Ridge
Permian
Sub-Mount Goodenough unconformity
Marine deposition
WRS
Alluvial deposition
1st order SB
BU
FS above Martin Creek Formation
Shallow marine progradation
Maximum transgression
Basin expansion HLFZ
Regional basin infill following first phase of extension
Normal fault bounded basin
Glossifungites surface
1st order SB
ROU
Breakup sequence
Early post-rift
Rift climax
Early syn-rift
Facies
Sandstone-dominant (marine origin; S5)
Interbedded (marine origin; S3/4)
Mudstone-dominant (marine origin; S1/2)
Sandstone-dominant (continental/fluvial; A1)
Interbedded (continental/overbank; A1/2)
Sequence stratigraphy
Trangressive systems tract
Highstand systems tract
Falling-stage systems tract
Lowstand systems tract

Figure 2-20 (previous page): Summary figure describing the sequence stratigraphic framework and important underlying tectonic events. Gamma-ray and lithostratigraphy curves are composite sections based on multiple data points.

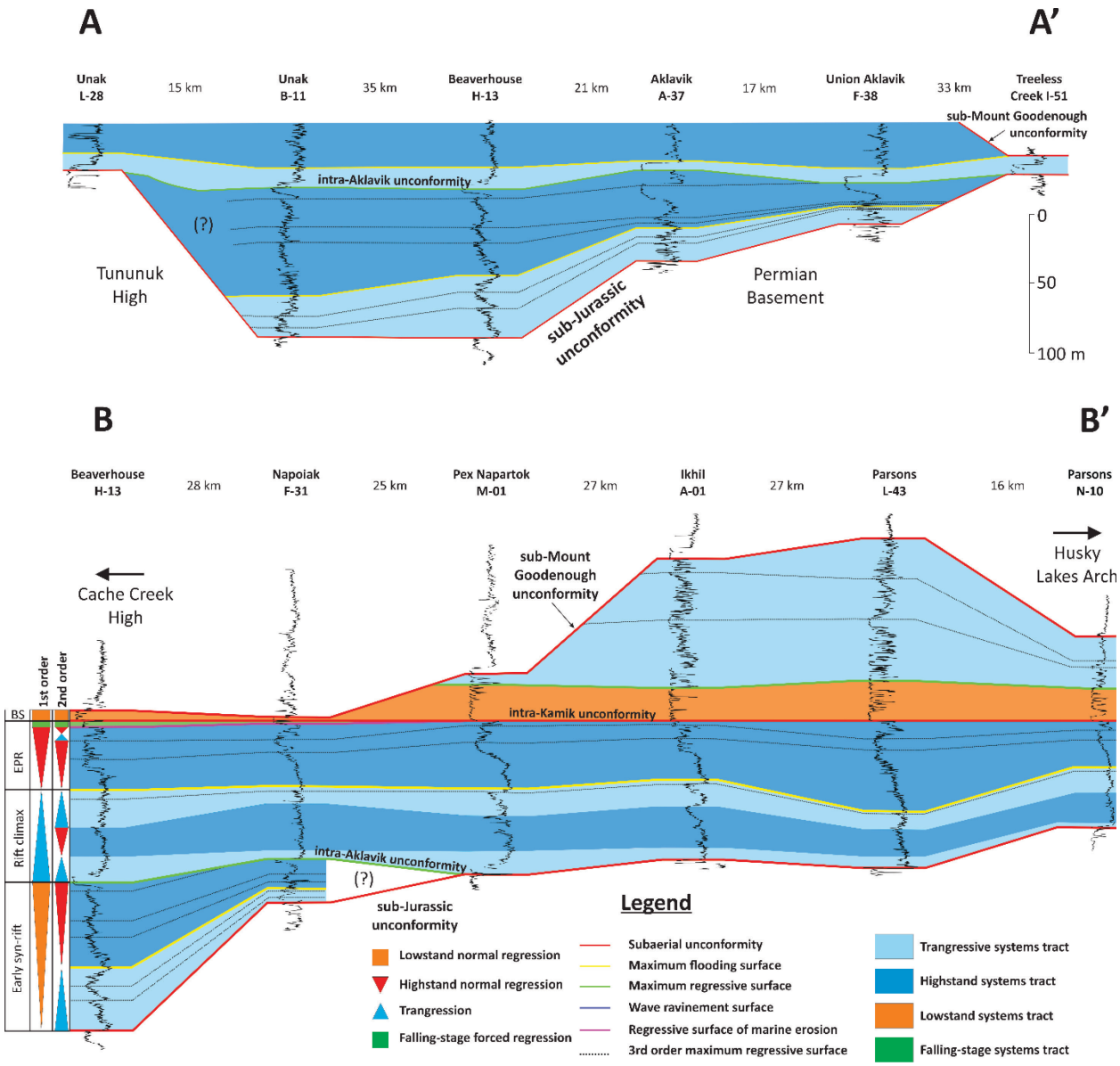

Figure 2-21: Sequence stratigraphic cross-section. Location of the cross-section shown in Fig. 1-3. Vertical scale in meters. RC: Rift climax, BS: Breakup sequence.

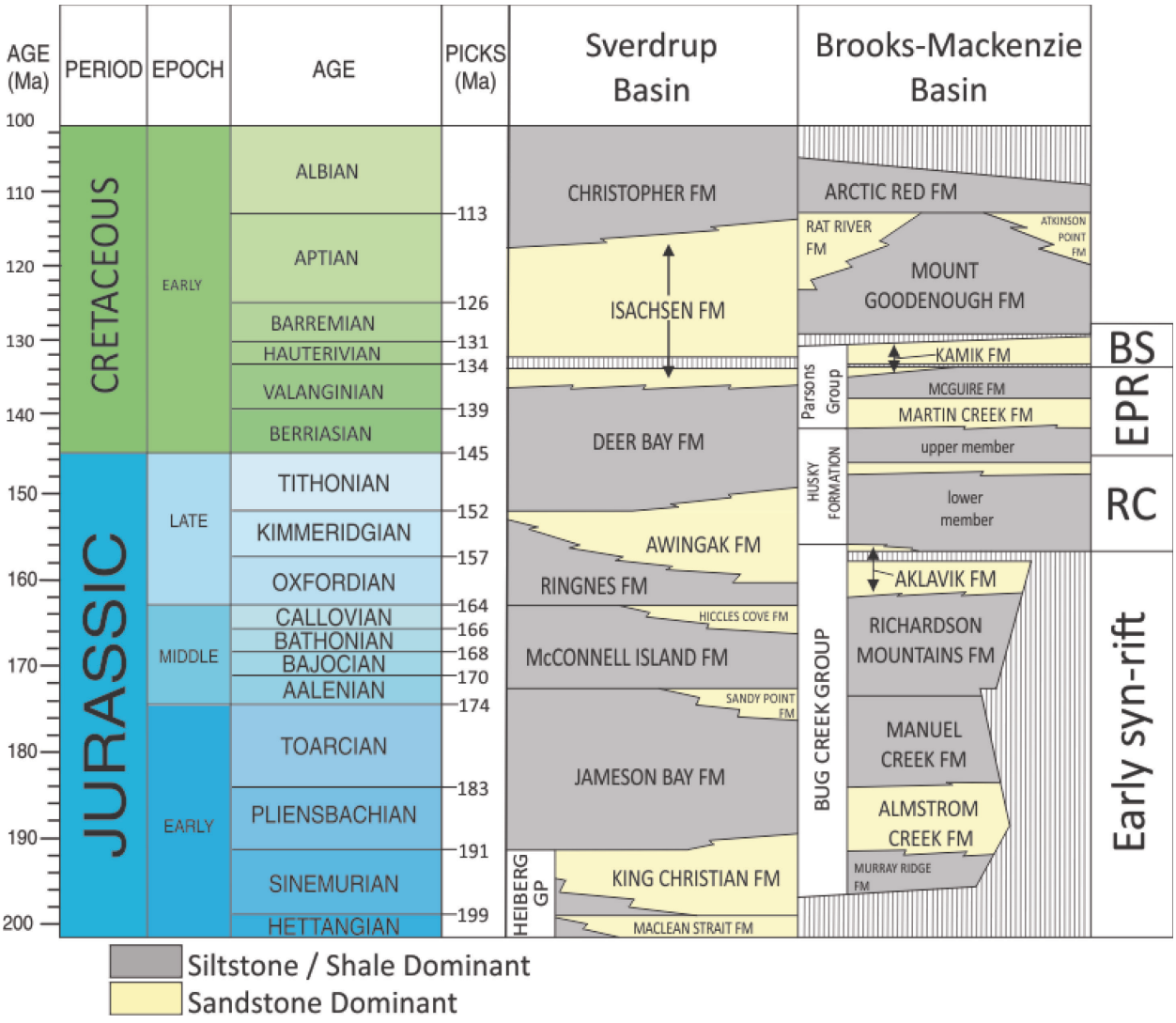

Figure 2-22: Comparing lithostratigraphic frameworks of the Brooks-Mackenzie Basin and Sverdrup Basin. RC: Rift climax, EPR: Early post-rift, BS: Breakup sequence.

BIBLIOGRAPHY

Balkwill, H.R., Cook, D.G., Detterman, R.L., Embry, A.F., Hakansson, E., Miall, A.D., Poulton, T.P., and Young, F.G., 1983. Arctic North America and northern Greenland. In: Moullade, M., and Nairn, A.E.M. (eds.), The Phanerozoic Geology of the World II, Elsevier, New York, p. 1 – 31.

Barnett, C. R., 2003. Integrated sedimentology and ichnology of the Jurassic Aklavik Formation, Northern Richardson Mountains and Mackenzie Delta, N.W.T. Unpublished M.Sc. Thesis, University of Alberta.

Brideaux, W.W., Chamney, T.P., Dunay, R.E., Fritz, W.H., Hopkins, W.S. Jr., Jeletzky, J.A., McGregor, D.C., Norford, B.S., Norris, A.W., Pedder, A.E.H., Sherrington, P.F., Sliter, W.V., Sweet, A.R., Uyeno, T.T., and Waterhouse, J.B., 1975. Biostratigraphic determinations of fossils from the subsurface of the District of Franklin and Mackenzie. Geological Survey of Canada Paper, 74-39.

Brozena, J.M., Childers, V.A., Lawver, L.A., Gahagan, L.M., Forsberg, R., Faleide, J.I., and Eldholm, O., 2003. New aerogeophysical study of the Eurasia Basin and Lomonosov Ridge: Implication for basin development. Geology, 31(9), p. 825 – 828.

Catuneanu, O., 2006. Principles of sequence stratigraphy. Elsevier, Amsterdam.

Catuneanu, O., 2019a. Model-independent sequence stratigraphy. Earth-Science Reviews, 188, p. 312 – 388.

Catuneanu, O., 2019b. Scale in sequence stratigraphy. Marine and Petroleum Geology, 106, p. 128 – 159.

Catuneanu, O., Abreu, V., Bhattacharya, J.P., Blum, M.D., Dalrymple, R.W., Eriksson, P.G., Fielding, C.R., Fisher, W.L., Galloway, W.E., Gibling, M.R., Giles, K.A., Holbrook, J.M., Jordan, R.,

Kendall, C.G.St.C., Macurda, B., Martinsen, O.J., Miall, A.D., Neal, J.E., Nummedal, D., Pomar, L., Posamentier, H.W., Pratt, B.R., Sarg, J.F., Shanley, K.W., Steel, R.J., Strasser, A., Tucker, M.E., and Winker, C., 2009. Towards the standardization of sequence stratigraphy. Earth-Science Reviews, 92(1-2), 1 – 33.

Chian, D., Jackson, H.R., Hutchinson, D.R., Shimeld, J.W., Oakey, G.N., Lebedeva-Ivanova, N., Li, Q., Saltus, R.W., and Mosher, D.C., 2016. Distribution of crustal types in Canada Basin, Arctic Ocean. Tectonophysics, 691, p. 8 – 30.

Collinson, J.D., 1969. The sedimentology of the Grindslow shales and the Kinderscout grit; a deltaic complex in the Namurian of northern England. Journal of Sedimentary Research, 39(1), 194 – 221.

Colpron, M., Crowley, J.L., Gehrels, G., Long, D.G.F., Murphy, D.C., Beranek, L., and Bickerton, L., 2015. Birth of the northern Cordilleran orogen, as recorded by detrital zircon in Jurassic synorogenic strata and regional exhumation in Yukon. Lithosphere, 7(5), p. 541 – 562.

Cook, F.A., Cofin, K.C., Lane, L.S., Dietrich, J.R., and Dixon, J., 1987. Structure of the southeast margin of the Beaufort-Mackenzie Basin, Arctic Canada, from crustal seismic-reflection data. Geology, 15(10), p. 931 – 935.

Dietrich, J.R., 1996. Seismic stratigraphy. In: Geological Atlas of the Beaufort-Mackenzie Area. J. Dixon (eds.), Miscellaneous Report, 59, p. 47 – 65.

Dixon, J., 1982. Jurassic and Lower Cretaceous subsurface stratigraphy of the Mackenzie Delta-Tuktoyaktuk Peninsula, N.W.T. Geological Survey of Canada Bulletin, 349.

Dixon, J., 1991. The Neocomian Parsons Group, northern Yukon and adjacent Northwest Territories. Geological Survey of Canada Bulletin, 406.

Dixon, J., 1997. Chapter 11: Cretaceous and Tertiary. In: The geology, mineral and hydrocarbon potential of northern Yukon Territory and northwestern District of Mackenzie. D.K. Norris (eds.), Geological Survey of Canada Bulletin, 422, p. 301 – 318.

Dixon, J., 2002. Description of some cores from the Beaufort-Mackenzie area, Northwest Territories. Geological Survey of Canada, Open File 4194.

Dixon, J., 2004. Jurassic-Lower Cretaceous (Oxfordian to Lower Aptian) (A contribution to the Geological Atlas of the northern Canadian mainland sedimentary basin). Geological Survey of Canada, Open File 4621.

Dixon, J., and Jeletzky, J.A., 1991. Stratigraphic nomenclature of Lower Cretaceous rocks in the northern Yukon and adjacent District of Mackenzie, Northwest Territories. Geological Survey of Canada Paper, 90-21.

Dixon, J., Lane, L.S., Dietrich, J.R., McNeil, D.H., and Chen, Z., 2019. Chapter 17: Geological History of the Late Cretaceous to Cenozoic Beaufort-Mackenzie Basin, Arctic Canada. In: The sedimentary basins in the United States and Canada. A.D. Miall (eds.), Elsevier, Amsterdam, p. 695 – 717.

Dott, R.H., and Bourgeois, J., 1982. Hummocky stratification: Significance of its variable bedding sequences. GSA Bulletin 93(8), p. 663-680.

Duke, W.L., 1985. Hummocky cross-stratification, tropical hurricanes, and intense winter storms. Sedimentology, 32(2), p. 167 – 194.

Embry, A.F., 1990. Geological and geophysical evidence in support of anticlockwise rotation of northern Alaska. Marine Geology, 93, p. 317 – 329.

Embry, A.F., and Dixon, J., 1990. The breakup unconformity of the Amerasia Basin, Arctic Ocean: Evidence from Arctic Canada. Geological Society of America Bulletin, 102(11), p. 1526 – 1534.

Falvey, D.A., 1974. The development of continental margins in plate tectonic theory. The APEGA Journal, 14(1), p. 95 – 107.

Gingras, M.K., MacEachern, J.A., and Dashtgard, S.E., 2011. Process ichnology and the elucidation of physico-chemical stress. Sedimentary Geology, 237(3-4), 115 – 134.

Gottlieb, E.S., Meisling, K.E., Miller, E.L., and Mull, C.G., 2014. Closing the Canada Basin: Detrital zircon geochronology relationship between the North Slope of Arctic Alaska and the Franklinian mobile belt of Arctic Canada. Geosphere, 10(6), p. 1366 – 1384.

Grantz, A., Eittreim, S., and Dinter, D.A., 1979. Geology and tectonic development of the continental margin north of Alaska. Tectonophysics, 15, p. 263 – 291.

Grantz, A., and May, S.D., 1982. Rifting history and structural development of the continental margin North of Alaska: Field Investigations of Margin Structure and Stratigraphy. In: J.S. Watkins and C.L. Drake (eds.), Studies in continental marine geology. American Association of Petroleum Geologists, Memoir 34, p. 77 – 100.

Grantz, A., Hart, P.E., and Childers, V.A., 2011. Geology and tectonic development of the Amerasia and Canada Basins, Arctic Ocean. In: Spencer, A.M., Embry, A.F., Gautier, D.L., and Sørenson, K. (eds.), Arctic Petroleum Geology, Memoir 35, Geological Society, London, p. 771 – 799.

Gupta, S., Cowie, P.A., Dawers, N.H., and Underhill, J.R., 1998. A mechanism to explain rift-basin subsidence and stratigraphic patterns through fault-array evolution. Geology, 26(7), p. 595 – 508.

Hadlari, T., Davis, W.J., Dewing, K., Heaman, L.M., Lemieux, Y., Ootes, L., Pratt, B.R., and Pyle, L.J., 2012. Two detrital zircon signatures for the Cambrian passive margin of northern Laurentia highlighted by new U-Pb results from northern Canada. GSA Bulletin, 124(7-8), p. 1155 – 1168.

Hadlari, T., Midwinter, D., Galloway, J.M., Dewing, K., and Durbano, A.M., 2016. Mesozoic rift to post-rift tectonostratigraphy of the Sverdrup Basin, Canadian Arctic. Marine and Petroleum Geology, 76, p. 148 – 158.

Hadlari, T., Millar, R.A., and Lane, L.S., 2020. The Eskimo Lakes fault zone renamed Husky Lakes fault zone, Tuktoyaktuk Peninsula, Northwest Territories. Geological Survey of Canada, Open File 8740.

Holz, M., Vilas-Boas, D.B., Troccoli, E.B., Santana, V.C., and Vidigal-Souza, P.A., 2017. Conceptual Models for Sequence Stratigraphy of Continental Rift Successions. In: Montenari, M. (eds.), Advances in Sequence Stratigraphy, Stratigraphy and Timescales 2, p. 119 – 186.

Hubbard, R.J., Edrich, S.P., and Rattey, R.P., 1987. Geologic evolution and hydrocarbon habitat of the 'Arctic Alaska Microplate'. Marine and Petroleum Geology, 4(1), p. 2 – 8.

James, N.P., and Dalrymple, R.W. (eds.), 2010. Facies models 4. Geological Association of Canada.

Jeletzky, J.A., 1960. Uppermost Jurassic and Cretaceous rocks, east flanks of Richardson Mountains between Stoney Creek and lower Donna River, Northwest Territories. Geological Survey of Canada Paper, 59-14.

Jeletzky, J.A., 1967. Jurassic and (?) Triassic rocks of the eastern slope of Richardson Mountains northwest District of Mackenzie. Geological Survey of Canada Paper, 66-50.

Jeletzky, J.A., 1980. Lower Cretaceous rocks od McDougall Pass area and some adjacent areas of north-central Richardson Mountains, northern Yukon Territory and northwest District of Mackenzie, N.W.T. Geological Survey of Canada Paper, 78-22.

Jervey, M.T., 1988. Quantitative geological modeling of siliciclastic rock sequences and their seismic expression. In: C.K. Wilgus, B.S. Hastings, C.G.St.C. Kendall, H.W. Posamentier, C.A. Ross and J.C. Van Wagoner (eds.), Sea-Level Changes: and Integrated Approach. Society Economic Paleontologists and Mineralogists, Spec. Publ. 42, p. 47 – 69.

Lemieux, Y., Hadlari, T., and Simonetti, A., 2011. Detrital zircon geochronology and provenance of Devono-Mississippian strata in the northern Canadian Cordilleran miogeocline. Canadian Journal of Earth Science, 48(2), 515 – 541.

MacEachern, J.A., and Pemberton, S.G., 1992. Ichnological aspects of Cretaceous shoreface successions and shoreface variability in the Western Interior Seaway of North America. In: Pemberton, S.G. (eds.), Application of Ichnology to Petroleum Exploration, A Core Workshop, SEPM, Core Workshop, 17, p. 57 – 84.

Matthews, W.A., and Guest, B., 2016. A practical approach for collecting large-n detrital zircon U-Pb data sets by quadrupole LA-ICP-MS. Geostandards and Geoanalytical Research, 41(2), p. 161 – 180.

Martins-Neto, M.A., and Catuneanu, O., 2010. Rift sequence stratigraphy. Marine and Petroleum Geology, 27(1), p. 247 – 253.

Miall, A.D., 1977. Lithofacies types and vertical profile models in braided river deposits: a summary. In: A.D. Miall (eds.), Fluvial Sedimentology. Canadian Society of Petroleum Geologists, Memoir 5, p. 597 – 604.

Miall, A.D., 1996. The geology of fluvial deposits: Sedimentary Facies, Basin Deposits, and Petroleum geology. Springer, Berlin.

Midwinter, D., Hadlari, T., Davis, W.J., and Dewing, K., 2016. Dual provenance signatures of the Triassic northern Laurentian margin from detrital-zircon U-Pb and Hf-isotopic analysis of Triassic-Jurassic strata in the Sverdrup Basin. Lithosphere, 8(6), p. 668 – 683.

Moore, J.G., 1992. A syn-rift to post-rift transition sequence in the Main Porcupine Basin, offshore Western Ireland. Geological Society, London, Special Publication, 62, p. 333 – 349.

Myhr, D.W., and Gunther, P.R., 1974. Lithostratigraphy and coal reflectance of a Lower Cretaceous deltaic succession in the Gulf Mobil Parson F-09 borehole, N.W.T. Geological Survey of Canada Paper, 74-18, p. 24 – 28.

Nelson, J.L., Colpron, M., Piercey, S.J., Dusel-Bacon, C., Murphy, D.C., and Roots, C.F., 2006. Paleozoic tectonic and metallogenic evolution of the pericratonic terranes in Yukon, northern British Columbia and eastern Alaska. In: M. Colpron and L.J. Nelson (eds.), Paleozoic Evolution and Metallogeny of the Pericratonic Terranes at the Ancient Pacific Margin of North America. Geological Association of Canada Special Paper 45, p. 323 – 360.

Nøttvedt, A., Gabrielsen, R.H., and Steel, R.J., 1995. Tectonostratigraphy and sedimentary architecture of rift basins, with reference to the northern North Sea. Marine and Petroleum Geology, 12(8), p. 881 – 901.

Pemberton, S.G., and Frey, R.W., 1984. The Glossifungites ichnofacies: Modern examples from the Georgia coast, U.S.A., In: H.A. Curran (eds.), Biogenic Structures: their use in interpreting depositional environments. Society of Economic Paleontologists and Mineralogists Special Publication, 35, p. 237 – 259.

Pemberton, S.G., MacEachern, J.A., Gingras, M.K., and Saunders, T.D.A., 2008. Biogenic chaos: Cryptobioturbation and the work of sedimentologically friendly organisms. Palaeogeography, Palaeoclimatology, Palaeoecology, 270(3-4), p. 273 – 279.

Plint, A.G., and Nummedal, D., 2000. The falling stage systems tract: recognition and importance in sequence stratigraphic analysis. Geological Society, London, Special Publication, 172, p. 1 – 17.

Poulton, T.P., 1997. Chapter 10: Jurassic. In: The geology, mineral and hydrocarbon potential of northern Yukon Territory and northwestern District of Mackenzie. D.K. Norris (ed.). Geological Survey of Canada Bulletin, 422, p. 267 – 297.

Poulton, T.P., Leskiw, K., and Audretsch, A., 1982. Stratigraphy and microfossils of the Jurassic Bug Creek Group of northern Yukon and adjacent Northwest Territories. Geological Survey of Canada Bulletin, 325.

Prosser, S., 1993. Rift-related linked depositional systems and their seismic expression. In: G.D. Williams and A. Dobb (eds.), Tectonics and seismic sequence stratigraphy. Geological Society, London, 71, p. 35 – 66.

Røhr, T.S., Andersen, T., Dypvik, H., and Embry, A.F., 2010. Detrital zircon characteristics of the Lower Cretaceous Isachsen Formation, Sverdrup Basin: source constraints from age and Hf isotope data. Canadian Journal of Earth Science, 47, p. 255 – 271.

Shepard, G.E., Müller, R.D., and Seton, M., 2013. The tectonic evolution of the Arctic Pangea breakup: Integrating constraints from surface geology and geophysics with mantle structure. Earth-Science Reviews, 124, p. 148 – 183.

Seilacher, D., 1967. Bathymetry of trace fossils. Marine Geology, 5(5-6), p. 413 – 428.

Soares, D.M., Alves, T.M., and Terrinha, P., 2012. The breakup sequence and associated lithospheric breakup surface: Their significance in the context of rifted continental margins (West Iberia and Newfoundland margins, North Atlantic). Earth and Planetary Science Letters, 355-256, p. 311 – 326.

Till, A.B., 2016. A synthesis of Jurassic and Early Cretaceous crustal evolution along the southern margin of the Arctic Alaska-Chukotka microplate and implications for defining tectonic boundaries active during opening of Arctic Ocean basins. Lithosphere, 8(3), p. 219 – 237.

Tullius, D.N., Leier, A.L., Galloway, J.M., Embry, A.F., and Pedersen, P.K., 2014. Sedimentology and stratigraphy of the Lower Cretaceous Isachsen Formation: Ellef Ringnes Island, Sverdrup Basin, Canadian Arctic Archipelago. Marine and Petroleum Geology, 57, p. 135 – 151.

Van Wagoner, J.C., 1995. Sequence stratigraphy and marine to nonmarine facies architecture of foreland basin strata, Book Cliffs, Utah, U.S.A. In: J.C. Van Wagoner and G.T. Bertram (eds.), Sequence stratigraphy of Foreland Basin Deposits. American Association of Petroleum Geologists Memoir, 64, p. 137 – 223.

Vial, P.R., Mitchum Jr., R. M., Todd, R.G., Widmier, J.M., Thomason III, S., Sangree, J.B., Bubb, J.N., and Hatledid, W.G., 1977. Seismic stratigraphy and global changes of sea-level. In: Seismic Stratigraphy – Applications to Hydrocarbon Exploration. C.E. Payton (ed.). American Association of Petroleum Geologists Memoir, 26, p. 49 – 212.

Vogt, P.R., Avery, O.E., 1974. Detailed magnetic surveys in the northeast Atlantic and Labrador Sea. Journal of Geophysical Research, 79(2), p. 363 – 389.

Wilson, R.C.L., 1975. Atlantic opening and Mesozoic continental margin basins of Iberia. Earth and Planetary Science Letters, 25(1), p. 33 – 43.

Chapter 3: Conclusions and future work

CONCLUSION

An ongoing scientific effort by a great number of researchers has reduced the uncertainty surrounding the opening of the Arctic Ocean since the initial concept was presented by Carey (1955). In this thesis, an attempt was made to add to this body of work by analyzing Jurassic to mid-Early Cretaceous strata deposited within the ancestral Brooks-Mackenzie Basin (Balkwill et al., 1983). Results and interpretations were based on an integrated data set, including core, outcrop, geophysical well-log, and detrital U-Pb zircon data. This integrated data set was then used to examine the sedimentology (e.g., Collinson, 1969), sequence stratigraphy (e.g., Catuneanu 2006, 2019a, b; Catuneanu et al., 2009), and underlying tectonic signatures (e.g., Prosser, 1993; Nøttvedt et al., 1995; Gupta et al., 1998; Soares et al., 2012). An attempt was made to relate these underlying tectonic signatures to the opening of the Arctic Ocean on a broader scale.

The main conclusions are as follows:

1. Sedimentology, stratigraphy, and stratigraphic geometry of the Jurassic to mid-Early Cretaceous strata within the study area are typical of a rift basin.
2. The sub-Jurassic unconformity likely represents the rift onset unconformity.
3. The Bug Creek Group represents early syn-rift strata and corresponds to a first-order LST. The primary source of sediment is the recycling of underlying strata.
4. The rift climax occurs just above the arenaceous member of the Husky Formation.
5. The timing of the rift climax in the study area appears to coincide with the timing of the rift climax in the Sverdrup Basin within the Deer Bay Formation.

6. The Husky to Martin Creek interval represents early post-rift deposits.
7. The influx of coarse-grained material within the Kamik Formation appears to coincide with a similar vertical facies succession in the Sverdrup Basin, which Hadlari et al. (2016) interprets as the breakup unconformity for the Arctic Ocean. This comparison is used to support the interpretation that the base-Kamik unconformity represents the breakup unconformity within the study area.
8. The Kamik Formation likely represents a breakup sequence (*sensu* Soares et al., 2012), terminating within the lowermost Mount Goodenough Formation.

FUTURE WORK

There is more work that could be done, both within the study area and outside of it. Within the study area, the two main additions would be the incorporation of seismic data and a more detailed examination of the detrital zircon data. First, there is some seismic data that is available within the Mackenzie Delta. Though data vintage may be an issue, attempts should be made to incorporate this data into the analysis. The potential of additional structural insights could be of great benefit. Furthermore, seismic stratigraphy could be a powerful tool to analyze the changing paleogeography on a regional scale. Second, because the primary focus of this thesis was sedimentology and sequence stratigraphy, only a preliminary assessment of the detrital zircon data was completed. A fuller attempt to link the detrital zircon signatures to regional trends and source areas should be undertaken. Some preliminary conclusions were drawn. However, a more integrated approach that included multiple pan-Arctic data sets could provide a deeper insight.

Another potential future contribution would be to expand this study to include younger strata. Here, the Jurassic to mid-Early Cretaceous was examined, which represents an approximately 70 Ma period. This period spans the opening of the Arctic Ocean, but younger strata will have to be examined to elucidate the effects of the North American Cordillera.

This study mainly focused on the Brooks-Mackenzie Basin, though attempts were made to correlate results to the Sverdrup Basin. Many similarities between the Brooks-Mackenzie and Sverdrup Basin were observed. This represents a good start, as this exercise has not yet been attempted with any detail. However, a broader future synthesis should include Arctic Alaska. Jurassic to mid-Early Cretaceous strata on Alaska's North Slope is also intimately related to the Brooks-Mackenzie and Sverdrup basins, as well as the formation of the Arctic Ocean. These three basins together demarcate the entire North American portion of the Arctic Ocean. Therefore, a synchronous examination of all three basins would provide additional insight, particularly regarding the potential identification of a breakup sequence. The best place to analyze Arctic Alaskan strata in relation to the formation of the Arctic Ocean would be within the Dinkum Graben System, which records the phases of extension within Arctic Alaska (Houseknecht and Connors, 2016).

BIBLIOGRAPHY

Balkwill, H.R., Cook, D.G., Detterman, R.L., Embry, A.F., Hakansson, E., Miall, A.D., Poulton, T.P., and Young, F.G., 1983. Arctic North America and northern Greenland. In: Moullade, M., and Nairn, A.E.M. (eds.), The Phanerozoic Geology of the World II, Elsevier, New York, p. 1 – 31.

Carey, S.W., 1955. The orocline concept in geotectonics. Paper and Proceedings of the Royal Society of Tasmania, 89, p. 255 – 288.

Catuneanu, O., 2006. Principles of sequence stratigraphy. Elsevier, Amsterdam.

Catuneanu, O., 2019a. Model-independent sequence stratigraphy. Earth-Science Reviews, 188, p. 312 – 388.

Catuneanu, O., 2019b. Scale in sequence stratigraphy. Marine and Petroleum Geology, 106, p. 128 – 159.

Catuneanu, O., Abreu, V., Bhattacharya, J.P., Blum, M.D., Dalrymple, R.W., Eriksson, P.G., Fielding, C.R., Fisher, W.L., Galloway, W.E., Gibling, M.R., Giles, K.A., Holbrook, J.M., Jordan, R., Kendall, C.G.St.C., Macurda, B., Martinsen, O.J., Miall, A.D., Neal, J.E., Nummedal, D., Pomar, L., Posamentier, H.W., Pratt, B.R., Sarg, J.F., Shanley, K.W., Steel, R.J., Strasser, A., Tucker, M.E., and Winker, C., 2009. Towards the standardization of sequence stratigraphy. Earth-Science Reviews, 92(1-2), 1 – 33.

Collinson, J.D., 1969. The sedimentology of the Grindslow shales and the Kinderscout grit; a deltaic complex in the Namurian of northern England. Journal of Sedimentary Research, 39(1), 194 – 221.

Houseknecht, D.W., and Connors, C.D., 2016. Dinkum Graben System beneath the Alaska Beaufort Shelf – Evidence for Mississippian to Early Cretaceous extension, and petroleum systems. AAPG Annual Convention and Exhibition, Calgary, Alberta, Canada.

Gupta, S., Cowie, P.A., Dawers, N.H., and Underhill, J.R., 1998. A mechanism to explain rift-basin subsidence and stratigraphic patterns through fault-array evolution. Geology, 26(7), p. 595 – 508.

Nøttvedt, A., Gabrielsen, R.H., and Steel, R.J., 1995. Tectonostratigraphy and sedimentary architecture of rift basins, with reference to the northern North Sea. Marine and Petroleum Geology, 12(8), p. 881 – 901.

Prosser, S., 1993. Rift-related linked depositional systems and their seismic expression. In: G.D. Williams and A. Dobb (eds.), Tectonics and seismic sequence stratigraphy. Geological Society, London, 71, p. 35 – 66.

Soares, D.M., Alves, T.M., and Terrinha, P., 2012. The breakup sequence and associated lithospheric breakup surface: Their significance in the context of rifted continental margins (West Iberia and Newfoundland margins, North Atlantic). Earth and Planetary Science Letters, 355-256, p. 311 – 326.

COMPREHENSIVE BIBLIOGRAPHY

Anfinson, O.A., Leier, A.L., Embry, A.F., and Dewing, K., 2012. Detrital zircon geochronology and provenance of the Neoproterozoic to Late Devonian Franklinian Basin, Canadian Arctic Islands. Geological Society of America Bulletin, 124(3-4), p. 415 – 430.

Anfinson, O.A., Embry, A.F., and Stockli, D.F., 2016. Geochronologic constraints on the Permian-Triassic northern source region of the Sverdrup Basin, Canadian Arctic Islands. Tectonophysics, 691, p. 206 – 219.

Balkwill, H.R., Cook, D.G., Detterman, R.L., Embry, A.F., Hakansson, E., Miall, A.D., Poulton, T.P., and Young, F.G., 1983. Arctic North America and northern Greenland. In: Moullade, M., and Nairn, A.E.M. (eds.), The Phanerozoic Geology of the World II, Elsevier, New York, p. 1 – 31.

Barnett, C. R., 2003. Integrated sedimentology and ichnology of the Jurassic Aklavik Formation, Northern Richardson Mountains and Mackenzie Delta, N.W.T. Unpublished M.Sc. Thesis, University of Alberta.

Beaufort Regional Environmental Assessment (BREA), 2013. Oil and Gas Exploration and Development Activity Forecast. Accessed August 28, 2020. <https://www.beaufortrea.ca/wp-content/uploads/2012/03/NCR-5358624-v4-BREA_-_FINAL_UPDATE_-_EXPLORATION_AND_ACTIVITY_FORECAST-__MAY_2013.pdf>

Brideaux, W.W., Chamney, T.P., Dunay, R.E., Fritz, W.H., Hopkins, W.S. Jr., Jeletzky, J.A., McGregor, D.C., Norford, B.S., Norris, A.W., Pedder, A.E.H., Sherrington, P.F., Sliter, W.V., Sweet, A.R., Uyeno, T.T., and Waterhouse, J.B., 1975. Biostratigraphic determinations of fossils from the subsurface of the District of Franklin and Mackenzie. Geological Survey of Canada Paper, 74-39.

Brozena, J.M., Childers, V.A., Lawver, L.A., Gahagan, L.M., Forsberg, R., Faleide, J.I., and Eldholm, O., 2003. New aerogeophysical study of the Eurasia Basin and Lomonosov Ridge: Implication for basin development. Geology, 31(9), p. 825 – 828.

Carey, S.W., 1955. The orocline concept in geotectonics. Paper and Proceedings of the Royal Society of Tasmania, 89, p. 255 – 288.

Catuneanu, O., 2006. Principles of sequence stratigraphy. Elsevier, Amsterdam.

Catuneanu, O., 2019a. Model-independent sequence stratigraphy. Earth-Science Reviews, 188, p. 312 – 388.

Catuneanu, O., 2019b. Scale in sequence stratigraphy. Marine and Petroleum Geology, 106, p. 128 – 159.

Catuneanu, O., Abreu, V., Bhattacharya, J.P., Blum, M.D., Dalrymple, R.W., Eriksson, P.G., Fielding, C.R., Fisher, W.L., Galloway, W.E., Gibling, M.R., Giles, K.A., Holbrook, J.M., Jordan, R., Kendall, C.G.St.C., Macurda, B., Martinsen, O.J., Miall, A.D., Neal, J.E., Nummedal, D., Pomar, L., Posamentier, H.W., Pratt, B.R., Sarg, J.F., Shanley, K.W., Steel, R.J., Strasser, A., Tucker, M.E., and Winker, C., 2009. Towards the standardization of sequence stratigraphy. Earth-Science Reviews, 92(1-2), 1 – 33.

Chian, D., Jackson, H.R., Hutchinson, D.R., Shimeld, J.W., Oakey, G.N., Lebedeva-Ivanova, N., Li, Q., Saltus, R.W., and Mosher, D.C., 2016. Distribution of crustal types in Canada Basin, Arctic Ocean. Tectonophysics, 691, p. 8 – 30.

Collinson, J.D., 1969. The sedimentology of the Grindslow shales and the Kinderscout grit; a deltaic complex in the Namurian of northern England. Journal of Sedimentary Research, 39(1), 194 – 221.

Colpron, M., and Nelson, J.L., 2009. A Palaeozoic Northwest Passage: incursion of Caledonian, Baltican and Siberian terranes into eastern Panthalassa, and the early evolution of the North American Cordillera. In: Cawood, P.A., and Kröner, A. (eds.), Earth Accretionary Systems in Space and Time, The Geological Society, London, Special Publication, 318, p. 273 – 307.

Colpron, M., Crowley, J.L., Gehrels, G., Long, D.G.F., Murphy, D.C., Beranek, L., and Bickerton, L., 2015. Birth of the northern Cordilleran orogen, as recorded by detrital zircon in Jurassic synorogenic strata and regional exhumation in Yukon. Lithosphere, 7(5), p. 541 – 562.

Cook, F.A., Cofin, K.C., Lane, L.S., Dietrich, J.R., and Dixon, J., 1987. Structure of the southeast margin of the Beaufort-Mackenzie Basin, Arctic Canada, from crustal seismic-reflection data. Geology, 15(10), p. 931 – 935.

Dietrich, J.R., 1996. Seismic stratigraphy. In: Geological Atlas of the Beaufort-Mackenzie Area. J. Dixon (eds.), Miscellaneous Report, 59, p. 47 – 65.

Dixon, J., 1982. Jurassic and Lower Cretaceous subsurface stratigraphy of the Mackenzie Delta-Tuktoyaktuk Peninsula, N.W.T. Geological Survey of Canada Bulletin, 349.

Dixon, J., 1991. The Neocomian Parsons Group, northern Yukon and adjacent Northwest Territories. Geological Survey of Canada Bulletin, 406.

Dixon, J., 1997. Chapter 11: Cretaceous and Tertiary. In: The geology, mineral and hydrocarbon potential of northern Yukon Territory and northwestern District of Mackenzie. D.K. Norris (eds.), Geological Survey of Canada Bulletin, 422, p. 301 – 318.

Dixon, J., 2002. Description of some cores from the Beaufort-Mackenzie area, Northwest Territories. Geological Survey of Canada, Open File 4194.

Dixon, J., 2004. Jurassic-Lower Cretaceous (Oxfordian to Lower Aptian) (A contribution to the Geological Atlas of the northern Canadian mainland sedimentary basin). Geological Survey of Canada, Open File 4621.

Dixon, J., and Jeletzky, J.A., 1991. Stratigraphic nomenclature of Lower Cretaceous rocks in the northern Yukon and adjacent District of Mackenzie, Northwest Territories. Geological Survey of Canada Paper, 90-21.

Dixon, J., Lane, L.S., Dietrich, J.R., McNeil, D.H., and Chen, Z., 2019. Chapter 17: Geological History of the Late Cretaceous to Cenozoic Beaufort-Mackenzie Basin, Arctic Canada. In: The sedimentary basins in the United States and Canada. A.D. Miall (eds.), Elsevier, Amsterdam, p. 695 – 717.

Døssing, A., Jackson, H.R., Matzka, J., Einarsson, I., Rasmussen, T.M., Olesen, A.V., and Brozena, J.M., 2013. On the origin of the Amerasia Basin and the High Arctic Large Igneous Province—Results of new aeromagnetic data. Earth and Planetary Science Letters, 363, p. 219 – 230.

Dott, R.H., and Bourgeois, J., 1982. Hummocky stratification: Significance of its variable bedding sequences. GSA Bulletin 93(8), p. 663-680.

Duke, W.L., 1985. Hummocky cross-stratification, tropical hurricanes, and intense winter storms. Sedimentology, 32(2), p. 167 – 194.

Embry, A.F., 1990. Geological and geophysical evidence in support of anticlockwise rotation of northern Alaska. Marine Geology, 93, p. 317 – 329.

Embry, A.F., 2000. Counterclockwise rotation of the Arctic Alaska Plate: Best available model or untenable hypothesis for the opening of the Amerasia Basin. Polarforschung, 68, p. 247 – 255.

Embry, A.F., and Dixon, J., 1990. The breakup unconformity of the Amerasia Basin, Arctic Ocean: Evidence from Arctic Canada. Geological Society of America Bulletin, 102(11), p. 1526 – 1534.

Falvey, D.A., 1974. The development of continental margins in plate tectonic theory. The APEGA Journal, 14(1), p. 95 – 107.

Gingras, M.K., MacEachern, J.A., and Dashtgard, S.E., 2011. Process ichnology and the elucidation of physico-chemical stress. Sedimentary Geology, 237(3-4), 115 – 134.

Gottlieb, E.S., Meisling, K.E., Miller, E.L., and Mull, C.G., 2014. Closing the Canada Basin: Detrital zircon geochronology relationship between the North Slope of Arctic Alaska and the Franklinian mobile belt of Arctic Canada. Geosphere, 10(6), p. 1366 – 1384.

Grantz, A., Eittreim, S., and Dinter, D.A., 1979. Geology and tectonic development of the continental margin north of Alaska. Tectonophysics, 15, p. 263 – 291.

Grantz, A., and May, S.D., 1982. Rifting history and structural development of the continental margin North of Alaska: Field Investigations of Margin Structure and Stratigraphy. In: J.S. Watkins and C.L. Drake (eds.), Studies in continental marine geology. American Association of Petroleum Geologists, Memoir 34, p. 77 – 100.

Grantz, A., Hart, P.E., and Childers, V.A., 2011. Geology and tectonic development of the Amerasia and Canada Basins, Arctic Ocean. In: Spencer, A.M., Embry, A.F., Gautier, D.L., and Sørenson, K. (eds.), Arctic Petroleum Geology, Memoir 35, Geological Society, London, p. 771 – 799.

Gupta, S., Cowie, P.A., Dawers, N.H., and Underhill, J.R., 1998. A mechanism to explain rift-basin subsidence and stratigraphic patterns through fault-array evolution. Geology, 26(7), p. 595 – 508.

Hadlari, T., Davis, W.J., Dewing, K., Heaman, L.M., Lemieux, Y., Ootes, L., Pratt, B.R., and Pyle, L.J., 2012. Two detrital zircon signatures for the Cambrian passive margin of northern Laurentia highlighted by new U-Pb results from northern Canada. GSA Bulletin, 124(7-8), p. 1155 – 1168.

Hadlari, T., Midwinter, D., Galloway, J.M., Dewing, K., and Durbano, A.M., 2016. Mesozoic rift to post-rift tectonostratigraphy of the Sverdrup Basin, Canadian Arctic. Marine and Petroleum Geology, 76, p. 148 – 158.

Hadlari, T., Midwinter, D., Poulton, T.P., and Matthews, W.A., 2017. A Pangean rim of fire: Reviewing the Triassic of western Laurentia. Lithosphere, 9(4), p. 579 – 582.

Hadlari, T., Millar, R.A., and Lane, L.S., 2020. The Eskimo Lakes fault zone renamed Husky Lakes fault zone, Tuktoyaktuk Peninsula, Northwest Territories. Geological Survey of Canada, Open File 8740.

Holz, M., Vilas-Boas, D.B., Troccoli, E.B., Santana, V.C., and Vidigal-Souza, P.A., 2017. Conceptual Models for Sequence Stratigraphy of Continental Rift Successions. In: Montenari, M. (eds.), Advances in Sequence Stratigraphy, Stratigraphy and Timescales 2, p. 119 – 186.

Hubbard, R.J., Edrich, S.P., and Rattey, R.P., 1987. Geologic evolution and hydrocarbon habitat of the 'Arctic Alaska Microplate'. Marine and Petroleum Geology, 4(1), p. 2 – 8.

Jakobsson, M., Mayer, L.A., Coakley, B., Dowdeswell, J.A., Forbes, S., Fridman, B., Hodnesdal, H., Noormets, R., Pedersen, R., Rebesco, M., Schenke, H.W. Zarayskaya, Y., Accettella, A.D., Armstrong, A., Anderson, R.M., Bienhoff, P., Camerlenghi, A., Church, I., Edwards, M., Gardner, J.V., Hall, J.K., Hell, B., Hestvik, O.B., Kristoffersen, Y., Marcussen, C., Mohammad, R., Mosher, D., Nghiem, S.V., Pedrosa, M.T., Travaglini, P.G., and Weatherall, P., 2012**.** The International

Bathymetric Chart of the Arctic Ocean (IBCAO) Version 3.0. Geophysical Research Letters, doi:10:1029/2012GL052219.

James, N.P., and Dalrymple, R.W. (eds.), 2010. Facies models 4. Geological Association of Canada.

Jeletzky, J.A., 1960. Uppermost Jurassic and Cretaceous rocks, east flanks of Richardson Mountains between Stoney Creek and lower Donna River, Northwest Territories. Geological Survey of Canada Paper, 59-14.

Jeletzky, J.A., 1967. Jurassic and (?) Triassic rocks of the eastern slope of Richardson Mountains northwest District of Mackenzie. Geological Survey of Canada Paper, 66-50.

Jeletzky, J.A., 1980. Lower Cretaceous rocks od McDougall Pass area and some adjacent areas of north-central Richardson Mountains, northern Yukon Territory and northwest District of Mackenzie, N.W.T. Geological Survey of Canada Paper, 78-22.

Jervey, M.T., 1988. Quantitative geological modeling of siliciclastic rock sequences and their seismic expression. In: C.K. Wilgus, B.S. Hastings, C.G.St.C. Kendall, H.W. Posamentier, C.A. Ross and J.C. Van Wagoner (eds.), Sea-Level Changes: and Integrated Approach. Society Economic Paleontologists and Mineralogists, Spec. Publ. 42, p. 47 – 69.

Lane, L.S., 1997. Canada Basin, Arctic Ocean: evidence against a rotational origin. Tectonophysics, 16(3), p. 309 – 322.

Lane, L.S., 2007. Devonian-Carboniferous paleogeography and orogenesis, northern Yukon and adjacent Arctic Alaska. Canadian Journal of Earth Science, 44(5), p. 679 – 694.

Lawver, L.A., and Scotese, C.R., 1990. A review of tectonic models for the evolution of the Canada Basin. In: Grantz, A., Johnson, G.L., and Sweeney, J.F. (eds.), The Arctic Ocean Region, The Geology of North America, 1, p. 593 – 618.

Lemieux, Y., Hadlari, T., and Simonetti, A., 2011. Detrital zircon geochronology and provenance of Devono-Mississippian strata in the northern Canadian Cordilleran miogeocline. Canadian Journal of Earth Science, 48(2), 515 – 541.

MacEachern, J.A., and Pemberton, S.G., 1992. Ichnological aspects of Cretaceous shoreface successions and shoreface variability in the Western Interior Seaway of North America. In: Pemberton, S.G. (eds.), Application of Ichnology to Petroleum Exploration, A Core Workshop, SEPM, Core Workshop, 17, p. 57 – 84.

Matthews, W.A., and Guest, B., 2016. A practical approach for collecting large-n detrital zircon U-Pb data sets by quadrupole LA-ICP-MS. Geostandards and Geoanalytical Research, 41(2), p. 161 – 180.

Martins-Neto, M.A., and Catuneanu, O., 2010. Rift sequence stratigraphy. Marine and Petroleum Geology, 27(1), p. 247 – 253.

Miall, A.D., 1977. Lithofacies types and vertical profile models in braided river deposits: a summary. In: A.D. Miall (eds.), Fluvial Sedimentology. Canadian Society of Petroleum Geologists, Memoir 5, p. 597 – 604.

Miall, A.D., 1996. The geology of fluvial deposits: Sedimentary Facies, Basin Deposits, and Petroleum geology. Springer, Berlin.

Midwinter, D., Hadlari, T., Davis, W.J., and Dewing, K., 2016. Dual provenance signatures of the Triassic northern Laurentian margin from detrital-zircon U-Pb and Hf-isotopic analysis of Triassic-Jurassic strata in the Sverdrup Basin. Lithosphere, 8(6), p. 668 – 683.

Miller, E.L., Gehrels, G.E., Pease, V., and Sokolov, S., 2010. Stratigraphy and U-Pb detrital zircon geochronology of Wrangel Islands, Russia: implications for Arctic paleogeography. AAPG Bulletin, 94(5), p. 665 – 692.

Moore, J.G., 1992. A syn-rift to post-rift transition sequence in the Main Porcupine Basin, offshore Western Ireland. Geological Society, London, Special Publication, 62, p. 333 – 349.

Myhr, D.W., and Gunther, P.R., 1974. Lithostratigraphy and coal reflectance of a Lower Cretaceous deltaic succession in the Gulf Mobil Parson F-09 borehole, N.W.T. Geological Survey of Canada Paper, 74-18, p. 24 – 28.

Nelson, J.L., Colpron, M., Piercey, S.J., Dusel-Bacon, C., Murphy, D.C., and Roots, C.F., 2006. Paleozoic tectonic and metallogenic evolution of the pericratonic terranes in Yukon, northern British Columbia and eastern Alaska. In: M. Colpron and L.J. Nelson (eds.), Paleozoic Evolution and Metallogeny of the Pericratonic Terranes at the Ancient Pacific Margin of North America. Geological Association of Canada Special Paper 45, p. 323 – 360.

Norris, D.K., 1985. Geology of the Northern Yukon and Northwest District of Mackenzie. Geological Survey of Canada, "A" Series Map 1581A. <https://doi.org/10.4095/120537>.

Norris, D.K. (eds.), 1997. Geology and Mineral and hydrocarbon potential of northern Yukon Territory and Northwestern District of Mackenzie, Geological Survey of Canada Bulletin, 422.

Nøttvedt, A., Gabrielsen, R.H., and Steel, R.J., 1995. Tectonostratigraphy and sedimentary architecture of rift basins, with reference to the northern North Sea. Marine and Petroleum Geology, 12(8), p. 881 – 901.

NRCan, 2019. About Geo-mapping for Energy and Minerals (GEM) program. Accessed June 2, 2020. <https://www.nrcan.gc.ca/science-data/earth-sciences/earth-sciences-resources/earth-sciences-federal-programs/gem-geo-mapping-energy-minerals/about-geo-mapping-energy-minerals-gem-program/21817>.

Pemberton, S.G., and Frey, R.W., 1984. The Glossifungites ichnofacies: Modern examples from the Georgia coast, U.S.A., In: H.A. Curran (eds.), Biogenic Structures: their use in interpreting depositional environments. Society of Economic Paleontologists and Mineralogists Special Publication, 35, p. 237 – 259.

Pemberton, S.G., MacEachern, J.A., Gingras, M.K., and Saunders, T.D.A., 2008. Biogenic chaos: Cryptobioturbation and the work of sedimentologically friendly organisms. Palaeogeography, Palaeoclimatology, Palaeoecology, 270(3-4), p. 273 – 279.

Plint, A.G., and Nummedal, D., 2000. The falling stage systems tract: recognition and importance in sequence stratigraphic analysis. Geological Society, London, Special Publication, 172, p. 1 – 17.

Poulton, T.P., 1997. Chapter 10: Jurassic. In: The geology, mineral and hydrocarbon potential of northern Yukon Territory and northwestern District of Mackenzie. D.K. Norris (ed.). Geological Survey of Canada Bulletin, 422, p. 267 – 297.

Poulton, T.P., Leskiw, K., and Audretsch, A., 1982. Stratigraphy and microfossils of the Jurassic Bug Creek Group of northern Yukon and adjacent Northwest Territories. Geological Survey of Canada Bulletin, 325.

Prosser, S., 1993. Rift-related linked depositional systems and their seismic expression. In: G.D. Williams and A. Dobb (eds.), Tectonics and seismic sequence stratigraphy. Geological Society, London, 71, p. 35 – 66.

Rickwood, F.K., 1970. The Prudhoe Bay Field. In: Adkinson, W.L., and Brosgè, W.P. (eds.), Proceedings of the geological seminar on the North Slope of Alaska, AAPG, Pacific Section, L1 – L11.

Røhr, T.S., Andersen, T., Dypvik, H., and Embry, A.F., 2010. Detrital zircon characteristics of the Lower Cretaceous Isachsen Formation, Sverdrup Basin: source constraints from age and Hf isotope data. Canadian Journal of Earth Science, 47, p. 255 – 271.

Shepard, G.E., Müller, R.D., and Seton, M., 2013. The tectonic evolution of the Arctic Pangea breakup: Integrating constraints from surface geology and geophysics with mantle structure. Earth-Science Reviews, 124, p. 148 – 183.

Seilacher, D., 1967. Bathymetry of trace fossils. Marine Geology, 5(5-6), p. 413 – 428.

Soares, D.M., Alves, T.M., and Terrinha, P., 2012. The breakup sequence and associated lithospheric breakup surface: Their significance in the context of rifted continental margins (West Iberia and Newfoundland margins, North Atlantic). Earth and Planetary Science Letters, 355-256, p. 311 – 326.

Tailleur, L.L., 1969. Rifting speculation of the geology of Alaska's North Slope. Oil and Gas Journal, 19, p. 128 – 130.

Till, A.B., 2016. A synthesis of Jurassic and Early Cretaceous crustal evolution along the southern margin of the Arctic Alaska-Chukotka microplate and implications for defining tectonic boundaries active during opening of Arctic Ocean basins. Lithosphere, 8(3), p. 219 – 237.

Tullius, D.N., Leier, A.L., Galloway, J.M., Embry, A.F., and Pedersen, P.K., 2014. Sedimentology and stratigraphy of the Lower Cretaceous Isachsen Formation: Ellef Ringnes Island, Sverdrup Basin, Canadian Arctic Archipelago. Marine and Petroleum Geology, 57, p. 135 – 151.

Van Wagoner, J.C., 1995. Sequence stratigraphy and marine to nonmarine facies architecture of foreland basin strata, Book Cliffs, Utah, U.S.A. In: J.C. Van Wagoner and G.T. Bertram (eds.), Sequence stratigraphy of Foreland Basin Deposits. American Association of Petroleum Geologists Memoir, 64, p. 137 – 223.

Vial, P.R., Mitchum Jr., R. M., Todd, R.G., Widmier, J.M., Thomason III, S., Sangree, J.B., Bubb, J.N., and Hatledid, W.G., 1977. Seismic stratigraphy and global changes of sea-level. In: Seismic Stratigraphy – Applications to Hydrocarbon Exploration. C.E. Payton (ed.). American Association of Petroleum Geologists Memoir, 26, p. 49 – 212.

Vogt, P.R., and Ostenso, N.A., 1970. Magnetic and gravity profiles across the Alpha Cordillera and their relation to Arctic sea-floor spreading. Journal of Geophysical Research, 75(26), p. 4925 – 4937.

Vogt, P.R., Avery, O.E., 1974. Detailed magnetic surveys in the northeast Atlantic and Labrador Sea. Journal of Geophysical Research, 79(2), p. 363 – 389.

Wilson, R.C.L., 1975. Atlantic opening and Mesozoic continental margin basins of Iberia. Earth and Planetary Science Letters, 25(1), p. 33 – 43.

Appendix A:

U-Pb detrital zircon data

Accepted Dates

Date (Ma)	$2s_{total}$ (ABS)
P-MR-103	
396.9	17.8
397.5	19.1
407.2	21.7
419.3	20.6
422.3	15.3
432.5	15.5
445.8	17.2
447.6	17.2
453.6	18.0
533.6	20.1
539.5	21.2
554.4	29.8
649.5	21.7
1089.9	38.3
1132.7	56.3
1144.6	29.8
1153.3	31.6
1198.9	33.5
1224.0	38.9
1232.5	50.3
1241.1	39.0
1306.7	37.7
1373.7	35.7
1381.0	44.7
1392.9	34.3
1429.2	49.5
1480.6	52.4
1489.8	42.5
1500.1	42.1
1502.1	45.4
1505.7	62.0
1511.3	43.2
1538.0	112.3
1544.4	52.8
1574.9	56.8
1584.5	97.4
1597.8	113.7
1624.1	64.7
1640.7	73.7
1640.7	71.5
1669.9	69.0
1696.7	94.7
1705.5	49.5
1752.4	98.6
1774.4	69.4
1776.1	47.1
1794.4	72.5
1802.7	63.0
1814.2	104.3
1837.0	67.8
1837.0	80.0
1884.6	61.5
1915.5	94.1
1917.0	27.6
1933.7	58.8
1941.3	104.8
1968.1	101.4
2116.8	87.1
2357.3	117.3
2652.9	124.4
2713.3	57.9
2802.3	33.3
SC-MR-203	
370.1	25.4
401.7	19.2
401.7	20.4
402.3	17.7
404.8	15.4
416.8	19.3
428.9	15.6
432.5	18.4
436.8	21.3
436.8	21.6
438.0	24.2
438.6	17.4
442.2	18.0
444.0	21.7
449.4	21.6
457.2	18.9
475.8	26.1
475.8	20.6
475.8	26.2
477.0	23.1
493.1	27.6
503.3	19.9
514.6	14.9
549.6	24.3
599.7	20.4
606.8	25.0
618.5	45.5
625.5	40.7
636.1	27.1
655.3	26.7
870.6	56.2
892.5	42.4
894.2	41.5
899.8	32.4
931.7	27.9
944.0	39.1
966.8	38.9
967.9	70.7
967.9	37.3
974.5	36.9
975.1	42.0
977.9	33.1
983.4	35.7
985.6	38.6
991.1	42.9
994.5	53.5
997.2	47.5
998.3	37.1
1014.9	42.7
1029.7	44.4
1030.8	52.9
1044.5	54.4
1046.7	34.6
1054.9	42.6
1061.0	48.9
1071.3	40.7
1078.4	38.0
1084.4	48.3
1088.2	48.8
1099.7	45.5
1105.1	73.1
1110.0	47.5
1112.2	38.3
1114.3	65.7
1118.1	42.6
1120.3	37.2
1126.8	38.1
1126.8	32.4
1141.9	64.3
1144.6	56.6
1148.9	47.6
1152.7	34.6
1153.3	45.2
1155.4	40.6
1183.9	46.1
1190.9	41.4
1192.0	48.3
1196.2	48.4
1201.6	64.1
1204.3	35.7
1208.5	53.4
1210.7	49.0
1211.2	41.2
1217.6	54.6
1228.3	41.6
1235.2	45.1
1235.7	38.6
1248.0	51.4
1249.6	40.2
1250.1	49.4
1283.5	54.3
1283.5	40.0
1292.4	78.1
1295.1	53.4
1302.4	51.7
1315.6	39.9
1329.8	48.1
1339.7	64.8
1355.4	72.3
1356.5	40.2
1362.2	43.2
1375.8	44.1
1381.5	63.8
1407.5	44.9
1414.7	45.4
1416.3	63.6
1435.4	58.2
1444.1	60.8
1447.8	44.1
1448.8	37.9
1452.4	49.7
1463.7	55.9
1464.2	68.8
1496.0	62.7
1498.0	115.5
1499.0	42.4
1499.6	43.9
1500.1	53.2
1514.9	39.6
1520.0	45.1

1520.0	53.7	1698.5	147.9	1867.3	58.4	2700.9	53.4	454.8	19.2	1048.4	52.9
1522.5	60.4	1698.5	89.5	1883.0	71.6	2717.7	103.4	482.4	17.8	1049.5	27.3
1523.0	49.9	1700.2	56.0	1893.9	75.7	2726.5	57.5	599.7	24.4	1060.4	54.7
1526.6	50.4	1710.8	88.7	1900.1	72.7	2728.2	39.2	605.0	22.9	1062.1	39.1
1531.7	49.8	1712.6	68.4	1904.7	83.1	2730.0	54.6	615.0	22.9	1064.8	30.4
1533.2	45.9	1712.6	87.7	1930.7	59.1	2730.9	50.8	615.0	25.0	1067.0	36.6
1588.3	81.7	1721.3	66.7	1942.8	41.6	2750.8	59.1	623.2	22.0	1073.0	35.6
1594.0	98.9	1723.0	97.0	1950.3	89.6	2765.3	43.1	646.6	25.8	1106.2	32.9
1597.8	80.2	1733.5	108.7	1968.1	103.4	2768.7	29.7	654.7	21.7	1110.5	71.6
1611.0	65.3	1738.6	67.9	1969.5	77.6	2792.3	59.8	683.8	35.4	1111.1	43.8
1614.8	88.3	1743.8	78.3	1972.5	66.3	2793.2	38.2	749.5	23.9	1115.4	31.8
1618.5	65.7	1755.8	48.6	1985.7	103.9	2801.5	45.9	939.5	44.8	1116.0	59.6
1620.4	145.8	1760.9	110.8	1987.1	46.3	2808.1	65.6	955.1	59.9	1119.2	33.6
1622.2	85.0	1764.3	69.4	2017.4	68.9	2811.4	53.0	968.4	34.3	1122.5	55.3
1625.9	78.7	1769.3	70.0	2028.8	60.7	**AC-MR-298**		969.0	32.5	1125.2	50.1
1627.8	66.7	1781.1	66.8	2030.2	92.3	363.5	16.8	974.0	31.8	1132.7	53.9
1633.4	103.6	1787.8	77.8	2030.2	49.4	366.5	16.4	976.2	41.1	1135.4	45.3
1642.6	88.4	1794.4	68.9	2035.9	52.8	392.0	21.0	996.1	40.3	1136.5	33.9
1648.1	59.0	1797.7	88.4	2069.3	35.7	392.6	15.3	996.7	35.3	1136.5	51.6
1648.1	89.1	1799.4	77.3	2088.5	76.1	398.1	19.1	997.2	28.2	1143.0	44.3
1653.6	72.3	1801.1	41.0	2139.3	62.1	404.1	16.3	1002.7	38.7	1143.0	47.8
1668.1	157.3	1804.4	55.0	2499.4	51.6	411.4	22.9	1005.5	57.9	1150.6	40.4
1669.9	72.4	1817.5	72.0	2512.6	55.0	413.8	16.3	1019.8	34.7	1152.2	32.3
1671.7	77.9	1825.6	91.0	2521.8	72.0	433.1	14.0	1024.8	35.5	1159.7	35.7
1671.7	96.7	1825.6	113.9	2536.8	54.7	433.1	20.2	1030.8	31.3	1160.8	36.3
1673.5	61.6	1833.7	122.7	2558.6	61.9	434.3	17.5	1030.8	34.9	1166.2	33.0
1680.7	69.5	1833.7	70.0	2567.5	85.9	436.8	36.8	1031.4	49.4	1173.2	38.1
1680.7	77.6	1837.0	62.8	2589.8	47.0	441.6	17.8	1034.7	46.0	1175.3	50.2
1680.7	57.1	1843.4	47.0	2601.3	97.2	441.6	19.7	1035.8	33.5	1179.6	49.1
1686.0	79.4	1845.0	88.0	2625.9	56.3	445.8	21.7	1044.5	40.7	1180.7	69.5
1694.9	153.3	1849.8	73.1	2685.7	74.6	451.2	26.3	1044.5	33.2	1186.1	41.6
1696.7	76.6	1857.8	119.8	2687.5	82.5	453.0	25.1	1045.1	32.2	1187.7	41.2

1197.8	37.2	1482.2	49.4	1662.6	66.3	1814.2	92.9	1953.2	60.3	2742.2	30.2
1200.0	42.8	1483.7	47.8	1668.1	67.2	1817.5	55.6	1962.2	116.0	2742.2	39.7
1207.5	95.1	1485.7	53.5	1673.5	56.9	1822.4	111.0	1965.1	55.5	2747.3	55.5
1230.9	69.1	1485.7	41.0	1675.3	93.0	1825.6	54.5	1969.5	94.3	2748.2	35.5
1249.0	30.7	1488.8	60.0	1678.9	53.4	1830.5	52.7	1972.5	72.6	2794.8	33.2
1250.1	59.4	1490.9	46.0	1678.9	104.1	1832.1	54.9	1979.8	144.5	2799.0	78.4
1260.7	71.2	1496.5	41.1	1680.7	63.5	1832.1	65.3	1994.4	65.2	2805.6	34.5
1263.9	41.0	1498.0	51.5	1686.0	99.8	1832.1	127.1	1994.4	45.1	2825.4	33.9
1285.6	50.6	1498.5	55.9	1686.0	111.0	1837.0	101.4	1995.9	43.4	2856.1	78.6
1297.7	61.7	1504.2	44.5	1689.6	97.0	1837.0	48.8	2011.7	52.8	2858.5	36.7
1299.3	42.2	1505.2	68.1	1696.7	76.1	1845.0	103.5	2020.3	34.4	2877.5	60.1
1313.5	40.3	1526.1	46.6	1703.8	57.7	1853.0	76.5	2021.7	127.4	**RM-MR-437**	
1355.4	69.1	1531.7	43.2	1707.3	58.1	1857.8	50.6	2030.2	44.3	399.9	22.5
1364.8	40.4	1545.9	99.8	1707.3	73.6	1857.8	67.2	2031.6	99.4	400.5	14.9
1370.0	46.4	1555.6	87.8	1717.8	126.5	1864.1	82.6	2042.9	78.1	404.1	18.9
1375.8	54.1	1565.3	97.3	1719.6	51.8	1867.3	80.7	2085.8	69.7	408.4	15.3
1377.9	46.3	1565.3	79.2	1738.6	68.5	1868.9	65.1	2128.7	72.2	419.3	18.9
1382.5	52.7	1576.8	80.6	1740.4	90.4	1873.6	146.4	2269.9	36.4	421.7	20.4
1386.7	75.4	1588.3	86.2	1745.5	44.8	1875.2	53.1	2285.4	41.6	422.3	15.8
1403.3	45.1	1609.1	90.2	1748.9	43.4	1892.4	62.6	2365.2	82.0	425.3	14.1
1403.8	42.6	1612.9	68.0	1754.1	71.3	1901.7	52.5	2382.0	46.6	425.3	20.0
1427.6	46.9	1618.5	65.4	1757.5	55.6	1910.9	62.4	2395.2	67.5	426.5	20.0
1428.7	39.2	1620.4	84.6	1765.9	56.8	1917.0	71.1	2432.2	69.6	426.5	21.2
1432.3	37.3	1622.2	63.0	1781.1	103.9	1923.1	56.8	2439.7	72.0	431.3	19.5
1443.6	44.5	1625.9	84.1	1781.1	61.2	1923.1	104.6	2506.5	54.4	433.1	25.9
1450.3	52.4	1637.0	59.3	1782.8	58.4	1924.6	85.7	2569.4	65.8	433.7	19.2
1451.4	42.7	1638.9	70.2	1794.4	44.0	1926.2	92.7	2604.1	60.8	442.8	17.0
1451.9	42.4	1642.6	195.3	1797.7	48.5	1927.7	56.0	2626.8	56.4	444.0	21.0
1471.4	50.0	1649.9	83.8	1799.4	197.8	1927.7	57.6	2674.8	55.0	447.6	16.8
1477.0	40.9	1649.9	150.9	1799.4	91.8	1933.7	52.1	2690.2	88.4	447.6	19.3
1477.7	138.6	1651.7	69.2	1799.4	71.2	1935.2	100.0	2703.6	40.3	509.2	19.0
1481.7	40.5	1653.6	102.7	1807.7	81.3	1953.2	70.5	2703.6	53.6	513.4	19.6

557.9	20.4	1022.0	33.6	1154.9	46.6	1443.6	45.3	1616.6	44.8	1755.8	50.4
633.1	26.7	1029.2	41.5	1157.6	34.7	1459.6	43.5	1622.2	46.9	1757.5	51.7
643.1	49.0	1029.2	46.4	1169.4	42.9	1461.6	38.7	1629.7	62.8	1767.6	43.1
654.1	26.6	1031.4	42.6	1173.2	35.1	1471.4	54.0	1629.7	65.5	1769.3	104.1
661.7	24.6	1044.0	38.6	1174.2	42.4	1473.4	44.9	1635.2	74.1	1774.4	114.8
676.8	28.0	1045.1	38.8	1180.2	33.5	1473.4	47.7	1640.7	95.0	1779.4	52.6
871.2	31.5	1047.8	36.0	1182.3	47.3	1477.6	38.7	1642.6	177.3	1786.1	61.8
897.6	27.1	1050.0	32.0	1183.4	34.8	1480.1	40.2	1646.2	110.3	1791.1	59.3
934.5	27.0	1054.4	34.8	1191.4	46.0	1483.7	52.3	1649.9	57.0	1794.4	64.5
937.3	33.1	1057.7	56.9	1194.1	49.2	1484.7	79.4	1651.7	79.0	1801.1	74.4
945.7	30.8	1063.1	28.4	1211.2	40.8	1485.7	46.8	1655.4	68.9	1802.7	66.1
947.9	41.5	1063.7	50.2	1212.8	63.8	1489.8	50.6	1657.2	96.7	1806.0	170.6
953.4	38.5	1067.5	54.0	1218.2	38.0	1490.4	41.1	1666.3	53.7	1819.1	54.6
957.9	49.7	1068.6	43.5	1225.6	39.5	1495.0	43.5	1671.7	99.7	1819.1	59.1
961.2	31.5	1072.4	37.2	1234.1	115.4	1500.1	49.5	1671.7	67.4	1825.6	77.6
965.1	32.8	1075.7	46.0	1243.7	37.6	1505.2	45.4	1675.3	59.7	1840.2	42.4
967.3	42.8	1076.3	34.4	1248.5	37.4	1511.3	62.5	1675.3	105.6	1864.1	57.3
967.9	43.6	1077.9	51.7	1251.2	40.0	1516.9	48.8	1675.3	56.7	1872.0	51.7
968.4	42.6	1080.1	40.4	1263.9	43.2	1516.9	64.4	1682.5	91.5	1873.6	81.1
971.2	40.6	1081.2	44.7	1282.9	41.3	1519.4	37.8	1684.2	172.7	1884.6	110.7
971.8	39.5	1082.8	54.8	1299.8	47.3	1522.5	53.3	1693.2	45.2	1886.1	87.9
982.8	55.2	1094.2	43.8	1304.0	39.4	1525.0	37.3	1702.0	77.3	1886.1	50.4
990.0	38.8	1099.1	43.1	1314.0	44.0	1533.7	37.7	1702.0	58.1	1904.7	70.7
997.8	35.4	1108.9	50.4	1318.2	60.3	1535.7	50.6	1719.6	162.7	1907.8	54.1
1002.2	29.2	1113.8	38.0	1320.9	44.6	1567.2	65.0	1721.3	61.5	1921.6	87.1
1003.3	32.1	1113.8	57.3	1324.0	40.9	1569.1	54.9	1724.8	61.4	1924.6	74.4
1004.4	56.6	1118.1	38.8	1347.6	42.2	1582.6	71.0	1733.5	102.1	1944.3	91.0
1006.6	67.3	1118.1	41.1	1356.5	43.7	1594.0	49.8	1736.9	83.4	1944.3	58.9
1009.4	29.4	1120.8	55.0	1420.9	38.7	1597.8	82.8	1736.9	56.7	1965.1	59.4
1009.9	38.4	1121.4	30.5	1423.0	65.2	1605.4	68.3	1747.2	69.4	1981.3	52.7
1011.0	51.5	1121.4	41.7	1433.8	45.2	1609.1	56.9	1754.1	101.8	1984.2	175.5
1014.3	35.6	1127.9	49.2	1435.4	51.6	1614.8	123.4	1754.1	120.5	1997.3	41.1

2013.1	75.3	414.4	24.7	1006.6	61.3	1362.2	40.9	1812.6	72.4	1936.7	65.4
2021.7	38.6	419.3	21.1	1007.2	28.3	1373.2	45.0	1827.3	72.2	1939.8	59.5
2045.7	70.2	420.5	18.0	1017.6	38.1	1384.6	54.0	1835.4	43.7	1950.3	110.3
2084.4	291.8	422.9	27.1	1019.8	42.6	1416.8	37.9	1856.2	153.2	1953.2	53.3
2091.2	67.9	424.1	24.5	1021.5	50.2	1432.8	43.2	1857.8	116.5	1953.2	61.5
2104.7	109.1	427.7	23.2	1026.4	48.6	1433.3	154.4	1861.0	82.0	1953.2	71.2
2246.9	89.6	428.3	19.3	1034.1	35.6	1463.3	141.0	1865.7	77.7	1953.2	84.2
2314.8	59.0	431.3	15.2	1040.1	57.2	1478.6	53.4	1867.3	65.7	1963.6	72.8
2368.5	114.5	434.3	16.7	1051.7	38.2	1482.2	39.5	1867.3	99.3	1965.1	53.9
2420.4	41.7	435.6	23.8	1056.0	36.9	1499.0	61.3	1868.9	67.3	1978.4	62.7
2538.8	50.2	442.2	16.5	1056.6	29.1	1522.1	139.4	1870.5	90.3	1979.8	47.5
2589.8	44.6	442.8	29.6	1070.8	50.8	1527.6	59.7	1879.9	70.7	1979.8	59.9
2634.3	44.6	442.8	18.0	1071.3	29.5	1537.8	60.1	1879.9	80.0	1981.3	75.5
2649.2	46.3	443.4	18.6	1082.3	56.5	1548.9	55.4	1884.6	67.3	1990.0	66.6
2690.2	48.1	450.6	20.3	1099.1	41.1	1629.7	51.5	1886.1	146.2	1991.5	126.6
2690.2	39.9	454.2	29.2	1130.6	55.4	1638.9	76.8	1890.8	89.4	1995.9	65.0
2721.2	62.3	459.0	25.9	1136.0	46.0	1642.6	122.3	1892.4	44.9	2000.2	70.9
2731.7	61.2	460.2	15.4	1146.8	30.4	1644.4	83.9	1897.0	68.3	2000.2	67.5
2738.7	55.7	464.4	20.2	1148.4	61.7	1648.1	123.6	1907.8	60.8	2003.1	122.4
2745.6	45.4	490.7	31.1	1164.6	56.2	1668.1	67.6	1909.4	59.9	2006.0	74.5
2754.2	39.4	575.0	22.0	1175.9	55.5	1673.5	102.9	1909.4	44.5	2010.3	67.1
2778.9	49.8	626.7	35.2	1182.3	43.1	1684.2	76.8	1910.9	64.6	2028.8	47.6
AK-MR-645		640.1	37.1	1217.6	46.1	1693.2	117.1	1912.4	63.7	2035.9	85.7
183.7	9.8	935.1	36.8	1244.2	43.3	1700.2	103.4	1915.5	51.4	2035.9	42.3
184.3	17.0	951.2	44.5	1258.1	50.7	1714.3	110.2	1915.5	43.5	2035.9	76.7
277.0	18.7	952.9	30.7	1292.4	77.7	1716.1	116.3	1920.1	67.8	2040.1	56.8
370.8	18.7	954.6	31.5	1297.7	91.5	1717.8	84.8	1923.1	59.1	2058.2	81.7
403.5	21.2	968.4	37.8	1303.0	70.2	1750.6	101.3	1929.2	131.8	2062.4	63.6
404.8	26.4	968.4	49.0	1308.2	49.6	1772.7	100.3	1929.2	107.8	2111.4	86.9
407.2	18.6	986.2	32.2	1316.1	57.2	1792.8	66.8	1930.7	76.6	2123.4	100.0
408.4	16.9	989.5	36.1	1319.3	57.3	1796.1	69.2	1930.7	134.2	2153.6	81.6
413.8	19.4	995.6	30.3	1325.6	47.4	1806.0	107.0	1930.7	35.1	2165.3	74.7

2208.5	73.1	370.8	15.5	551.4	20.5	1050.6	38.4	1163.0	35.6	1404.9	52.1
2255.4	47.8	370.8	15.8	554.9	20.7	1066.4	33.8	1170.5	57.2	1405.4	48.0
2263.9	130.2	377.4	16.0	557.3	26.1	1067.0	53.8	1172.1	37.2	1418.3	42.3
2299.6	92.4	378.1	13.2	564.4	28.4	1067.0	39.0	1179.1	43.4	1421.4	51.3
2300.8	53.9	381.7	15.7	573.3	30.5	1076.3	37.6	1187.1	42.8	1426.6	49.6
2301.9	43.9	384.7	15.4	620.9	23.6	1079.0	56.9	1188.2	44.4	1427.1	41.2
2310.1	73.2	387.8	13.6	641.3	37.3	1084.4	35.0	1190.3	48.6	1428.7	44.0
2319.5	52.3	388.4	20.0	661.7	26.9	1088.8	59.7	1207.5	102.6	1431.8	45.7
2337.9	103.3	401.7	16.3	669.8	23.1	1089.9	35.4	1210.1	43.2	1441.1	39.1
2391.9	52.3	413.2	20.3	897.0	29.2	1089.9	42.7	1223.5	73.1	1447.8	38.2
2396.3	53.4	413.8	23.1	916.6	31.1	1092.1	44.7	1227.8	41.2	1464.2	52.5
2416.0	65.5	413.8	18.6	917.8	31.3	1093.1	33.9	1229.9	39.3	1467.8	49.3
2444.0	58.2	416.2	27.1	917.8	32.7	1096.4	45.9	1232.5	42.9	1471.9	56.9
2473.5	94.0	421.7	19.4	928.4	31.1	1101.8	43.7	1244.2	38.3	1474.5	43.5
2479.8	88.0	422.9	19.4	936.7	38.2	1102.4	31.6	1260.7	37.8	1489.3	50.2
2567.5	52.9	425.3	18.1	952.9	24.7	1104.6	43.9	1261.2	50.6	1490.4	55.7
2614.6	65.6	426.5	22.2	962.3	30.6	1113.2	53.0	1276.6	52.3	1497.5	56.3
2624.0	31.7	428.3	13.9	965.7	32.7	1113.8	35.8	1284.0	39.2	1503.6	52.7
2678.4	45.5	435.0	15.5	968.4	31.7	1122.5	48.3	1294.0	48.1	1504.2	58.7
2693.7	32.9	439.2	15.8	969.0	44.7	1124.1	52.8	1300.3	41.1	1508.2	42.3
2708.9	63.8	443.4	16.9	969.0	45.0	1125.2	52.1	1307.2	37.9	1531.2	48.1
2724.7	67.0	452.4	18.0	969.0	48.6	1126.8	34.1	1311.4	43.7	1533.7	47.6
2765.3	50.5	459.0	22.6	982.8	33.7	1128.4	38.8	1323.0	38.7	1536.7	47.0
2770.4	64.3	459.0	27.5	983.4	40.0	1139.8	40.7	1328.2	41.3	1584.5	102.1
2791.5	64.0	461.4	17.3	1000.5	41.2	1139.8	47.7	1329.3	46.9	1605.4	129.1
2803.2	83.8	467.4	19.3	1003.3	32.7	1141.9	41.1	1329.8	37.7	1609.1	66.5
2803.2	73.9	508.6	19.7	1024.2	42.6	1148.9	42.2	1351.8	50.9	1612.9	103.6
2840.8	59.7	520.5	18.8	1029.2	53.3	1154.3	55.0	1365.3	46.6	1631.5	122.6
2866.4	94.5	521.1	38.4	1034.7	32.4	1157.6	64.3	1368.0	54.4	1640.7	138.0
P-BC-33		524.7	21.7	1035.2	51.3	1157.6	44.9	1370.6	47.2	1642.6	65.2
351.9	13.9	525.9	18.8	1036.9	42.0	1159.7	48.9	1387.2	50.2	1646.2	105.1
361.6	14.4	533.6	20.1	1040.7	30.8	1163.0	43.9	1398.6	40.5	1649.9	104.2

1657.2	67.7	1830.5	105.7	1953.2	57.8	2708.0	55.9	552.0	16.0	1111.1	30.9
1664.5	54.2	1832.1	75.2	1985.7	49.9	2716.0	42.4	567.4	28.8	1117.6	32.5
1669.9	110.1	1838.6	52.2	1990.0	92.6	2721.2	48.2	599.2	26.5	1118.1	27.3
1673.5	71.4	1846.6	67.9	2004.5	62.6	2728.2	56.0	680.3	23.8	1127.3	35.7
1682.5	62.2	1846.6	104.6	2014.6	55.1	2743.0	49.5	868.9	21.6	1132.2	44.5
1686.0	222.5	1849.8	73.1	2047.1	84.5	2754.2	42.5	892.5	22.8	1138.7	43.2
1693.2	51.6	1854.6	104.0	2051.3	80.1	2788.2	39.9	967.3	41.9	1143.5	55.6
1694.9	86.6	1861.0	58.5	2062.4	45.8	2795.7	57.0	975.1	29.0	1158.6	40.5
1700.2	102.0	1861.0	96.8	2066.6	75.3	3099.9	110.2	981.7	28.8	1174.8	34.2
1709.1	54.9	1862.5	79.7	2092.5	100.3	3115.3	41.0	1006.0	51.2	1180.2	39.7
1724.8	138.5	1864.1	50.9	2124.7	61.7	**AK-BC-195**		1012.1	29.1	1181.8	31.7
1736.9	102.9	1868.9	94.7	2212.3	98.7	366.5	11.9	1013.8	29.5	1208.5	27.1
1736.9	94.8	1872.0	87.2	2334.5	41.3	374.4	12.5	1018.2	34.4	1214.4	34.8
1765.9	58.7	1873.6	97.3	2335.6	42.4	386.4	10.8	1018.7	40.3	1279.2	34.0
1769.3	52.9	1878.3	67.8	2370.8	63.9	409.6	17.5	1020.9	31.6	1297.2	36.3
1777.7	105.2	1881.5	121.1	2419.3	45.6	421.7	13.6	1025.9	31.4	1327.7	36.4
1786.1	63.0	1886.1	93.0	2505.5	49.4	424.1	14.8	1025.9	23.9	1341.8	47.3
1787.8	192.6	1889.3	112.8	2512.6	60.7	424.1	16.7	1028.1	25.8	1349.2	49.6
1787.8	81.5	1892.4	62.0	2517.7	42.0	425.6	10.8	1033.6	31.5	1353.3	33.4
1787.8	94.3	1897.0	78.8	2539.8	61.8	427.1	15.6	1041.2	36.6	1371.1	39.0
1791.1	188.3	1903.2	60.4	2554.7	62.1	427.7	14.1	1044.5	33.4	1376.3	33.4
1794.4	91.1	1915.5	97.1	2554.7	54.4	428.1	11.4	1049.5	28.7	1460.6	35.7
1802.7	108.2	1918.5	50.8	2562.6	65.4	430.7	18.3	1056.6	30.1	1461.6	44.4
1807.7	93.5	1920.1	80.1	2567.5	37.3	434.3	20.1	1059.3	33.7	1468.8	42.1
1809.3	87.5	1923.1	77.2	2573.3	31.5	440.4	13.8	1073.0	38.1	1504.7	37.1
1815.9	66.6	1927.7	83.5	2580.1	62.5	442.8	19.2	1087.7	41.5	1580.7	57.9
1815.9	74.4	1929.2	88.3	2622.1	43.8	444.0	13.5	1090.4	39.5	1607.2	88.7
1817.5	53.4	1930.7	50.5	2622.1	64.6	448.1	12.2	1090.4	41.7	1627.8	79.8
1822.4	100.8	1932.2	59.2	2657.5	65.7	457.8	12.7	1097.0	29.7	1637.0	54.9
1824.0	62.0	1938.3	99.1	2663.0	54.7	543.7	25.9	1098.0	40.6	1644.4	47.3
1824.0	103.4	1945.8	71.6	2665.7	59.3	544.3	21.4	1102.4	39.7	1651.7	46.3
1825.6	86.0	1945.8	102.3	2689.3	167.5	548.4	22.4	1105.6	27.0	1651.7	42.4

1662.6	65.8	1857.8	58.9	1909.4	43.8	1947.3	47.5	2239.5	37.2	242.9	14.9
1664.5	45.7	1861.0	43.3	1909.4	31.6	1951.7	31.3	2253.0	34.6	351.3	16.3
1671.7	65.6	1862.5	71.3	1909.4	32.0	1953.2	43.9	2279.4	35.0	390.8	20.0
1680.7	81.1	1862.5	46.1	1912.4	30.6	1954.7	50.7	2280.6	33.1	396.9	26.8
1689.6	52.9	1865.7	36.1	1912.4	43.4	1957.7	41.2	2284.2	52.3	397.5	17.1
1700.2	37.2	1868.9	53.6	1912.4	56.6	1962.2	71.5	2333.3	45.3	397.5	15.7
1700.2	151.5	1870.5	69.9	1914.0	61.8	1962.2	93.8	2341.4	37.0	401.1	19.1
1702.0	39.4	1872.0	44.4	1915.5	41.8	1974.0	40.3	2353.9	27.4	416.2	26.2
1705.5	57.1	1872.0	76.9	1915.5	52.6	1981.3	30.9	2358.4	54.5	421.7	16.4
1714.3	66.9	1873.6	46.5	1917.0	51.9	1984.2	47.9	2359.5	27.8	425.9	24.9
1721.3	31.7	1875.2	44.0	1918.5	43.6	1988.6	43.4	2383.1	35.9	430.7	22.8
1723.0	59.3	1875.2	73.3	1918.5	46.0	1988.6	102.7	2388.6	32.8	430.7	17.3
1724.8	69.3	1875.2	44.1	1920.1	37.4	2006.0	29.3	2393.0	28.1	433.1	23.3
1726.5	82.0	1876.7	42.2	1921.6	36.9	2023.1	39.5	2402.9	39.2	434.3	20.4
1731.7	43.5	1884.6	36.4	1921.6	60.6	2024.5	65.6	2421.4	37.9	437.4	25.8
1733.5	75.4	1884.6	63.5	1921.6	34.1	2034.5	38.0	2455.7	43.6	437.4	19.8
1735.2	47.0	1886.1	31.2	1923.1	50.5	2058.2	87.1	2481.8	40.7	438.0	18.7
1776.1	66.5	1887.7	32.6	1923.1	33.3	2063.8	42.2	2553.7	40.7	449.4	23.6
1791.1	39.9	1889.3	37.4	1923.1	40.7	2070.7	41.1	2652.9	60.5	450.0	26.1
1797.7	82.1	1890.8	52.9	1926.2	44.7	2089.8	49.1	2676.6	65.3	503.9	18.2
1799.4	34.8	1895.5	32.6	1927.7	34.8	2093.9	32.5	2688.4	64.0	505.1	21.6
1802.7	51.7	1897.0	32.0	1930.7	30.4	2096.6	41.1	2717.7	35.4	514.6	23.3
1806.0	50.1	1898.6	37.5	1930.7	35.7	2098.0	51.6	2722.1	47.7	520.5	26.3
1824.0	39.6	1900.1	32.0	1930.7	45.2	2107.4	50.4	2730.0	45.0	561.4	22.1
1830.5	43.9	1900.1	33.3	1933.7	28.6	2120.8	53.2	2732.6	35.6	580.9	39.1
1833.7	96.1	1900.1	36.7	1933.7	53.5	2131.4	47.0	2737.0	32.0	614.4	27.2
1837.0	77.3	1901.7	88.5	1933.7	45.5	2164.0	55.1	2746.5	55.1	614.4	31.6
1838.6	80.5	1901.7	31.5	1935.2	34.6	2176.9	44.3	2748.2	26.7	622.6	25.4
1841.8	51.2	1903.2	31.0	1938.3	29.1	2212.3	63.5	2752.5	35.2	622.6	20.8
1845.0	54.4	1904.7	40.2	1938.3	43.7	2230.9	51.3	3045.1	27.3	627.9	26.9
1848.2	38.5	1907.8	36.1	1939.8	40.1	2230.9	56.1	3148.2	30.1	735.2	26.8
1854.6	41.9	1907.8	35.2	1941.3	39.2	2230.9	38.0	**HK-MC-60**		787.9	61.9

926.7	44.8	1094.8	31.8	1466.8	42.5	1700.2	60.9	1941.3	169.3	2238.3	79.0
927.8	42.7	1097.5	32.9	1470.4	46.5	1703.8	56.0	1942.8	91.9	2239.5	75.4
927.8	41.8	1101.8	31.7	1471.4	44.2	1709.1	75.6	1942.8	96.6	2256.6	94.2
933.4	32.1	1110.5	50.5	1472.4	65.2	1714.3	117.8	1945.8	58.5	2263.9	133.5
935.6	32.0	1119.7	40.2	1474.5	73.2	1723.0	47.6	1950.3	49.8	2292.5	43.1
957.9	44.6	1126.8	39.6	1481.7	57.5	1728.3	89.7	1956.2	67.7	2298.4	96.7
969.5	57.1	1137.6	73.6	1482.2	52.6	1731.7	59.1	1956.2	50.1	2331.0	76.2
971.8	41.4	1139.2	35.0	1500.6	53.1	1738.6	81.6	1957.7	87.5	2359.5	63.8
986.7	31.6	1143.5	38.8	1501.1	45.8	1765.9	72.7	1957.7	83.0	2367.4	67.9
1000.5	39.9	1157.0	51.1	1521.5	46.1	1777.7	78.8	1965.1	57.7	2394.1	89.9
1007.2	33.4	1158.6	44.0	1525.0	48.7	1810.9	100.1	1966.6	131.4	2409.5	124.4
1027.5	34.6	1165.1	29.6	1531.7	43.4	1820.8	153.4	1971.0	134.4	2411.7	83.3
1028.6	36.9	1167.3	46.2	1535.2	52.1	1824.0	105.9	1971.0	150.7	2437.6	81.5
1033.6	34.6	1169.9	72.3	1538.3	68.5	1830.5	67.5	1976.9	64.4	2448.2	79.1
1033.6	29.5	1178.5	39.9	1540.8	51.7	1846.6	70.8	1978.4	72.0	2473.5	50.5
1038.5	31.9	1180.2	55.1	1547.4	51.7	1854.6	66.2	1979.8	66.6	2481.8	111.0
1040.7	50.7	1195.2	58.3	1565.3	82.9	1859.4	65.3	1981.3	89.5	2497.3	133.8
1042.3	60.2	1209.6	55.0	1578.8	97.3	1865.7	104.1	1987.1	102.8	2569.4	46.4
1044.5	39.0	1221.9	48.3	1629.7	91.2	1889.3	81.6	2003.1	114.2	2659.3	47.9
1047.3	51.4	1228.8	62.9	1637.0	107.5	1892.4	49.2	2011.7	92.1	2692.0	41.0
1048.4	51.6	1240.5	41.3	1638.9	105.9	1897.0	69.2	2020.3	56.0	2710.7	59.0
1053.8	31.1	1275.0	45.7	1657.2	97.0	1900.1	64.3	2035.9	173.8	2731.7	51.4
1053.8	43.2	1315.1	46.1	1659.0	71.1	1903.2	85.4	2070.7	56.9	2738.7	58.7
1065.9	47.6	1318.2	37.5	1660.8	49.6	1903.2	74.5	2070.7	52.5	2742.2	155.2
1071.3	42.5	1329.3	47.9	1666.3	91.1	1906.3	88.7	2095.3	74.2	2759.4	47.5
1072.4	38.6	1345.5	53.5	1668.1	63.7	1909.4	83.6	2118.1	82.5	2778.1	66.3
1082.8	49.0	1358.6	42.5	1671.7	72.5	1915.5	65.0	2122.1	56.5	2785.6	58.7
1090.4	47.5	1363.3	62.2	1677.1	71.9	1926.2	66.1	2153.6	70.9	2840.0	46.8
1092.1	43.5	1396.6	59.3	1678.9	87.6	1927.7	82.4	2154.9	97.2	3093.2	42.8
1092.6	38.5	1400.7	51.2	1686.0	116.7	1936.7	77.4	2169.2	87.8	3118.6	57.6
1094.2	61.8	1427.7	101.4	1689.6	74.8	1936.7	76.3	2214.8	61.0	3731.2	24.4
1094.8	43.3	1463.2	59.6	1693.2	119.6	1939.8	73.2	2218.5	70.3	**MC-GG-13**	

147.2	10.8	448.2	16.6	846.4	33.9	1056.0	33.0	1175.3	42.5	1451.4	50.8
206.8	14.7	448.8	25.5	908.8	58.0	1058.8	34.6	1178.0	57.4	1464.7	60.1
230.5	11.4	457.2	34.2	940.6	34.0	1058.8	43.1	1197.3	56.0	1464.7	65.0
242.9	10.7	474.0	25.0	954.0	49.9	1059.9	40.1	1204.8	48.7	1468.3	58.1
285.0	12.6	522.3	25.6	965.7	30.5	1063.1	55.6	1209.1	43.4	1476.5	42.7
289.3	11.1	537.2	29.1	972.9	34.8	1066.4	31.7	1217.6	37.2	1479.6	38.5
303.5	13.5	537.8	23.9	979.0	65.3	1069.2	41.1	1221.9	48.1	1484.2	63.1
309.0	13.5	540.1	30.0	987.8	42.3	1074.6	43.0	1228.8	69.7	1486.8	53.4
313.9	14.9	544.9	31.9	987.8	45.1	1075.7	50.8	1258.6	42.0	1488.8	41.4
318.8	14.1	559.1	33.9	988.9	30.9	1076.3	34.7	1260.2	43.6	1490.4	54.2
353.1	20.6	559.7	27.5	992.2	26.9	1096.4	42.9	1316.7	61.7	1493.4	57.0
368.3	17.7	560.9	24.7	994.5	37.1	1099.1	46.4	1322.4	44.6	1525.6	67.8
373.8	14.8	562.6	25.4	998.9	37.6	1102.9	39.4	1325.1	39.7	1526.6	64.9
378.7	19.4	563.2	22.4	1001.1	48.0	1104.0	46.5	1325.6	38.0	1545.4	55.5
381.7	14.9	565.0	26.3	1005.5	35.2	1112.2	42.6	1331.9	36.6	1586.4	196.8
386.6	17.0	565.6	27.3	1006.0	31.8	1115.4	54.8	1334.0	63.3	1597.8	85.7
386.6	20.9	569.7	35.5	1022.6	50.7	1120.3	60.4	1340.8	50.6	1599.7	107.5
391.4	17.2	575.6	24.1	1024.2	53.0	1125.7	56.3	1344.4	52.9	1607.2	103.5
396.3	28.1	580.3	24.7	1028.6	40.5	1126.8	66.5	1357.5	48.6	1612.9	96.0
400.5	14.1	586.8	27.2	1028.6	42.7	1129.5	46.2	1362.2	46.5	1620.4	63.2
404.8	26.7	587.4	33.8	1030.8	53.6	1132.7	38.0	1364.8	39.5	1622.2	109.7
407.2	21.2	593.3	36.3	1031.4	53.7	1134.9	34.5	1368.0	43.5	1624.1	106.2
408.4	16.8	615.0	30.1	1033.6	34.6	1136.0	36.7	1370.0	43.9	1635.2	115.5
409.0	18.6	615.0	28.2	1033.6	56.9	1137.6	63.0	1381.0	45.2	1637.0	75.0
410.8	15.3	632.6	30.0	1035.2	45.2	1150.0	48.8	1395.5	57.9	1659.0	77.5
413.8	21.2	634.9	28.1	1036.9	34.0	1153.8	62.2	1397.1	50.8	1677.1	68.8
416.8	19.8	643.1	26.9	1038.0	30.7	1161.9	34.3	1400.2	51.8	1677.1	46.5
419.3	15.0	653.6	36.4	1039.6	65.1	1162.4	35.7	1416.3	57.3	1677.1	75.6
424.1	26.3	664.6	27.7	1041.8	40.7	1164.6	59.6	1416.8	45.6	1678.9	151.5
433.7	19.5	665.8	28.9	1047.3	35.5	1168.3	33.5	1417.8	64.3	1678.9	103.2
435.0	22.6	704.0	31.3	1051.7	39.6	1169.9	42.3	1435.4	41.7	1682.5	101.3
439.8	21.7	762.1	25.6	1052.2	43.8	1169.9	59.3	1447.8	48.8	1684.2	83.4

1689.6	70.1	1846.6	105.3	2806.5	69.9	461.4	18.3	1007.2	53.8	1098.6	38.0
1689.6	76.2	1859.4	63.5	2813.1	78.9	470.4	26.7	1016.0	41.0	1098.6	49.6
1691.4	50.1	1861.0	71.8	2834.3	63.8	486.0	20.4	1020.4	53.4	1100.2	59.2
1694.9	84.6	1868.9	93.9	3053.4	54.7	514.0	21.2	1020.4	38.2	1103.5	61.3
1696.7	91.2	1872.0	84.2	3101.3	35.0	533.0	23.3	1024.2	41.6	1108.9	52.8
1696.7	57.7	1883.0	83.0	3433.6	204.2	533.6	31.7	1027.5	50.7	1113.2	50.4
1700.2	106.9	1892.4	172.3	**K-GG-75**		533.6	28.3	1027.5	35.4	1118.7	34.9
1700.2	86.9	1900.1	55.4	159.2	8.6	535.4	21.3	1030.3	43.5	1119.2	49.7
1702.0	75.4	1900.1	70.8	164.0	8.3	536.0	23.5	1031.4	54.5	1123.0	34.4
1705.5	127.4	1900.1	67.9	227.4	13.2	539.5	31.3	1032.5	42.1	1124.6	47.3
1705.5	94.5	1904.7	68.5	233.0	17.4	541.9	33.7	1033.0	27.9	1130.0	49.2
1710.8	62.3	1926.2	86.2	238.6	9.0	546.1	19.0	1033.0	37.5	1133.8	62.8
1714.3	54.4	1957.7	69.0	318.8	16.3	562.6	30.3	1033.6	55.5	1139.2	47.3
1714.3	65.7	1971.0	62.9	368.3	16.1	582.7	25.1	1037.4	39.1	1145.7	55.2
1714.3	120.9	1978.4	68.7	404.8	19.1	603.3	20.4	1038.5	36.0	1151.6	50.1
1717.8	104.9	2003.1	54.3	406.0	20.5	612.7	32.0	1050.6	39.9	1167.3	53.0
1719.6	113.9	2026.0	71.4	409.6	18.5	622.0	33.2	1050.6	66.2	1167.8	42.7
1730.0	96.4	2027.4	90.1	409.6	27.7	641.9	28.7	1055.5	39.5	1168.9	43.6
1747.2	55.4	2034.5	46.4	410.8	22.1	757.0	37.5	1057.1	43.0	1195.7	41.3
1760.9	66.9	2099.3	86.3	410.8	25.8	920.6	44.2	1057.1	32.7	1196.8	144.0
1762.6	72.1	2119.4	76.6	413.2	21.7	927.3	33.8	1061.5	38.6	1218.2	81.1
1767.6	62.1	2131.4	71.4	415.0	16.8	928.9	46.7	1070.3	48.4	1218.2	43.5
1767.6	59.8	2170.5	86.9	415.6	22.9	944.5	49.9	1071.9	43.5	1235.2	48.9
1786.1	43.6	2314.8	80.6	426.5	23.9	949.5	39.8	1075.2	52.2	1235.2	29.6
1787.8	84.0	2345.9	110.1	433.7	21.0	957.3	35.1	1081.7	32.4	1238.4	50.9
1789.4	69.2	2567.5	131.1	435.6	15.3	962.3	51.8	1082.8	37.6	1240.0	39.0
1794.4	84.1	2623.1	68.9	439.2	35.9	966.2	40.4	1083.3	43.1	1270.8	43.4
1799.4	44.9	2667.5	35.2	449.4	17.9	985.1	42.2	1087.2	42.0	1293.5	57.3
1801.1	92.8	2683.9	41.9	453.6	21.5	989.5	49.8	1087.2	53.0	1296.7	46.5
1802.7	78.7	2735.2	71.5	455.4	18.2	990.6	36.6	1088.8	62.8	1298.8	60.1
1815.9	88.3	2767.0	49.0	458.4	24.7	1001.1	63.5	1091.5	40.6	1300.9	63.2
1822.4	60.8	2776.4	67.4	459.0	24.1	1006.6	68.8	1097.0	32.1	1304.0	36.2

1307.2	57.9	1574.9	118.8	1750.6	49.3	1960.7	59.5	246.0	14.1	662.9	29.1
1315.6	38.9	1584.5	89.9	1759.2	69.7	1962.2	89.8	255.9	15.8	843.0	43.2
1315.6	54.9	1595.9	102.8	1762.6	111.3	1969.5	74.3	257.8	20.8	926.1	49.3
1333.5	41.4	1616.6	58.0	1764.3	107.8	2040.1	79.8	368.9	14.2	927.3	39.4
1334.0	50.9	1620.4	94.9	1765.9	51.9	2065.2	87.5	374.4	16.9	929.5	30.7
1334.5	67.1	1622.2	101.3	1774.4	62.9	2084.4	86.3	385.3	18.0	937.9	56.5
1347.6	53.1	1622.2	68.9	1779.4	78.4	2099.3	107.4	396.9	20.1	946.8	40.0
1378.9	65.1	1629.7	74.8	1782.8	72.9	2115.4	82.8	409.0	20.1	947.9	50.7
1391.4	46.3	1629.7	58.0	1786.1	54.3	2167.9	72.4	415.6	24.8	987.3	32.9
1414.7	61.9	1635.2	69.7	1787.8	54.5	2197.2	46.9	418.1	20.5	989.5	49.6
1422.5	52.4	1637.0	67.6	1792.8	74.5	2279.4	63.7	423.5	21.8	995.6	69.1
1426.6	50.2	1637.0	102.8	1794.4	64.5	2384.2	36.3	430.1	19.6	998.3	58.3
1430.7	40.8	1637.0	82.5	1794.4	73.7	2426.8	48.1	433.1	21.2	1001.1	25.2
1431.3	51.2	1638.9	91.8	1796.1	65.0	2505.5	53.4	435.0	18.3	1003.8	35.2
1432.8	52.9	1638.9	68.4	1806.0	107.4	2639.0	71.0	436.8	18.3	1006.0	32.5
1436.4	62.3	1644.4	76.1	1806.0	82.8	2662.1	155.5	440.4	19.0	1008.8	36.2
1441.1	44.4	1646.2	67.6	1825.6	100.6	2685.7	78.2	440.4	26.3	1019.3	47.0
1450.8	44.6	1653.6	64.9	1827.3	88.8	2703.6	67.9	442.8	27.7	1021.5	51.1
1459.6	48.1	1657.2	85.7	1828.9	114.2	2719.5	76.0	446.4	19.9	1022.6	38.5
1467.8	47.5	1657.2	137.3	1832.1	106.0	2782.3	90.5	449.4	24.3	1023.7	36.8
1470.4	39.9	1678.9	85.8	1835.4	108.9	2818.8	60.8	557.3	25.6	1032.5	28.5
1472.9	51.7	1686.0	115.5	1838.6	94.0	2825.4	37.8	578.6	21.4	1035.2	29.5
1481.1	54.0	1686.0	75.4	1861.0	90.6	2826.2	52.0	589.2	20.6	1035.8	41.0
1508.2	51.9	1691.4	153.3	1867.3	54.4	2995.3	73.3	602.1	26.5	1046.2	29.1
1527.1	44.4	1691.4	49.5	1868.9	65.0	3201.1	35.9	605.6	23.2	1048.9	33.4
1531.7	57.9	1693.2	81.9	1890.8	49.1	3208.0	59.2	608.5	32.0	1055.5	33.6
1537.8	47.3	1696.7	283.6	1900.1	71.0	**MGE-MGE-94**		609.1	41.2	1056.6	44.1
1539.9	119.7	1700.2	118.0	1914.0	97.4	150.7	6.2	616.8	23.0	1056.6	31.5
1545.4	46.3	1710.8	72.3	1915.5	125.1	155.4	11.7	621.4	29.5	1058.2	53.8
1545.4	48.4	1714.3	74.2	1917.0	54.7	160.4	14.8	631.4	32.6	1058.8	54.0
1545.9	92.8	1721.3	119.7	1924.6	62.2	162.3	10.7	633.7	30.6	1059.3	51.9
1569.1	107.8	1745.5	88.8	1953.2	52.4	244.1	10.2	655.3	32.8	1063.7	46.4

1066.4	49.4	1276.1	51.5	1571.1	93.5	1760.9	70.2	1878.3	50.2	2360.7	45.8
1067.0	42.6	1285.6	40.7	1601.6	124.9	1760.9	71.3	1889.3	81.7	2367.4	45.9
1074.1	34.0	1289.8	42.3	1605.4	73.2	1762.6	91.0	1895.5	60.0	2378.6	84.9
1074.6	43.0	1307.2	55.2	1609.1	136.0	1762.6	67.3	1898.6	103.7	2395.2	65.4
1077.9	32.5	1307.7	41.9	1618.5	62.1	1764.3	67.2	1914.0	98.7	2440.8	51.3
1077.9	86.4	1323.0	48.2	1620.4	102.3	1765.9	101.2	1918.5	61.8	2460.9	52.3
1083.3	87.5	1329.3	49.9	1622.2	95.4	1767.6	47.3	1923.1	55.6	2464.1	51.9
1086.6	36.5	1332.9	37.8	1644.4	145.8	1767.6	70.5	1935.2	56.2	2533.8	72.7
1093.7	32.4	1365.9	62.4	1649.9	88.3	1769.3	78.1	1979.8	73.4	2553.7	43.1
1110.0	33.6	1371.6	50.6	1651.7	78.9	1769.3	97.6	1979.8	56.1	2626.8	37.6
1111.6	38.1	1392.4	53.4	1653.6	71.4	1771.0	112.7	2017.4	112.2	2677.5	61.8
1120.8	35.8	1397.1	60.7	1653.6	82.3	1771.0	70.7	2018.8	64.9	2687.5	34.2
1123.0	44.7	1419.4	49.9	1653.6	80.4	1777.7	75.7	2052.7	168.3	2706.2	48.1
1132.2	91.2	1420.9	47.7	1668.1	76.1	1784.4	41.3	2055.5	74.3	2708.0	73.5
1143.0	121.4	1422.0	47.7	1686.0	63.8	1784.4	90.2	2096.6	149.3	2716.8	84.5
1144.6	39.8	1433.8	58.4	1691.4	107.7	1787.8	78.0	2098.0	223.4	2718.6	58.0
1167.3	29.9	1439.0	47.0	1700.2	67.1	1794.4	99.7	2153.6	77.4	2723.0	28.8
1167.8	33.8	1448.3	44.1	1703.8	115.3	1796.1	49.0	2161.4	117.0	2746.5	111.6
1171.6	49.9	1450.3	43.0	1709.1	85.9	1796.1	164.8	2164.0	61.4	2746.5	49.2
1176.9	47.1	1451.4	47.2	1712.6	76.5	1801.1	120.0	2190.9	88.3	2767.9	49.4
1180.7	48.6	1466.3	55.0	1712.6	101.5	1809.3	67.9	2201.0	57.4	2767.9	71.2
1182.3	45.9	1467.3	44.5	1716.1	99.3	1809.3	122.8	2216.0	117.9	2768.7	30.0
1183.9	39.5	1484.7	71.1	1719.6	61.8	1814.2	119.6	2218.5	131.3	2793.2	54.1
1190.9	36.1	1492.9	42.1	1721.3	58.8	1815.9	71.9	2240.8	135.7	2801.5	147.1
1191.4	46.6	1500.1	83.6	1730.0	51.2	1820.8	73.0	2263.9	66.6	2840.8	69.6
1194.1	57.8	1506.7	65.3	1731.7	69.1	1822.4	63.9	2269.9	96.2	3004.6	56.2
1196.2	43.8	1515.9	42.4	1738.6	109.0	1845.0	108.2	2283.0	99.1	3093.2	47.7
1196.8	65.9	1531.7	53.7	1743.8	73.2	1846.6	121.4	2285.4	65.4	3184.1	57.9
1238.4	58.7	1539.8	53.3	1745.5	77.4	1856.2	47.9	2287.8	76.4	**HK-MGE-18**	
1250.1	62.0	1555.6	122.9	1748.9	48.3	1859.4	70.6	2336.8	89.8	97.0	7.1
1260.7	67.0	1557.5	67.3	1750.6	68.4	1868.9	65.7	2353.9	71.5	179.3	9.4
1262.8	60.7	1565.3	103.8	1754.1	52.9	1875.2	93.9	2359.5	61.2	193.7	12.1

308.4	14.4	640.1	34.8	1053.8	28.4	1212.3	40.2	1466.3	40.5	1680.7	71.0
358.0	26.4	650.6	25.9	1060.4	33.0	1212.8	70.9	1479.6	46.7	1680.7	79.4
372.6	15.6	672.2	28.1	1061.5	61.3	1228.8	40.3	1480.1	48.6	1694.9	84.1
375.6	21.7	716.2	27.2	1063.7	37.7	1235.2	38.7	1484.7	51.2	1700.2	104.4
380.5	17.2	778.2	28.2	1065.9	37.4	1252.2	49.4	1485.7	44.1	1705.5	64.0
389.0	26.2	792.4	36.1	1067.0	44.1	1268.7	39.9	1495.0	74.6	1707.3	67.5
399.3	19.8	811.2	29.9	1075.7	43.2	1289.8	51.4	1500.1	62.4	1712.6	55.4
403.5	17.5	888.6	62.0	1080.6	42.7	1293.5	53.0	1501.6	56.7	1714.3	123.6
412.6	23.3	912.2	73.3	1085.5	35.5	1297.7	42.0	1511.8	60.9	1724.8	85.3
415.0	18.9	946.2	39.1	1088.8	54.7	1318.2	48.3	1517.4	51.0	1735.2	62.8
419.3	19.7	957.3	39.6	1089.9	43.1	1320.9	48.6	1541.8	55.0	1738.6	97.1
422.9	22.7	966.8	57.7	1092.6	35.5	1330.8	52.0	1548.4	58.5	1742.1	73.7
424.7	23.5	967.3	50.9	1093.7	31.6	1340.3	40.6	1576.8	76.4	1747.2	82.0
425.3	16.7	973.4	35.9	1095.3	46.4	1347.6	47.9	1590.2	104.4	1754.1	62.9
430.7	17.2	979.0	79.1	1098.0	50.9	1350.7	55.1	1595.9	127.7	1760.9	104.4
435.0	20.7	981.2	33.8	1103.5	62.9	1358.6	49.2	1595.9	75.8	1764.3	69.5
435.6	19.0	991.7	57.8	1110.0	38.8	1371.6	49.6	1599.7	108.1	1771.0	91.7
436.8	21.5	998.3	34.1	1112.7	40.2	1375.8	48.1	1612.9	86.5	1772.7	98.5
441.6	18.8	1001.1	33.2	1125.2	60.3	1377.9	63.0	1616.6	122.7	1776.1	69.5
447.0	21.5	1003.8	56.5	1127.3	39.7	1381.5	48.5	1622.2	76.5	1777.7	61.9
453.0	24.0	1004.4	46.4	1131.1	48.0	1384.1	55.3	1627.8	75.4	1779.4	55.3
461.4	27.7	1006.0	54.3	1139.8	55.1	1385.1	58.1	1635.2	57.0	1779.4	109.0
466.2	30.4	1007.7	30.8	1142.5	46.4	1395.0	35.7	1637.0	97.9	1782.8	102.9
484.2	22.0	1008.8	36.1	1146.2	45.6	1405.4	48.4	1640.7	161.0	1786.1	201.0
534.8	23.5	1019.3	51.3	1151.6	38.0	1411.6	50.1	1651.7	109.5	1791.1	138.2
544.9	27.7	1020.4	32.6	1157.0	44.0	1414.2	38.4	1653.6	111.3	1796.1	75.0
562.6	21.2	1023.1	73.9	1165.6	53.6	1435.9	49.7	1659.0	94.8	1799.4	70.7
583.9	44.1	1023.1	46.6	1166.2	41.3	1445.7	53.7	1660.8	90.5	1817.5	52.0
606.8	35.4	1028.6	34.7	1171.0	49.7	1448.8	42.8	1671.7	59.4	1825.6	53.0
623.2	30.3	1032.5	34.7	1171.6	34.4	1450.8	53.3	1675.3	96.1	1833.7	89.0
627.9	32.6	1039.1	37.6	1175.3	143.6	1460.6	52.9	1677.1	83.6	1840.2	83.6
635.5	25.1	1039.1	31.2	1175.9	36.7	1464.2	44.6	1677.1	67.1	1841.8	80.3

1845.0	54.2	2726.5	54.3	408.4	16.3	600.9	28.0	1038.0	29.6	1214.4	38.7
1849.8	88.0	2727.4	50.0	409.0	14.2	605.6	28.5	1041.2	39.3	1215.5	39.8
1851.4	66.3	2740.4	54.6	411.4	13.3	613.2	20.7	1042.9	31.6	1217.6	42.4
1853.0	138.6	2741.3	84.5	412.6	15.1	616.8	23.3	1044.0	45.5	1217.6	38.6
1884.6	80.0	2744.8	32.5	416.8	16.2	617.3	18.2	1055.5	50.2	1228.8	84.4
1886.1	47.5	2744.8	74.0	417.5	29.1	622.6	24.5	1057.1	30.2	1241.1	48.6
1890.8	99.0	2744.8	45.9	429.5	16.4	623.2	25.3	1061.5	35.4	1242.7	44.2
1904.7	71.9	2745.6	24.5	431.3	13.9	637.2	25.7	1063.7	33.6	1248.5	35.3
1923.1	60.3	2751.7	54.0	431.9	23.7	653.6	28.5	1065.9	40.7	1249.0	40.4
1941.3	197.0	2754.2	53.2	435.6	16.3	667.5	32.3	1068.1	34.0	1253.3	44.7
1945.8	82.9	2755.9	53.3	436.2	19.1	668.7	26.7	1071.3	36.3	1260.7	38.7
1953.2	98.1	2764.5	60.9	442.2	26.1	704.0	22.4	1081.7	35.0	1260.7	38.8
1954.7	58.6	2775.5	57.9	442.8	14.5	769.6	24.8	1081.7	33.1	1268.7	45.7
1962.2	71.7	2846.5	82.0	450.0	17.5	802.1	44.6	1082.8	39.1	1290.3	51.6
1971.0	77.1	2850.5	90.8	450.6	17.1	951.2	27.1	1086.6	29.5	1295.6	38.7
1978.4	77.7	2895.5	65.1	454.8	21.7	953.4	45.1	1086.6	39.9	1325.6	34.7
1997.3	62.7	2896.3	71.5	455.4	18.5	972.3	26.7	1098.0	38.4	1326.1	37.7
2001.6	83.7	2998.1	56.9	456.0	17.0	981.7	41.3	1120.8	31.7	1327.7	48.7
2021.7	68.1	**MGE-MGE-425**		457.8	15.4	985.1	31.2	1124.1	30.1	1330.8	39.7
2047.1	140.6	166.1	8.4	460.8	18.8	987.8	40.9	1126.2	32.5	1340.3	44.7
2091.2	131.2	218.7	9.0	465.6	17.8	1003.8	35.9	1130.6	33.0	1347.6	38.3
2157.5	78.8	246.0	13.0	466.2	15.1	1011.0	26.5	1132.2	35.7	1349.2	37.0
2164.0	52.4	307.2	12.8	466.8	23.4	1016.5	26.8	1133.8	38.8	1358.0	34.3
2525.8	89.3	317.0	13.2	467.4	15.9	1017.6	50.8	1137.1	40.8	1360.7	41.6
2527.8	123.8	318.8	15.5	553.8	19.4	1018.7	39.2	1138.7	35.7	1365.9	42.8
2588.8	45.0	320.7	14.0	567.9	23.7	1019.8	25.0	1144.6	37.1	1405.4	35.1
2619.3	61.0	341.5	13.9	585.0	22.8	1022.0	29.6	1154.9	35.7	1408.0	49.6
2652.9	139.7	361.0	12.0	593.9	20.0	1023.1	58.0	1178.5	45.7	1412.1	36.3
2687.5	56.1	404.1	18.3	596.2	22.3	1024.2	46.6	1180.7	34.5	1418.3	41.2
2692.8	37.0	406.0	17.7	597.4	24.3	1030.8	37.3	1190.3	33.8	1428.2	45.6
2707.1	48.7	406.6	15.9	597.4	19.0	1035.2	37.6	1192.0	57.7	1429.2	51.5
2712.4	86.6	407.2	14.8	599.2	22.2	1036.3	42.5	1198.9	35.5	1461.1	52.6

1484.7	40.3	1865.7	49.3	2767.0	32.0	602.1	22.8	1118.7	41.6	1539.3	54.0
1497.0	44.9	1895.5	107.3	**MGE-RR**		612.1	25.8	1123.0	42.2	1573.0	48.7
1501.1	41.2	1895.5	69.9	153.6	6.7	617.9	33.1	1124.6	39.4	1584.5	85.0
1514.9	43.9	1903.2	43.6	160.8	8.8	629.0	24.8	1154.9	31.9	1597.8	73.1
1515.9	37.8	1924.6	43.4	161.7	7.3	630.8	23.2	1166.7	37.6	1607.2	67.1
1518.4	41.9	1942.8	71.9	195.6	11.3	637.2	25.7	1194.6	41.0	1620.4	68.5
1522.0	33.3	1944.3	39.8	282.4	9.1	639.6	18.5	1220.8	40.1	1620.4	81.1
1528.1	46.7	1962.2	50.7	359.8	14.3	639.6	24.5	1266.0	31.0	1620.4	51.6
1544.9	46.2	1966.6	62.0	382.3	17.8	646.0	21.4	1267.1	35.2	1622.2	106.6
1620.4	68.8	2008.8	36.5	393.8	18.3	658.8	34.8	1294.5	35.6	1633.4	59.8
1624.1	71.5	2020.3	52.6	398.7	14.8	660.5	22.6	1301.4	44.4	1659.0	62.4
1642.6	80.7	2047.1	134.5	398.7	19.1	664.6	34.3	1325.6	44.1	1662.6	81.0
1651.7	93.5	2058.2	48.4	404.8	14.4	685.5	19.4	1327.2	36.3	1677.1	86.7
1657.2	65.2	2069.3	55.3	408.4	25.3	893.1	30.4	1339.2	41.1	1678.9	81.6
1662.6	50.5	2080.3	59.8	410.8	14.2	949.5	32.7	1342.4	34.3	1723.0	39.3
1668.1	82.9	2098.0	407.1	415.0	14.9	988.9	36.7	1344.4	46.7	1752.4	75.5
1684.2	53.3	2110.1	50.2	415.0	13.6	990.6	43.0	1357.5	39.6	1774.4	44.4
1687.8	90.8	2135.3	79.8	416.2	17.0	1001.1	83.5	1360.7	35.5	1786.1	42.7
1733.5	53.1	2139.3	142.8	418.1	21.1	1016.0	49.1	1379.9	38.0	1814.2	75.0
1742.1	78.0	2298.4	38.5	418.1	15.2	1017.6	26.6	1388.8	47.9	1817.5	43.5
1762.6	39.9	2366.3	35.1	420.5	14.3	1022.6	32.6	1389.3	42.5	1830.5	87.3
1771.0	101.7	2560.6	42.6	428.3	18.2	1027.0	34.5	1398.6	51.3	1837.0	61.8
1774.4	30.9	2696.4	50.4	433.1	21.1	1030.8	41.3	1426.6	40.8	1849.8	61.7
1781.1	44.1	2700.9	27.6	447.0	18.2	1035.8	32.9	1438.5	37.9	1862.5	54.8
1791.1	59.1	2717.7	46.2	450.0	17.0	1036.9	41.2	1450.8	35.2	1868.9	55.2
1814.2	145.5	2719.5	29.5	462.6	15.4	1041.2	43.3	1455.5	38.9	1868.9	124.2
1817.5	46.2	2730.9	37.6	527.7	23.2	1054.4	26.4	1459.1	39.9	1886.1	48.0
1817.5	49.1	2733.5	43.5	531.2	25.0	1064.2	41.8	1471.9	36.1	1889.3	62.2
1827.3	55.7	2734.3	56.2	534.2	24.3	1085.5	45.9	1474.5	45.5	1890.8	57.6
1845.0	77.7	2738.7	38.8	542.5	17.5	1091.0	31.1	1499.0	53.6	1900.1	72.9
1856.2	83.9	2744.8	36.0	582.1	26.6	1109.4	51.4	1504.1	104.2	1904.7	43.6
1862.5	71.5	2766.2	40.7	588.0	27.4	1116.5	30.4	1515.4	46.3	1918.5	91.0

1932.2	56.5
1942.8	61.1
1954.7	71.9
2134.0	75.4
2235.8	57.2
2277.1	42.8
2286.6	73.7
2304.3	48.1
2384.2	67.7
2406.2	49.4
2488.1	47.5
2490.1	47.1
2571.4	50.5
2610.8	47.8
2674.8	34.8
2700.0	52.9
2719.5	33.6
2722.1	37.4
2722.1	48.0
2735.2	41.3
2811.4	32.8
2907.1	72.4
3102.6	30.9